Critical slowing down and error analysis of lattice QCD simulations

D I S S E R T A T I O N

zur Erlangung des akademischen Grades

d o c t o r   r e r u m   n a t u r a l i u m
(Dr. Rer. Nat.)
im Fach Physik

eingereicht an der
Mathematisch-Naturwissenschaftliche Fakultät I
Humboldt-Universität zu Berlin

von
Herrn M.Sc. Francesco Virotta

Präsident der Humboldt-Universität zu Berlin:
Prof. Dr. Jan-Hendrik Olbertz

Dekan der Mathematisch-Naturwissenschaftliche Fakultät I:
Prof. Dr. Andreas Herrmann

Gutachter:
1. Prof. Dr. Ulrich Wolff
2. Priv. Doz. Dr. Rainer Sommer
3. Prof. Dr. Luigi Del Debbio

eingereicht am: 03.01.2012
Tag der mündlichen Prüfung: 21.02.2012

Abstract

In this work we investigate the critical slowing down of lattice QCD simulations. We perform a preliminary study in the quenched approximation where we find that our estimate of the exponential auto-correlation time scales as $\tau_{\exp}(a) \sim a^{-5}$, where a is the lattice spacing. In unquenched simulations with $O(a)$ improved Wilson fermions we do not obtain a scaling law but find results compatible with the behavior that we find in the pure gauge theory. The discussion is supported by a large set of ensembles both in pure gauge and in the theory with two degenerate sea quarks. We have moreover investigated the effect of slow algorithmic modes in the error analysis of the expectation value of typical lattice QCD observables (hadronic matrix elements and masses). In the context of simulations affected by slow modes we propose and test a method to obtain reliable estimates of statistical errors. The method is supposed to help in the typical algorithmic setup of lattice QCD, namely when the total statistics collected is of $O(10)\tau_{\exp}$. This is the typical case when simulating close to the continuum limit where the computational costs for producing two independent data points can be extremely large. We finally discuss the scale setting in $N_{\mathrm{f}} = 2$ simulations using the Kaon decay constant f_{K} as physical input. The method is explained together with a thorough discussion of the error analysis employed. A description of the publicly available code used for the error analysis is included.

Zusammenfassung

In dieser Arbeit untersuchen wir das Critical Slowing down der Gitter-QCD Simulationen. Wir führen eine Vorstudie in der quenched Approximation durch, in der wir feststellen, dass unsere Schätzung der exponentiellen Autokorrelation wie $\tau_{\mathrm{exp}}(a) \sim a^{-5}$ skaliert, wobei a der Gitterabstand ist. In unquenched Simulationen mit $\mathrm{O}(a)$-verbesserten Wilson-Fermionen finden wir ein ähnliches Skalierungsgesetz. Die Diskussion wird von einem großen Satz an Ensembles sowohl in reiner Eichtheorie als auch in der Theorie mit zwei entarteten Seequarks unterstützt. Wir haben darüber hinaus die Wirkung von langsamen algorithmischen Modi in der Fehleranalyse des Erwartungswertes von typischen Gitter-QCD-Observablen (hadronische Matrixelemente und Massen) untersucht. Im Kontext der Simulationen, die durch langsame Modi betroffen sind, schlagen wir vor und testen eine Methode, um zuverlässige Schätzungen der statistischen Fehler zu bekommen. Diese Methode soll in dem typischen Simulationsbereich der Gitter-QCD helfen, nämlich dann, wenn die gesamte erfasste Statistik $\mathrm{O}(10)\tau_{\mathrm{exp}}$ ist. Dies ist der typische Fall bei Simulationen in der Nähe des Kontinuumslimes, wo der Rechenaufwand für die Erzeugung von zwei unabhängigen Datenpunkten sehr groß sein kann. Schließlich diskutieren wir die Skalenbestimmung in $N_{\mathrm{f}} = 2$-Simulationen mit der Kaon Zerfallskonstante f_{K} als experimentellem Input. Die Methode wird zusammen mit einer gründlichen Diskussion der angewandten Fehleranalyse erklärt. Eine Beschreibung der öffentlich zugänglichen Software, die für die Fehleranalyse genutzt wurde, ist eingeschlossen.

Contents

Contents

1. Introduction

Some of the most successful predictions of modern theoretical high energy physics can be summarized in what has been known in the last 50 years as the standard model (SM) of particle physics [80, 85]. The model describes elementary interactions in terms of quantum fields and is largely built around two principles: renormalizability and gauge symmetry [83]. The requirement of renormalizability can be understood in the context of effective field theories [86] where contributions in low energy observables coming from non-renormalizable interactions are suppressed (the nature of the suppression is model dependent but can generally be represented as a factor proportional to a negative power of some high energy scale).

The nature of gauge symmetry, on the other hand, is generally thought to be more fundamental than renormalizability. The low energy symmetries of the SM are usually thought as remnant from the breaking of a larger symmetry group that characterizes the theory at high energies and in this sense gauge invariance is expected to hold all the way up to the grand-unification scale.

The gauge symmetries of the SM are $U(1) \times SU(2)$ [84], associated with the electro-weak force, and $SU(3)$ that is associated with the strong force that binds quarks into hadrons [79]. The electro-weak force is mediated by photons and the W and Z bosons and successfully describes electro-magnetic interactions (e.g. scattering of charged particles and, to a very high precision, the anomalous magnetic moment of charged leptons) and weak decays. The strong, mediated by gluons, acts between particles that carry the quantum numbers of color, namely quarks and gluons themselves. The theory of quarks and gluons alone is quantum chromodynamics (QCD).

One of the distinctive features of QCD is that it describes particles, namely the hadrons, whose elementary constituents are not directly accessible by experiment. This observation known as color confinement [87] on the one hand and asymptotic freedom on the other hand, i.e. the fact that the theory at high energy approaches the free field theory since the renormalized coupling slowly vanishes [82, 81, 67, 24], are indeed its most peculiar properties.

In order to explore the phenomenological consequences of the SM and QCD many different techniques have been developed in the course of the years. An important class is perturbative methods: these are mostly effective if deviations from a known solution (free field) can be parametrized by a small quantity, that is typically the coupling constant. Even though perturbation theory is a valuable and reliable tool [66], in some regimes it fails and does not give correct predictions. This in particular is the case of QCD when the energy scale is below the mass of the nucleon, and the theory becomes strongly coupled. For some quantities, e.g. the hadron masses, perturbative computations do not work and other methods must be applied.

1. Introduction

Lattice QCD (LQCD) is a non-perturbative formulation of QCD [87]. This means that all the non-linear aspects that characterize the low energy behaviour of QCD are kept into account. As any other formulation of most quantum field theories, also LQCD introduces a regulator, that in the specific case is a space-time lattice. Due to the nature of the UV regulator LQCD formulated in a finite space-time volume can be solved numerically, since then it only consists of a finite number of quantum mechanical degrees of freedom. Many techniques have been developed and physical observables have been computed since LQCD was first introduced, and in the late years some of these computations have begun to enter the realm of precision physics.

The lattice numerical approach to QCD is based on methods analogue, at least in the spirit, to the ones used in statistical mechanics. In particular the algorithms used for "solving" the path integral use the Markov Chain Monte Carlo (MCMC) procedure to sample a very large space of states in a seemingly efficient way. Since the lattice method relies on a discretization of space-time in hyper-cubic cells with edges whose typical size is $a \sim 0.05 - 1$ fm, a necessary step in computations is the removal of the cutoff, i.e. an extrapolation to zero lattice spacing done by computing observables at more than one value of a. As the lattice spacing gets smaller the correlation length diverges and the theory approaches a critical point in a statistical mechanics sense. The increased correlation length generally implies a larger computational effort in order to generate data points that are not correlated to each other, in a phenomenon that is known as algorithmic critical slowing down (CSD). The correlations of data generated by a MCMC are called auto-correlations (this reflects the fact that we do not specifically refer to correlation between different observables, but to correlation between subsequent estimations of the same observable). In Ch. 5 and Ch. 6 we investigate the extent of CSD in MCMC computations of LQCD. The observable that we use for studying CSD is the topological charge. This observable has notoriously long auto-correlations for virtually all algorithms used for either pure Yang-Mills theory or QCD, and it has been studied over the years using link-update algorithms for pure gauge theory [11] and also in QCD with molecular dynamics based algorithms [1, 2, 3, 34].

Reliable computations mean full control of both statistical and systematic effects. A possible source of systematic error arises when a computation is done at small lattice spacing with an algorithm that severely suffers from CSD. In extreme cases the effective algorithmic ergodicity could be lost since only a small region of the relevant state space is explored (we work with finite, even though sometimes very large, computational resources). We see no evidence for such effect in the computations that we have performed, even at lattice spacings as small as ~ 0.045 fm.

We have also investigated methods to improve the estimate of statistical errors of physical observables computed with an MCMC algorithm in presence of large auto-correlations. These methods have been applied to the error analysis of typical LQCD observables and we find that our method improves the standard statistical error analysis in difficult cases.

2. Background theory

QCD is a field theory describing interactions of quarks and gluons. The starting point for most QCD calculations is the expression of the path integral used for defining vacuum expectation values with respect to the action functional $S_{\text{QCD}}[\Phi]$. In this context the v.e.v. of a two point function is

$$\langle \Phi_1(x_1)\Phi_2(x_2) \rangle = \frac{1}{Z} \int \mathcal{D}\Phi \; \Phi_1(x_1)\, \Phi_2(x_2) \; \mathrm{e}^{i\, S_{\text{QCD}}[\Phi]} \tag{2.1}$$

where Φ stands for quark and gluon fields and $\Phi_i(x_i)$ for fields or field components localized at the space–time point x_i. The normalization Z is given by the functional integral

$$Z = \int \mathcal{D}\Phi \; \mathrm{e}^{i\, S_{\text{QCD}}[\Phi]} \; . \tag{2.2}$$

In lattice QCD the Minkowsky space–time formulation is rarely used (for its bad convergence properties due to the fact that the functional integral is over a phase). The two point function of eq. (2.1) can indeed be analytically continued to a Euclidean green function by choosing time to be a purely imaginary quantity (Wick rotation). In the Euclidean formulation the expression in (2.2) becomes equivalent to the partition function of a (four dimensional) statistical mechanics system:

$$Z = \int \mathcal{D}\Phi \, \mathrm{e}^{-S_{\text{QCD}}^{\text{E}}[\Phi]} \; . \tag{2.3}$$

An advantage of using Euclidean instead of Minkowsky space comes from the fact that the n-point function in Euclidean space is a real analytic function in its arguments with power singularities at coinciding points (all the necessary mathematics is in ref. [65]). In the following we will restrict the discussion to the Euclidean theory, therefore from here on we drop the unnecessary superscript E.

2.1. The continuum Euclidean action

Quarks are spin 1/2 particles that carry the quantum number of color. Quark fields are thus described by 4–spinors:

$$\psi_{\alpha,c}^{(f)}(x) \; , \quad \overline{\psi}_{\alpha,c}^{(f)}(x) \tag{2.4}$$

where $x = (x_0, x_1, x_2, x_3)$ is the Euclidean space position with the zeroth dimension conventionally taken to be the time, $\alpha = 1, 2, 3, 4$ is the Dirac index and $c = 1, 2, 3$ is the color index. Quarks $\psi_{\alpha,c}^{(f)}$ come also in different flavors f: even though there are six known flavors in Nature, for most calculations only a subset is considered. For better

readability in the following text sub– and superscripts will not be shown, unless necessary for resolving ambiguities.

One of the basic principles of QCD is gauge invariance, the statement that different colors are completely equivalent. Gauge transformations are local rotations in color space: given a matrix $\Omega(x) \in \mathrm{SU}(3)$ at each point x, the transformation law for quark fields is given by:

$$\psi(x) \to \psi'(x) = \Omega(x)\psi(x) , \quad \overline{\psi}(x) \to \overline{\psi}'(x) = \overline{\psi}(x)\Omega(x)^\dagger . \tag{2.5}$$

According to the gauge principle physics for ψ and ψ' must be exactly the same implying that the gauge group must be a symmetry of both the action and the measure. Since quarks are spin $1/2$ particles, they obey the Dirac wave equation or, equivalently, the free field action must have the form

$$S_\mathrm{F}^0[\psi,\overline{\psi}] = \int \mathsf{d}^4x\ \overline{\psi}(x)(\gamma_\mu \partial_\mu + m)\psi(x) ; \tag{2.6}$$

where the γ–matrices obey the Euclidean anti–commutation relation

$$\{\gamma_\mu, \gamma_\nu\} = 2\delta_{\mu\nu}\mathbb{1}_{4\times 4} . \tag{2.7}$$

While the action in eq. (2.6) is invariant under a global (space–time independent) $\mathrm{SU}(3)$ rotation, it is not invariant under the gauge transformations of eq. (2.5) due to their local nature. The action that satisfies the equivalence

$$S_\mathrm{F}[\psi, \overline{\psi}, A] \equiv S_\mathrm{F}[\psi', \overline{\psi}', A'] \tag{2.8}$$

is found by introducing a new field $A_\mu(x) \in \mathfrak{su}(3)$, known as the gauge boson, with transformation properties imposed so that the extra contribution that comes from the derivative acting on $\Omega(x)$ is cancelled. The action S_F is thus obtained by substituting the ∂_μ in eq. (2.6) with the covariant derivative defined as:

$$\partial_\mu \longrightarrow D_\mu(x) = \partial_\mu + iA_\mu(x) \tag{2.9}$$

and imposing the transformation law for the gauge boson:

$$A_\mu(x) \to A'_\mu(x) = \Omega(x)A_\mu(x)\Omega(x)^\dagger + i(\partial_\mu\Omega(x))\Omega(x)^\dagger . \tag{2.10}$$

The gauge invariant fermionic action is thus given by

$$S_\mathrm{F}[\psi, \overline{\psi}, A] = \sum_{f=1}^{N_\mathrm{f}} \int \mathsf{d}^4x\ \overline{\psi}^{(f)}(x) \left(\gamma_\mu D_\mu(x) + m^{(f)}\right) \psi^{(f)}(x) , \tag{2.11}$$

while the action of the gluon field A_μ is the Yang-Mills action

$$S_\mathrm{G}[A] = \frac{1}{2g_0^2} \int \mathsf{d}^4x\ \mathrm{tr}[F_{\mu\nu}(x)F^{\mu\nu}(x)] \tag{2.12}$$

where the field tensor $F_{\mu\nu}$ is the commutator of the covariant derivative

$$F_{\mu\nu}(x) = -i[D_\mu(x), D_\nu(x)] = \partial_\mu A_\nu - \partial_\nu A_\mu + i[A_\mu, A_\nu] \,. \tag{2.13}$$

The continuum action of Euclidean QCD that enters the expression of the path integral eq. (2.3) is thus the sum of the gluon and fermion part and is given by:

$$S_{\text{QCD}}^{\text{E}}[\psi, \overline{\psi}, A] = S_{\text{F}}[\psi, \overline{\psi}, A] + S_{\text{G}}[A] \,. \tag{2.14}$$

The continuum formulation that we have given so far has been defined only on a very formal level. To make expressions as the one in eq. (2.1) mathematically meaningful, the path integral measure $\mathcal{D}\Phi$ has to be defined. All known definitions of the measure regularize the path integral in some way (a regularization can be understood as a cutoff that removes the UV degrees of freedom). If the relevant field configurations (those that are relevant for the computation of the expectation value of some observable of interest) are smooth then the regularized theory should approach a well defined continuum limit when the UV regulator is gradually removed and the fields are properly renormalized. The regularization scheme in which we are interested and that is mostly used for non-perturbative computations is known as lattice quantum field theory.

2.2. Lattice quantum chromodynamics

Lattice QCD is Euclidean QCD regularized with a 4–dimensional lattice. This is most often (but not necessarily) done in a finite volume of $\mathbb{R}^4$. In this case a lattice $\Lambda \subset \mathbb{Z}^4$ is the set of points

$$\Lambda = \{n = (n_0, n_1, n_2, n_3) \mid n_i = 0, 1, \ldots, N_i - 1\} \tag{2.15}$$

used to label the position coordinates in Euclidean space (lattice sites)

$$x = (x_0, x_1, x_2, x_3) \equiv a(n_0, n_1, n_2, n_3)$$

where we adopt the convention that the zeroth dimension represents Euclidean time and has physical extent $T = aN_0 \equiv aN_T$ while the region of space is a cube whose size is $L = a(N_1 = N_2 = N_3) \equiv aN_L$. The constant a is the lattice spacing used for converting from dimensionless lattice units to physical units.

2.2.1. Gauge fields on the lattice

The action of lattice QCD can be deduced through a reasoning similar to the one that lead us to the continuum action of eq. (2.14). The quark fields $\psi(x)$ on the lattice have a finite number of degrees of freedom and are described by Dirac spinors on the sites of Λ:

$$\psi(x) = \psi(an) \,, \quad \overline{\psi}(x) = \overline{\psi}(an) \,, \tag{2.16}$$

with anti–periodic boundary conditions in time and periodic in all other directions. A possible lattice discretization of the partial derivative is given by the forward difference operator

$$\partial_\mu^{\mathrm{f}}\psi(x) = \frac{1}{a}(\psi(x + a\hat\mu) - \psi(x)) \tag{2.17}$$

where $\hat\mu$ denotes the unit versor in the space–time direction specified by μ. If local SU(3) invariance is required to be a symmetry of the discretized action as it was required for the continuum, we can immediately see that it is not possible to attribute any definite meaning to the difference in eq. (2.17). We must instead first parallel–transport $\psi(x + a\hat\mu)$ along the link that connects it to $\psi(x)$ such that under eq. (2.5) they both transforms in the same way. The one–link–parallel–transporter is an SU(3) matrix that is assigned to each link (directed segment that connects neighboring sites)

$$U(x;\mu) \in \mathrm{SU}(3) \tag{2.18}$$

$$U(x;\mu)^\dagger \tag{2.19}$$

and has gauge transformation properties

$$U(x;\mu) \to U'(x,\mu) = \Omega(x)U(x;\mu)\Omega(x + a\hat\mu)^\dagger \ . \tag{2.20}$$

The gauge covariant forward and backward lattice derivatives are thus given by

$$\begin{aligned}
\nabla_\mu^{\mathrm{f}}\psi(x) &= \frac{1}{a}\left(U(x;\mu)\psi(x + a\hat\mu) - \psi(x)\right)\\
\nabla_\mu^{\mathrm{b}}\psi(x) &= \frac{1}{a}\left(\psi(x) - U(x - a\hat\mu;\mu)^\dagger\psi(x - a\hat\mu)\right) \ .
\end{aligned} \tag{2.21}$$

The relation between lattice and continuum derivative of eq. (2.9) is made explicit by introducing the gauge transporter along a link:

$$U(x;\mu) \equiv \mathcal{T}\exp\left\{ia\int_0^1 dt A_\mu(x + a(1 - t)\hat\mu)\ ,\right\} \tag{2.22}$$

where $\mathcal{T}\exp$ denotes the path ordered exponential. The transporter in eq. (2.22) is formulated in the continuum and the equivalence to the lattice link variable holds only if in the continuum limit relevant lattice fields are smooth functions. Following this heuristic argument at small lattice spacing the link variable is

$$U(x;\mu) = 1 + iaA_\mu(x) + O(a^2)\ , \tag{2.23}$$

that when inserted in eq. (2.21) reproduces the continuum expression of eq. (2.9) (up to cutoff effects).

The Wilson gauge action

Gauge links can be used to define gauge invariant local objects by taking the trace of products of link variables along closed paths. The most local, non–trivial object of this kind that one can think of is the parallel transporter around a plaquette $U(x; \mu, \nu)$, defined as a product of four link variables:
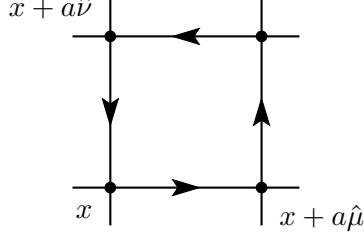
$$U(x; \mu, \nu) = \left[U(x; \mu) U(x + a\hat{\mu}; \nu) U(x + a\hat{\nu}; \mu)^\dagger U(x; \nu)^\dagger \right] . \tag{2.24}$$

As originally shown by Wilson in ref. [87] the plaquette is the ingredient out of which we construct the lattice gauge action, known as Wilson action:

$$S_{\mathrm{G}}[U] = \frac{\beta}{6} \sum_{x \in a\Lambda} \sum_{\mu, \nu} \mathrm{tr} \left[\mathbb{1} - U(x; \mu, \nu) \right] , \tag{2.25}$$

where $\beta = 6/g_0^2$ (in group $SU(N)$ the standard definition is $\beta = 2N/g_0^2$).

The naive continuum limit of the Wilson action corresponds to the Yang-Mills action of eq. (2.12) up to corrections of $O(a^2)$. This can be shown substituting the following approximation of the link variable

$$U(x; \mu) = \mathrm{e}^{iaA_\mu(x) + O(a^2)} , \tag{2.26}$$

equivalent up to $O(a^2)$ to the covariant exponential of eq. (2.22), in the expression of the plaquette and iteratively applying the Baker-Campbell-Hausdorff formula

$$\exp\{\lambda A\} \exp\{\lambda B\} = \exp \left\{ \lambda(A + B) + \frac{\lambda^2}{2}[A, B] + O(\lambda^3) \right\} \tag{2.27}$$

to the product of non–commuting exponentials. It is thus possible to show that the plaquette reduces to the form

$$U(x; \mu, \nu) = \mathrm{e}^{ia^2 F_{\mu\nu} + O(a^3)} . \tag{2.28}$$

When the exponential in eq. (2.28) is expanded and inserted in eq. (2.25) one obtains

$$S_{\mathrm{G}}[U] = \frac{a^4}{2g_0^2} \sum_{x \in a\Lambda} \sum_{\mu, \nu} \mathrm{tr}\, F_{\mu\nu}(x)^2 + O(a^2) , \tag{2.29}$$

7

where we have used the fact that the trace of the exponent in eq. (2.28) vanishes since it is an element of the lie algebra. Moreover no scalar (hyper-cubic symmetry group invariant) quantity of dimension 5 can be formed, so the lattice artifacts are of $O(a^2)$. This argument can be generalized to show that any gauge invariant object that is symmetric under the lattice rotation group (local closed paths properly summed so to be invariant under the cubic group) would have lead to the correct formal continuum limit expression, since besides the trivial term proportional to the identity matrix and the $F_{\mu\nu}^2$ term, there is no other gauge invariant operator with dimension ≤ 4. By following this logic, it is also possible to argue that lattice gauge actions are always $O(a)$ improved. In ref. [4, 18] one can find an alternative (generalizable to arbitrary dimensions and gauge groups) way to prove the equivalence between the Wilson and the standard formulation of the action through a non-Abelian formulation of the Stokes theorem.

2.3. Fermions on the lattice

The lattice covariant derivatives of eq. (2.21) can be used to write the simplest gauge invariant discretization of the continuum fermion action:

$$S_{\mathrm{F}} \overset{?}{=} a^4 \sum_x \overline{\psi}(x) \left(\gamma_\mu \frac{\nabla_\mu^{\mathrm{f}} + \nabla_\mu^{\mathrm{b}}}{2} + m \right) \psi(x) \,. \tag{2.30}$$

This natural prescription turns out to be not suitable for most calculations due to the (so called) doubling problem, that we briefly illustrate. Particles in a quantum field theory are identified with poles in the propagator. In the case of a free Dirac particle described by the action in eq. (2.30) where gauge fields have been set to unity, the propagator in momentum space is given by

$$S(p) = [i\gamma_\mu \widetilde{p}_\mu + m]^{-1} \quad \text{with} \quad \widetilde{p}_\mu = \frac{1}{a} \sin(ap_\mu) \,, \tag{2.31}$$

where $\pi/a \leq p_\mu \leq \pi/a$ varies in the first Brillouin zone of the lattice. The coordinate space propagator is given by the Fourier transform

$$\langle \psi(x)\overline{\psi}(0) \rangle = \int_{-\frac{\pi}{a}}^{\frac{\pi}{a}} \frac{\mathrm{d}^4 p}{(2\pi)^4} \, \mathrm{e}^{ipx} \, S(p) \,. \tag{2.32}$$

$S(p)$ has 16 poles, corresponding to 16 particles propagating in the free theory. Even if the proceeding argument has been formulated in the free field theory, since the interacting theory is believed to be asymptotically free, we can expect that doublers would show up also in full QCD (at least in the small lattice spacing limit). Furthermore as a theorem by Nielsen and Ninomiya stated in ref. [63] shows, doublers generally affect lattice regularization schemes. The theorem asserts that assuming some general properties of the lattice fermion action, including unitarity, symmetry under the cubic group, locality of the action and continuum chiral symmetry (in the form $\gamma_5 S_{\mathrm{F}} = -S_{\mathrm{F}} \gamma_5$) the spectrum of free fermions is always doubled (the doubling indeed occurs along each dimension, so

in D dimensions we end up with 2^D propagating fermions).

2.3.1. Wilson fermions

When we introduced the Wilson action eq. (2.25) we argued that the choice of discretization is not unique. The same holds true also in the case of the fermion action: even if the naive choice of eq. (2.30) has turned out to be unsuitable for most computations, there still exist many alternative discretizations that yield the same formal continuum limit and remove doublers. One of the simplest modification to the naive prescription was suggested by Wilson. The proposal amounts to add an extra term to the action, such that the free momentum space propagator reads

$$S(p) = [m + i\gamma_\mu \widetilde{p}_\mu + r\frac{a}{2}\overline{p}_\mu^2]^{-1} \quad \text{with} \quad \overline{p}_\mu = \frac{2}{a}\sin(\frac{a}{2}p_\mu) \qquad (2.33)$$

where the parameter r is usually set equal to one (if equal to zero we recover the naive discretization). In the Wilson formulation doublers are effectively removed by the momentum dependent mass–like term $\overline{p}_\mu^2$ that does not change the low energy spectrum of the theory since it vanishes for components with $p_\mu = 0$. Four–momenta at the corners of the Brillouin zone instead see an extra contribution to the mass equal to $2r/a$, so that the poles of the doublers propagators are shifted up and their total (bare) mass is effectively increased by an amount inversely proportional to the lattice spacing. It can be shown that the case $r = 1$ is special in this respect and doublers are altogether removed. The Wilson-Dirac operator in position space is thus given by

$$D_\mathrm{W} = \gamma_\mu(\nabla_\mu^\mathrm{f} + \nabla_\mu^\mathrm{b}) - r\frac{a}{2}\nabla_\mu^\mathrm{f}\nabla_\mu^\mathrm{b} , \qquad (2.34)$$

and the corresponding action for N_f flavours is

$$S_\mathrm{F} = a^4 \sum_{f=1}^{N_\mathrm{f}} \sum_x \overline{\psi}^{(f)}(x)(D_\mathrm{W} + m_f)\psi^{(f)}(x) . \qquad (2.35)$$

The Wilson term is irrelevant: in the continuum limit the physics described by the action in eq. (2.35) is expected to be the same as in eq. (2.11). The fact that the extra term is mass–like (its Dirac structure is trivial) can be related to the explicit breaking of chiral symmetry of the mass-less theory, but in the light of Nielsen and Ninomiya theorem this does not come unexpectedly.

2.3.2. Improved Wilson fermions

Calculations done at finite lattice spacing suffer from discretization effects of $O(a^z)$, where z is positive. In practice these effects imply that energy levels and on–shell matrix elements computed on the lattice approach their continuum limit at a rate that asymptotically is a power in the lattice spacing. We have seen before that for the Wilson action $z = 2$, while Wilson fermions suffer from stronger effects of $O(a)$. The removal

of this linear leading behavior can be done following the scheme outlined in ref. [77, 78] known as Symanzik improvement program. The improvement strategy consists in writing an effective action in powers of the lattice spacing a, and to consider terms of dimension $d \geq 5$ as corrections that can be used to improve the action. For the $O(a)$ improvement of the lattice QCD action with Wilson fermions a single independent dimension–5 operator is sufficient, the Pauli term

$$\overline{\psi}(x)\sigma_{\mu\nu}F_{\mu\nu}(x)\psi(x) \tag{2.36}$$

where $\sigma_{\mu\nu} = i\,[\gamma_\mu, \gamma_\nu]/2$. For the improved lattice action we thus obtain

$$S_{\text{Impr}} = S_{\text{G}} + S_{\text{F}} + c_{\text{sw}}(g_0)a^5 \sum_{f=1}^{N_{\text{f}}} \sum_x \sum_{\mu\nu} \overline{\psi}^{(f)}(x)\frac{i}{4}\sigma_{\mu\nu}\widehat{F}_{\mu\nu}\psi^{(f)}(x) \, , \tag{2.37}$$

where $\widehat{F}_{\mu\nu}$ is a discretized form of the field strength tensor and the coefficient $c_{\text{sw}}(g_0)$ is named Sheikholeslami–Wohlert coefficient from ref. [73], where the improved action (2.37) was proposed for the first time.

2.4. Hadron spectroscopy

One of the goals of lattice calculations is to confirm QCD as the theory describing quarks and their interactions. The simplest quantities involving quarks that one can compute on the lattice are the masses of the hadrons. As we will see correlation functions are important ingredients for such computations. In particular we will consider correlators of local products of fields

$$C(x_1 - x_2) = \langle O_1(x_1)\, O_2(x_2) \rangle = \frac{1}{Z} \int \mathcal{D}\Phi \; O_2(x_2)\, O_1(x_1)\, \mathrm{e}^{-S[\Phi]} \tag{2.38}$$

where periodic boundary conditions are assumed and the $O_i(x_i)$ are commonly referred to as interpolators of the physical states corresponding to the set of quantum numbers that are carried by them. Interpolators correspond to Hilbert space operators $\widehat{O}(x)$ or $\widehat{O}^\dagger(x)$ that annihilate or create states in a definite space-time point with the quantum numbers of the particles that we want to analyze.

2.4.1. Transfer matrix and correlation functions

The Hilbert space $\mathcal{H}$ of a lattice field theory can be described as a direct product

$$|\mathbf{\Phi}\rangle = \prod_x |\mathbf{\Phi}(x)\rangle \tag{2.39}$$

of the vectors corresponding to quantum mechanical degrees of freedom that live on each space–time point. The definition in the case of a lattice gauge theory is slightly more complicated by the constraint of gauge invariance, but still a Hilbert space can be defined (see ref. [64, 39, 9]). The Hilbert space that is used in ref. [38] for defining the transfer

matrix $\mathbb{T}$ has support on the spacial sub-lattice $\Lambda_0 = L \times L \times L \subset \Lambda$, we call this space $\mathcal{H}_{\Lambda_0}$. The integral operator $\mathbb{T}$ then describes the evolution of a state over a time interval of the size of a single lattice spacing a. The operator $\mathbb{T}$ is bounded, self–adjoint and since it is defined in a finite volume it has a completely discrete spectrum. Moreover it is positive definite and the largest eigenvalue ω_0 is non–degenerate. If $\mathbb{T}$ exists (this is e.g. guaranteed for the Wilson fermion action) then it is possible to define an Hamiltonian operator $\widehat{H}$ as

$$a\widehat{H} = -\ln(\mathbb{T}/\omega_0) \tag{2.40}$$

with the properties

$$\widehat{H} = \widehat{H}^\dagger \quad \text{and} \quad \langle \boldsymbol{\Phi} | \widehat{H} | \boldsymbol{\Phi} \rangle \geq 0 \ \ \forall \ |\boldsymbol{\Phi}\rangle \in \mathcal{H} \ . \tag{2.41}$$

The spectrum of the Hamiltonian $\widehat{H}|n\rangle = E_n|n\rangle$ is ordered in correspondence to the energy eigenvalues

$$E_0 < E_1 \leq E_2 \leq \ldots \tag{2.42}$$

where with $\widehat{H}|0\rangle = E_0$ we denote the unique vacuum state. The energy of the vacuum is arbitrary and within quantum field theory all physical results only depend on energy differences, for this reason without loss of generality we can set $E_0 = 0$ (this is already the case for the definition of $\widehat{H}$ given in eq. (2.40)).

The importance of the transfer matrix in a lattice formulation of quantum field theory is given by the fact that it bridges the Hamiltonian to the path integral formulation:

$$Z \equiv \operatorname{tr} \mathbb{T}^{T/a} = \operatorname{tr} e^{-T\widehat{H}} = \int \mathcal{D}\Phi \, e^{-S[\Phi]} \ . \tag{2.43}$$

This equivalence is extremely important for the computation of quantities on the lattice and their subsequent interpretation, the reason being that typical lattice computations use stochastic methods to estimate quantities defined in the path integral formulation (r.h.s of eq. (2.43)), while the physical interpretation of the result has to resort to the Hamiltonian formalism, mainly through the decomposition of correlation functions over the spectrum of the Hamiltonian operator.

Lattice correlators

To give a quantum mechanical interpretation of the correlator of two fields in eq. (2.38) one defines the operators corresponding to fields at $t = 0$ as $\widehat{O}(\vec{x}) \leftrightarrow O(0, \vec{x})$. The correlator in eq. (2.38) will then be expressed as a trace of products of operators on $\mathcal{H}_{\Lambda_0}$

$$\begin{aligned}
C(t_1 - t_2) &\overset{t_1 \geqq t_2}{=} \frac{1}{Z} \operatorname{tr} \left[\mathbb{T}^{t_2/a} \, \widehat{O}_2(0) \, \mathbb{T}^{(t_1-t_2)/a} \, \widehat{O}_1(0) \, \mathbb{T}^{(T-t_1)/a} \right] \\
&= \frac{1}{Z} \operatorname{tr} \left[e^{-\widehat{H}(T-t_1+t_2)} \, \widehat{O}_2(0) \, e^{-\widehat{H}(t_1-t_2)} \, \widehat{O}_1(0) \right] \ ,
\end{aligned} \tag{2.44}$$

where we have set $\vec{x}_1 = \vec{x}_2 = 0$. The spectral decomposition of expression (2.44) is done by properly inserting unit operators

$$\mathbb{1} = \sum_n |n\rangle\langle n| \tag{2.45}$$

where the sum runs over the entire spectrum (i.e. n labels all possible quantum states) and in terms of the time difference $t = t_1 - t_2$ we have

$$C(t) = \sum_{m,n} \langle n|\widehat{O}_1(0)|m\rangle\langle m|\widehat{O}_2(0)|n\rangle \mathrm{e}^{-tE_n - (T-t)E_m} \bigg/ \sum_n \mathrm{e}^{-TE_n} . \tag{2.46}$$

In large volume calculations, where one typically has $TE_1 \gtrsim 8$, the expression is sometimes simplified to its infinite time extent limit

$$\lim_{T\to\infty} C(t) = \sum_n \langle 0|\widehat{O}_2(0)|n\rangle\langle n|\widehat{O}_1(0)|0\rangle \mathrm{e}^{-tE_n} . \tag{2.47}$$

2.4.2. Masses and decay constants

One of the simplest and most widely computed correlators corresponds to the creation of a pseudo–scalar particle at time zero and its annihilation at time t. The pseudo–scalar particle that we discuss is the pion. A possible interpolator of the (charged) pion is the following

$$P^+(t, \vec{x}) = \overline{\psi}^d(t, \vec{x})\gamma_5\psi^u(t, \vec{x}) \tag{2.48}$$

and

$$\overline{P}^+(t, \vec{x}) = -\overline{\psi}^u(t, \vec{x})\gamma_5\psi^d(t, \vec{x}) = -P^-(t, \vec{x}) , \tag{2.49}$$

where ψ^u and ψ^d denote, respectively, the up and down quark fermionic fields. Since we are generally interested in the energy of a particle with a specific momentum, it is useful to introduce the Fourier transformed fields

$$\widetilde{P}^+(t, \vec{p}) = a^3 \sum_{\vec{x}} P^+(t, \vec{x})\mathrm{e}^{-i\vec{p}\vec{x}} \tag{2.50}$$

$$P^+(t, \vec{x}) = \frac{1}{V} \sum_{\vec{p}} \widetilde{P}^+(t, \vec{p})\mathrm{e}^{i\vec{p}\vec{x}} \tag{2.51}$$

where $V = L^3$ is the physical volume of the lattice while the lattice momentum components (with periodic boundary conditions) are given by

$$p_i = \frac{2\pi}{L}k_i , \quad \text{with} \quad k_i = -\frac{N_i}{2} + 1, \dots, \frac{N_i}{2}. \tag{2.52}$$

A correlator that can be used for measuring the properties of a pion with a definite momentum is thus

$$\langle \widetilde{P}^+(t,\vec{p})\,\overline{P}^+(0,\vec{0})\rangle = a^3 \sum_{\vec{x}} \mathrm{e}^{-i\vec{p}\vec{x}}\,\langle P^+(t,\vec{x})\,\overline{P}^+(0,\vec{0})\rangle\,, \tag{2.53}$$

where the expression can be interpreted as a source of the pseudo-scalar current sitting at the origin and a sink of definite three-momentum on a time-slice $t \geq 0$. A spectral decomposition analog to the one in eq. (2.47) can be obtained by first introducing the Hilbert space operators associated with the interpolating fields of the pseudo-scalar current, $\widehat{P}^+(\vec{x})$ and $\widehat{P}^-(\vec{x})$. After the insertion of the unit operator expanded on the energy-momentum (and possibly other remaining quantum numbers labelled by n) eigenstates, with normalization

$$\langle \vec{p}, n | \vec{q}, n' \rangle = 2E_n(\vec{p})V\,\delta_{\vec{p}\vec{q}}\delta_{nn'} \tag{2.54}$$

where $\delta_{\vec{p}\vec{q}} = \prod_i \delta_{p_i q_i}$, we obtain (with the further assumption that the vacuum is translation invariant)

$$\langle \widetilde{P}^+(t,\vec{p})\,\overline{P}^+(0,\vec{0})\rangle$$
$$= \frac{a^3}{V} \sum_{\vec{x},\vec{q},n} \frac{\mathrm{e}^{-i(\vec{p}-\vec{q})\vec{x}}\,\mathrm{e}^{-tE_n(\vec{q})}\,\langle 0|\widehat{P}^+(\vec{0})\,|\vec{q},n\rangle\langle \vec{q},n|\,\widehat{\overline{P}}^+(\vec{0})|0\rangle}{2E_n(\vec{q})}$$
$$= \sum_n \frac{\mathrm{e}^{-tE_n(\vec{p})}\,\left|\langle 0|\widehat{P}^+(\vec{0})\,|\vec{p},n\rangle\right|^2}{2E_n(\vec{p})}\,. \tag{2.55}$$

Since pions are the particles with lowest mass having the quantum numbers of (2.48), the energy of the first excited state in eq. (2.55) is

$$E_1^2(\vec{p}) = M_\pi^2 + \vec{p}^2 \tag{2.56}$$

and the leading asymptotic behavior of the correlator at zero spatial momentum is then given by

$$\sum_{\vec{x}} \langle P^+(t,\vec{x})\,P^-(0,\vec{0})\rangle \sim \frac{\left|\langle 0|\widehat{P}^+(\vec{0})|\vec{0},\pi\rangle\right|^2}{2M_\pi}\,\mathrm{e}^{-t\,M_\pi}\,, \tag{2.57}$$

where $|\vec{0},\pi\rangle$ is the eigenstate corresponding to a single pion at rest. The matrix element in (2.57) can be expressed in terms of low energy quantities by making use of the axial ward identities. To find this relation we need a second quantity, the axial current (that is also an interpolator of the pion field)

$$A_\mu(x) = \overline{\psi}^u(x)\gamma_\mu\gamma_5\psi^d(x)\,. \tag{2.58}$$

The (bare) decay constant of the pion is defined as the matrix element of the axial current

between the vacuum and a single pion state with momentum $\vec{p}$

$$\langle 0|\widehat{A}_\mu(\vec{0})|\vec{p}, \pi\rangle = p_\mu f_\pi. \tag{2.59}$$

From the path integral by performing local infinitesimal transformation of the fields one can derive the Ward identities (see for example ref. [41, 21]) associated with the flavour and chiral symmetries of the action, these operator identities on the lattice hold as expectation values. From an axial transformation it is possible to derive the Partial Conservation of the Axial Current in Euclidean space (PCAC relation):

$$\langle \partial_\mu A_\mu(x) O_{\text{ext}}(y)\rangle \overset{x \neq y}{=} 2M_{\text{PCAC}} \langle P^+(x) O_{\text{ext}}(y)\rangle , \tag{2.60}$$

where M_{PCAC} is the bare quark mass and O_{ext} is an arbitrary external source. If in this expression we set $O_{\text{ext}}(y) = P^+(y)$ and combine it with eq. (2.59) we obtain for the value of the bare matrix element in eq. (2.57):

$$\left|\langle 0|\widehat{P}^+(\vec{0})|\vec{0}, \pi\rangle\right| \sim \frac{M_\pi^2 f_\pi}{2M_{\text{PCAC}}} . \tag{2.61}$$

These quantities are bare, to connect them to physical ones it is necessary to renormalize the operators. Here we do not wish to discuss the details of non-perturbative renormalization. The only needed fact that we want to stress is that renormalization is done multiplicatively with factors that are functions only of the bare coupling (see e.g. ref. [14] and references thereon).

2.5. Wilson flow

The Wilson flow, also known as Yang-Mills gradient flow, is an analytical tool freshly introduced in the context of LQCD in ref. [45, 47]. Using the words of Martin Lüscher: "flows in field space may allow new insights in the physical mechanisms described by highly non-linear QFT such as QCD".

The Wilson flow is a flow of SU(3) gauge fields

$$B_\mu(x)|_{t_{\text{W}}=0} = i A_\mu(x) \tag{2.62}$$

described by a set of gauge invariant partial differential equations that are linear in the flow time t_{W}:

$$\partial_{t_{\text{W}}} B_\mu(x) = D'_\nu G_{\nu\mu}(x) \tag{2.63}$$

where the field tensor and the derivative are defined as

$$G_{\mu\nu}(x) = \partial_\mu B_\nu(x) - \partial_\nu B_\mu(x) + [B_\mu(x), B_\nu(x)] \tag{2.64}$$

$$D'_\mu = \partial_\mu + [B_\mu(x), \cdot] . \tag{2.65}$$

The term on the right of eq. (2.63) is proportional to the gradient of the action (eq. (2.12))

along the flow, for this reason the equations describe a trajectory in field space that flows towards the stationary points of the Yang-Mills action. The gradient flow has been studied in perturbation theory: in ref. [51] it has been shown that the fields $B_\mu(x)$ at time $t_W > 0$ are renormalized and are connected to the renormalized boundary fields $(A_R)_\mu(x)$ in a universal way that is specified by the renormalization group equation. A consequence is that gauge invariant quantities built from the fields $B_\mu(x)$ as

$$E = \frac{1}{4}\operatorname{tr} G_{\mu\nu}G_{\mu\nu} \tag{2.66}$$

do not require renormalization.

The linearized form of the flow equations can be solved analytically: the solution shows explicitly that the flow is a smoothing operation on the gauge field at the boundary $t_W = 0$, more precisely in ref. [47] the action of the flow has been described as an averaging operation on the gauge potential over a sphere whose mean-square radius is equal to $\sqrt{8t_W}$.

2.5.1. Lattice regularization

The Wilson flow can also be studied non-perturbatively on the lattice. While at short times t_W perturbation theory is expected to work, numerical simulations in LQCD allow to investigate its properties at large values of t_W. In ref. [47] the proposed lattice discretization of eq. (2.63) is the gradient of the Wilson action, eq. (2.25)

$$\partial_{t_W} V_{t_W}(x;\mu) = -g_0^2 S_G[V_{t_W}]V_{t_W}(x;\mu)\,, \quad \text{with} \quad V_0(x;\mu) = U(x;,\mu) \tag{2.67}$$

this choice is not unique and it does not have to be the same as the gauge action of the theory (the one used for the computation of quantities at $t_W = 0$). Universality actually ensures that differences coming from the choice of the term that generates the flow, as long that it has the correct symmetries and normalizations, vanish proportionally to a positive power of the lattice spacing.

As previously remarked the flow is some sort of smoothing operation on the gauge field. From eq. (2.67) it is actually possible to see that the flow on the lattice is generated by a sequence of infinitesimal stout link smearing steps [59].

A gauge invariant observable that can be easily computed on the lattice is the average plaquette from which it is possible to work out a discretization of eq. (2.66)

$$E(t_W) = 2\sum_{x\in a\Lambda}\sum_{\mu,\nu}\operatorname{tr}[\mathbb{1} - V_{t_W}(x;\mu,\nu)] \tag{2.68}$$

where $V_{t_W}(x;\mu,\nu)$ is the plaquette field built out of the fields $V_{t_W}(x;\mu)$.

2.6. Topological charge

The topological charge is a pure gauge quantity that in the continuum is given by the integral of the field strength tensor times its dual F^*

$$Q_{\text{top}} = \frac{1}{32\pi^2} \int \mathsf{d}^4 x \; \text{tr} \left[F_{\mu\nu}(x) F^*_{\mu\nu}(x) \right] . \tag{2.69}$$

In continuum QCD it is possible to show that the value of this integral is an integer and that it is equal to the difference of right handed and left handed zero modes of the Dirac operator. On the lattice with a chiral Dirac operator, it is also possible to have an integer charge by counting its zero modes. A less computationally intensive way that is also applicable to the case of the Wilson Dirac operator (that explicitly breaks chiral symmetry) is to calculate the topological charge on smoothed gauge configurations using e.g. HYP smearing introduced in refs. [30, 29] and then using an $\text{O}(a^2)$ discretization of the continuum expression in eq. (2.69). This definition is not expected to give (and indeed does not give) integer values of the charge, but it is still useful for determining properties of the algorithm (e.g. as an indicator on how fast infrared lattice modes are moving in simulation time). More recently in ref. [22] a method has been developed for computing renormalizable spectral quantities (e.g. the spectral density of the Hermitian Dirac operator) also within the Wilson-Dirac formulation of lattice QCD. In ref. [49] the technique developed in ref. [22] has been applied to the computation of the topological susceptibility (i.e. $\left\langle Q^2_{\text{top}} \right\rangle / V$). In the same work the values of the topological susceptibility computed with the spectral projectors have been compared with values computed using the Wilson flow as a smoothing operator and the two methods have been found to give the same value within statistical errors.

3. Algorithms

One of the characteristic aspects of Lattice QCD is its numerical nature. The hard computational core of the non–perturbative approach consists in evaluating the path integral on powerful computers. Lattice configurations must be generated numerically and algorithms have been devised with this goal in mind. After a general introduction to the Markov chain Monte Carlo (MCMC) methods we will introduce the Hybrid Monte Carlo algorithm.

3.1. Generating lattice configurations

The lattice QCD path integral formulation can be used to define a probability density in gauge configuration space that can be sampled with a Metropolis [56] algorithm, as is done in statistical mechanics. The quantities that are computed in lattice simulations are expectation values of observables

$$\langle O \rangle = \frac{1}{Z} \int \mathcal{D}\psi \mathcal{D}\overline{\psi} \mathcal{D}U \, O[U, \overline{\psi}, \psi] \, \mathrm{e}^{-S[U, \psi, \overline{\psi}]} \tag{3.1}$$

where the measure for the quark fields is

$$\mathcal{D}\psi = \prod_{x \in a\Lambda} \prod_{f,\alpha,c} \mathrm{d}\psi_{\alpha,c}^{(f)}(x) \quad \mathcal{D}\overline{\psi} = \prod_{x \in a\Lambda} \prod_{f,\alpha,c} \mathrm{d}\overline{\psi}_{\alpha,c}^{(f)}(x) \, . \tag{3.2}$$

The anti-commuting quark fields become on the lattice a countable collection of Grassmann numbers whose rules of integrations are discussed in text books as ref. [21] while for the gauge fields we have

$$\mathcal{D}U = \prod_{x \in a\Lambda} \prod_{\mu=0}^{3} \mathrm{d}U(x; \mu) \tag{3.3}$$

where the proper measure of the single link gauge variable (that is an SU(3) matrix) is the Haar measure over the group manifold whose definition can also be found in ref. [21]. In eq. (3.1) the observable O might stand for a two point function analogue to the one in eq. (2.1), while with Z we denote the partition function and S can stand for any action formulated on the lattice (but we will later restrict our attention to either the Wilson gauge action or the Wilson-Dirac action).

For notational convenience we now restrict our discussion to a path integral over the gauge degrees of freedom alone. As it will be shortly clarified this is a sensible simplification since the fermionic degrees of freedom can be "integrated out" at the expense of making the action more complex. An importance sampling Monte Carlo

calculation approximates the path integral as an average over a sample of N gauge field configurations U_i, distributed according to a probability density $\propto e^{-S[U]}$. The path integral expectation value of the observable is then expressed as

$$\langle O \rangle = \lim_{N \to \infty} \frac{1}{N} \sum_{i=1}^{N} O[U_i] \, . \tag{3.4}$$

Since in actual computations the sum in eq. (3.4) is truncated, the expectation value comes with an error that decreases with the square root of the number of configurations included and is proportional to the standard deviation. The justification of the Monte Carlo method and of the error formula lies in the law of large numbers and the central limit theorem as thoroughly discussed in ref. [58, 35].

3.1.1. Integrating the fermionic part of the action

In the Feynman path integral formulation, fermions are described by Grassmann variables. In the case of the lattice QCD measure, eq. (3.2), one has $O(V)$ (here V is the volume in lattice units) anti-commuting variables and since V variables span an algebra with 2^V generators, this makes it extremely impractical (actually impossible) to simulate systems with more than a handful of degrees of freedom *naively* on a computer. In the following we show how the Grassmann fields can be integrated at the expense of a more complicated formulation of the action and of the observables that could otherwise contain an explicit dependence on the fermionic degrees of freedom as well.

Since the Wilson-Dirac action of eq. (2.35) is bilinear in the fermionic variables we can perform a Berezin integration over the Grassmann numbers that enter the definition of the LQCD partition function

$$Z = \int \mathcal{D}U \int \mathcal{D}\overline{\psi} \, \mathcal{D}\psi \, e^{-S_{\mathrm{G}}[U] - S_{\mathrm{F}}[\overline{\psi}, \psi, U]} \, . \tag{3.5}$$

This reformulates the fermionic integral as a product of determinants

$$\int \mathcal{D}\overline{\psi} \, \mathcal{D}\psi \, e^{-S_{\mathrm{G}}[U] - S_{\mathrm{F}}[\overline{\psi}, \psi, U]} = \det D_1 \ldots \det D_{N_{\mathrm{f}}} \, e^{-S_{\mathrm{G}}[U]}, \tag{3.6}$$

where $D_f = D_{\mathrm{W}}[U] + M_{\mathrm{f}}$ is the fermion matrix for the quark flavour f. In this way the reduction to fewer degrees of freedom is given at the cost of a much greater complexity in the action. Indeed the extremely high computational costs of lattice QCD simulations lie exactly in the inclusion of the fermion determinant, either computed directly or stochastically estimated.

An important property that can be used to modify the expression in eq. (3.6) and render it more suitable for numerical computations is the γ_5-Hermiticity of the Wilson-Dirac operator

$$\gamma_5 \, D_{\mathrm{W}} \, \gamma_5 = D_{\mathrm{W}}^{\dagger} \tag{3.7}$$

this property, that can be explicitly checked, holds also for other formulations of the

lattice Dirac operator. An easy to show property of γ_5-Hermitian operators is that their spectrum is composed of either real or complex conjugated pairs of eigenvalues. This means also that the determinant in eq. (3.6) is real.

In the two degenerate flavor approximation the factor in eq. (3.6) is the square of the determinant. Using γ_5-Hermiticity it can be shown to be the determinant of a positive (semi)-definite Hermitian matrix:

$$(\det D_f)^2 = \det D_f \det \gamma_5 D_f \gamma_5 = \det(D_f D_f^\dagger) \,. \tag{3.8}$$

For positive matrices it is possible to unambiguously define the matrix logarithm, and in this way also define the effective action of the two flavour theory

$$S_{\text{eff}}[U] = S_{\text{G}}[U] - \text{tr} \ln D_f D_f^\dagger \,. \tag{3.9}$$

that only depends on the gauge fields.

The effective action S_{eff} can in principle be used directly in MC calculations, but still eq. (3.9) requires the computation of the determinant of a very large matrix (or the matrix logarithm that is also a very expensive operation). This is feasible only when the lattice volume is small otherwise it would take too much computational effort. An alternative technique well defined only for Hermitian positive matrices (like the product $DD^\dagger$) is to give a stochastic estimate of the determinant, based on the Gaussian path integral identity

$$\det DD^\dagger = \int \mathcal{D}\chi^\dagger \mathcal{D}\chi \, \text{e}^{-\chi^\dagger (D^\dagger D)^{-1}\chi} \,, \tag{3.10}$$

where the new pair of fields χ and $\chi^\dagger$ have the same number of degrees of freedom as the original fermion field but are normal c-numbers and for this reason are called pseudo-fermions. Starting from (3.10) there are many methods that allow more or less efficient ways to compute the effect of sea quarks while partly bypassing the computational burden of the determinant. A discussion regarding the inclusion of single flavours follows in sec. 3.3.2.

3.2. Markov chains

The probability distribution that we would like to sample is the weight in the path integral whose general form is

$$W(q) = \frac{\text{e}^{-S[q]}}{\int \mathcal{D}q \, \text{e}^{-S[q]}} \, \mathcal{D}q \,, \tag{3.11}$$

namely a Boltzmann probability density with a properly defined lattice measure $\mathcal{D}q$. In this context we will often refer to the notion of state, that we generally denote with q. In lattice QCD a state is usually thought as a single gauge configuration U, but a state might as well represent something much more simple (a $\mathbb{Z}_2$ number, for example).

In general Boltzmann weights defined in eq. (3.11) can not be computed directly, the

difficulty lies in calculating the normalization factor Z. It is known though since a long time [56] that there is a class of stochastic processes, called Markov processes, suitable for addressing this difficulty in an efficient way, since they allow to bypass the need to compute the partition function.

3.2.1. Stationary stochastic processes

Before introducing Markov processes we define some terminology specific to stochastic processes, of which a comprehensive introduction can be found in ref. [68]. By random process we mean a function $Q(t)$ that has a single deterministic argument t and whose values are random variables. The argument t is generally called Monte Carlo (MC) time. In our specific case the function evaluates to a gauge configuration U_t, labelled with a discrete time index t. The set of possible values of the function $Q(t)$, $\mathcal{Q} = \{q\}$, is called state space. This space can be either continuous (as is the case of lattice QCD gauge links, where the state space is also compact and simply connected) or discrete (as in some statistical mechanics systems like the Potts model where $\mathcal{Q} = \mathbb{Z}_n^V$, with V denoting the volume of the system).

Since the function $Q(t)$ is random each repetition of the computation at MC time t will, in general, yield a different value q. For this reason a single record of a stochastic process is merely one out of a whole collection of possible records that might have been computed. The set of all possible records is called the *ensemble* while each particular record we call a *realization* of the process, *replica* or *chain* (all three expressions are used, though in different contexts).

Probability distributions that do not depend on MC time (like the one in eq. (3.11)) are usually sampled with stationary stochastic processes. These processes are invariant under a shift of the MC time origin (statistical properties of the ensemble do not explicitly depend on the MC time).

3.2.2. Markov processes

A Markov process is a stochastic process with a one–time–step dependence. If we consider a realization of a Markov process where we have a configuration q, the next element of the chain will be in state q' with a probability given by the conditional distribution

$$P(q' \leftarrow q) \tag{3.12}$$

that does not depend on any previous state of the chain. The conditional distribution $P(q' \leftarrow q)$ is generally called transition (or Markov) matrix. The term matrix is strictly correct only when discussing discrete state spaces of finite extent (e.g. $\mathbb{Z}_n^V$). For simplicity of discussion we will from now on ignore the fact that the state space of lattice QCD is not discrete and will therefore use simple summation where a more rigorous treatment would introduce integrals over the state space with an appropriate definition of measure.

Markov processes are classified based on several properties of the transition matrix P. For all stochastic matrices we have

- $P(q' \leftarrow q)$ are square $|\mathcal{Q}| \times |\mathcal{Q}|$, where $|\mathcal{Q}|$ denotes the number of elements in the state space.

- All rows of $P(q' \leftarrow q)$ consist of non-negative real numbers, with $\sum_{q'} P(q' \leftarrow q) = 1$

In ref. [74] it is shown that some properties common to all Markov processes are simple consequences of this definition, namely

- Eigenvalues λ_n of $P(q' \leftarrow q)$ lie in the unit circle: $|\lambda_n| \leq 1$, where an eigenpair is defined as the solution of

$$\sum_{q \in \mathcal{Q}} P(q' \leftarrow q)\xi_n(q) = \lambda_n \xi_n(q') \tag{3.13}$$

- There is at least one eigenvalue λ_0 equal to one,

- The product of Markov matrices is a Markov matrix,

with the product of two stochastic matrices defined through the Chapman-Kolmogorov equation

$$P^{s+t}(q' \leftarrow q) = \sum_{q'' \in \mathcal{Q}} P^t(q' \leftarrow q'')P^s(q'' \leftarrow q) . \tag{3.14}$$

A sequence of Markov matrices generates a Markov chain. To make this statement concrete one must first specify the starting probability density $\Pi(q)$, i.e. the probability density from which we draw the first element of the chain q_0. We assume that $\Pi(q)$ is arbitrary (besides satisfying $\sum_{q \in \mathcal{Q}} \Pi(q) = 1$ and $0 \leq \Pi(q) \leq 1$). Further we define the sequence of probability densities

$$\Pi_t(q) = \sum_{q' \in \mathcal{Q}} P^t(q \leftarrow q')\Pi(q') . \tag{3.15}$$

A realization of length N of the process will then consist of a configuration q_N drawn from the probability density $\Pi_N(q)$ plus all the intermediate outcomes of the process starting from q_0:

$$\mathcal{R}_N^r = \{q_0^r \rightarrow q_1^r \rightarrow q_2^r \rightarrow \ldots \rightarrow q_N^r\} , \tag{3.16}$$

where the index r labels different realizations and it will be needed when discussing the errors in Monte Carlo computations.

All simulation algorithms of lattice QCD are believed to belong to the class of *regular* Markov chains, often called ergodic. Ergodic chains are the ones for which the probability to go from any state to any other in a finite number of steps n (where n does not depend on the starting/ending state) is greater than zero:

$$\exists \, n > 0 : \forall q \, \text{and} \, q' \in \mathcal{Q}, \; P^n(q' \leftarrow q) > 0 , \tag{3.17}$$

further spectral properties that hold for ergodic transition matrices are:

- There is exactly one unit eigenvalue

- The chain is asymptotically stationary.

The existence of exactly one unit eigenvalue is a direct consequence of the fact that there is a probability greater than zero to reach any corner of the state space in a finite amount of MC time. Asymptotic stationary means that

$$\forall\, \Pi(q)\,, \; \lim_{t\to\infty} \Pi_t(q) = \Pi_{\mathrm{eq}}(q)\,, \tag{3.18}$$

where $\Pi_{\mathrm{eq}}(q)$ is the unique equilibrium distribution ($\Pi_{\mathrm{eq}}(q) \propto \xi_0(q)$). The consequence of this property is that with an algorithm that simulates an ergodic Markov process it is possible to sample configurations from a unique equilibrium distribution starting from an arbitrary distribution $\Pi(q)$. The equilibrium distribution is reached as an asymptotic regime of the process in a period of MC time that is called equilibration or *thermalization* time. The characteristic time scale for thermalization is a property of the Markov process and, as we will show later, for ergodic chains it is a characteristic time τ_{exp} that can be expressed in terms of the spectrum of the stochastic matrix.

3.2.3. Metropolis algorithm

In a Monte Carlo calculation with importance sampling we want to produce a Markov chain with a stationary probability distribution given by

$$\Pi_{\mathrm{eq}}(q) = W(q)\,, \tag{3.19}$$

where in a QCD computation $W(q) \propto \mathrm{e}^{-S_{\mathrm{eff}}}$ is the weight in the path integral with S_{eff} (of the two degenerate flavours theory) given in eq. (3.9). A sufficient condition that ensures that the asymptotic probability density of a Markov chain is equal to $W(q)$ is that the transition matrix satisfies *detailed balance*

$$P(q' \leftarrow q)W(q) = P(q \leftarrow q')W(q') \tag{3.20}$$

for any pair of states q and q'. A simple algorithm which satisfies eq. (3.20) is the Metropolis algorithm that we now state. Starting with a configuration q_0 one iterates the following steps for $t = 0, 1, 2 \dots$

1. Generate a candidate state q according to some *a priori* symmetric proposal $P_{\mathrm{G}}(q \leftarrow q_t)$
$$q_t \to q \quad \text{with} \quad P_{\mathrm{G}}(q \leftarrow q_t) = P_{\mathrm{G}}(q_t \leftarrow q)\,. \tag{3.21}$$

2. Compute
$$P_{\mathrm{A}}(q \leftarrow q_t) = \min\left(1, \frac{W(q)}{W(q_t)}\right)\,. \tag{3.22}$$

3. With probability $P_{\mathrm{A}}(q \leftarrow q_t)$ set $q_{t+1} = q$, otherwise set $q_{t+1} = q_t$.

The complete transition matrix of this algorithm is given by

$$P(q' \leftarrow q) = P_A(q' \leftarrow q)P_G(q' \leftarrow q) + \delta_{qq'}\left(1 - a(q)\right), \tag{3.23}$$

where $a(q)$ is the probability that the proposed value is accepted, given q

$$a(q) = \sum_{q'} P_A(q' \leftarrow q)P_G(q' \leftarrow q), \tag{3.24}$$

so $1 - a(q)$ is the probability of remaining in the state q. As already anticipated one of the properties of this algorithm is that the probability of acceptance $P_A(q' \leftarrow q)$ does not depend on the normalization constant in eq. (3.11). Detailed balance is a property of this algorithm: in eq. (3.23) it is clearly satisfied by the Dirac delta, while for the remaining part of the expression one quickly sees that

$$P_A(q' \leftarrow q)P_G(q' \leftarrow q)W(q) = \tag{3.25}$$

$$\min\left(1, \frac{W(q')}{W(q)}\right) P_G(q' \leftarrow q)W(q) = \tag{3.26}$$

$$\min\left(P_G(q' \leftarrow q)W(q), P_G(q \leftarrow q')W(q')\right) = \tag{3.27}$$

$$\min\left(1, \frac{W(q)}{W(q')}\right) P_G(q \leftarrow q')W(q'), \tag{3.28}$$

completing the proof.

3.3. Hybrid Monte Carlo

We now concentrate on one of the most widely used algorithms for generating lattice QCD gauge configurations with dynamical fermions. HMC is a Metropolis algorithm in which a new configuration is proposed by integrating a set of classical equations of motion. The particular nature of the proposal method allows to update the gauge fields globally while keeping the acceptance rate high. The advantage of global vs. local updates is significant with dynamical fermions due to the non-local nature of the effective action, eq. (3.9).

3.3.1. Molecular Dynamics and Equilibrium Ensemble

The basic process underlying the HMC method is a completely deterministic evolution of the field of gauge links U_t in the MC time τ. In the classical Hamiltonian formalism gauge variables play the role of positions while the action plays the role of the quantum mechanical potential. To complete the Hamiltonian picture we must also introduce the momentum variable canonically conjugated to the gauge links. For this purpose we recall that gauge links are elements of SU(3) and as such can be written as exponentials of elements of the $\mathfrak{su}(3)$ algebra. The exponential is parametrized on the basis of the

generators T_a:

$$U(x;\mu) = \exp\left(iA_\mu(x)\right) = \exp\left(i\sum_{a=1}^{8} \omega^{(a)}(x;\mu)T_a\right) , \qquad (3.29)$$

where the $\omega^{(a)}(x;\mu)$ are eight real parameters. Each link variable $U(x;\mu)$ can now be related to eight real momentum variables $\pi^{(a)}(x;\mu)$ conjugated to $\omega^{(a)}(x;\mu)$. By combining them with the generators we introduce the momentum matrices

$$\Pi(x;\mu) = \sum_{a=1}^{8} \pi^{(a)}(x;\mu)T_a , \qquad (3.30)$$

that are themselves elements of the algebra.

The Hamiltonian on the lattice is then given by

$$H[\Pi, U] = T[\Pi] + S_G[U] + S_F[U] \qquad (3.31)$$

with the kinetic term given by

$$T[\Pi] = \sum_{x,\mu} \text{Tr}\,\Pi(x;\mu)^2 , \qquad (3.32)$$

where the trace is taken over the color and Dirac indices. The fermionic part of the action will in general also depend on the pseudo-fermions of eq. (3.10), but we ignore now this complication that will be addressed later. The joint probability distribution is given by

$$W(\Pi, U) = \frac{e^{-T[\Pi]}e^{-S[U]}}{\int \mathcal{D}\Pi \; e^{-T[\Pi]} \int \mathcal{D}U \; e^{-S[U]}} \, \mathcal{D}\Pi\mathcal{D}U , \qquad (3.33)$$

with the conjugated momentum field measure being the product

$$\mathcal{D}\Pi = \prod_{x\in a\Lambda} \prod_{\mu=0}^{3} d\pi(x;\mu) . \qquad (3.34)$$

In eq. (3.33) the Gaussian field distribution of the momenta ($\propto e^{-T[\Pi]}$) and the weight that occurs in the path integral ($\propto e^{-S[U]}$) factorize, so that when computing expectation values of observables (that do not depend on the unphysical conjugated momenta) the Gaussian integral associated with the canonical momenta cancels.

Microcanonical and Hybrid Molecular Dynamics

One of the first attempt to use auxiliary momenta has been the microcanonical approach in ref. [5]. The method was subsequently abandoned (a major drawback is that the microcanonical expectation value is equivalent to the canonical only in the infinite volume) but the concept of approximating the equilibrium distribution $W(\Pi, U)$ by integrating Hamilton's equations has remained and is still present in nowadays most advanced

dynamical fermions algorithms. The equations of motion for a gauge field are generally given in their differential form

$$
\begin{aligned}
\frac{dU(x;\mu)}{d\tau} &= i\Pi(x;\mu)U(x;\mu) \\
\frac{d\Pi(x;\mu)}{d\tau} &= -F(x;\mu) \,, \quad F(x;\mu) = \sum_{a=1}^{8} T_a \frac{\partial S[e^{i\omega T_a}U(x;\mu)]}{\partial\omega}\bigg|_{\omega=0}
\end{aligned}
\tag{3.35}
$$

where in the action we put in evidence the link w.r.t which we want to perform the derivative. A rigorous derivation of the expressions on the r.h.s can be found in ref. [36]. The initial conditions are arbitrary but if the the dynamics is mixing (absence of invariant tori) the MD time evolution can in principle explore the entire surface of constant energy.

Since the momenta $\Pi(x;\mu)$ form a Gaussian field it is easy to draw them directly from the exact equilibrium distribution. This observation inspired the technique of hybrid algorithms explored in ref. [17, 15], where the momentum field is periodically refreshed from the equilibrium distribution, in the attempt to accelerate the speed at which the phase space is explored.

Numerical integrators of the equations of motion

The HMD forms a Markov chain and if we were able to integrate eq. (3.35) exactly, it would yield a "perfect" Metropolis step: a symmetric proposal since the classical dynamics is time reversible and an acceptance step that would never fail since the Hamiltonian flow conserves the energy exactly. The problem comes from the fact that Hamilton's equation of lattice QCD is a complex non-linear system of differential equations and analytical integration is clearly out of question. Any algorithm practically realizable must thus adopt a suitable numerical integration scheme, but numerical solutions of eq. (3.35) do not generally conserve neither the Hamiltonian nor do they automatically satisfy the reversibility property that ensures detailed balance of the Metropolis algorithm. Indeed many approximate integration schemes are known for Hamiltonian dynamics but the ones that turn out to satisfy the detailed balance condition of eq. (3.20) are the ones that are reversible and area preserving. In particular we will describe here the leapfrog integrator.

Numerical integration over an interval of length τ_{traj} is done by discretizing it in N steps, each of length ϵ. Following the discussion in ref. [46] we build the leapfrog integrator combining two simple transformations of the fields, each transformation acting independently either on the momentum or on the gauge field

$$
T_{\mathrm{P}}(\epsilon): \quad
\begin{aligned}
\Pi(x;\mu) \\
U(x;\mu)
\end{aligned}
\longrightarrow
\begin{aligned}
\Pi'(x;\mu) &= \Pi(x;\mu) - \epsilon\, F[U(x;\mu)] \\
U'(x;\mu) &= U(x;\mu)
\end{aligned}
\tag{3.36}
$$

and

$$T_{\mathrm{U}}(\epsilon): \quad \begin{matrix} \Pi(x;\mu) \\ U(x;\mu) \end{matrix} \quad \longrightarrow \quad \begin{matrix} \Pi'(x;\mu) = \Pi(x;\mu) \\ U'(x;\mu) = \mathrm{e}^{i\Pi(x;\mu)\epsilon}\, U(x;\mu) \end{matrix} \qquad (3.37)$$

where F is the force already defined in eq. (3.35).

The first of the two transformations evolves momenta while the second one the gauge links. A step of the integrator of size ϵ evolves both fields in the molecular dynamics time direction with the schema

$$T_{\mathrm{P}}(\epsilon/2)\, T_{\mathrm{U}}(\epsilon)\, T_{\mathrm{P}}(\epsilon/2) \qquad (3.38)$$

in such a way that the first to advance by half a step is the momentum field, followed by an update of the gauge field and finally the momentum field covers the second half of a step. This alternation of full and half steps has also given the name to the procedure. Following the Hamiltonian flow along a longer trajectory in phase space can be done by chaining together many atomic steps:

$$\mathfrak{I}[\epsilon, N] \quad \equiv \quad \{T_{\mathrm{P}}(\epsilon/2)\, T_{\mathrm{U}}(\epsilon)\, T_{\mathrm{P}}(\epsilon/2)\}^N \,, \quad N = \frac{\tau_{\mathrm{traj}}}{\epsilon} \,. \qquad (3.39)$$

The algorithm can easily be shown to be symmetric under reversal of canonical time (this corresponds to changing the sign of the momentum field). The property of area preservation states that the Jacobian of the map defined through eq. (3.38) has unit determinant. This follows from

$$\det \frac{\partial(\Pi', U')}{\partial(\Pi, U)} = 1 \,, \qquad (3.40)$$

in both eq. (3.36) and eq. (3.37), and it implies the preservation of the path integral measure, that in turn is needed for the detailed balance, since the probability density that enters eq. (3.20) in the case of LQCD is given by $W(\Pi, U)$ of eq. (3.33).

3.3.2. HMC for two degenerate flavours

All numerical integration schemes introduce step size errors. The leapfrog algorithm is a second order method, meaning that in an integration of trajectory length τ_{traj} at small step size ϵ, deviations from the Hamiltonian are proportional to ϵ^2. In both the microcanonical and the HMD method expectation values of observables suffer of the discretization error due to the finite step size, and these values must therefore be extrapolated to the limit of $\epsilon = 0$. Systematic errors of this kind can be completely kept under control by the Metropolis method: this simple observation was first made in ref. [16] that introduced the Hybrid Monte Carlo algorithm that merges the hybrid method with the Metropolis Monte Carlo acceptance step.

With dynamical fermions the Hamiltonian of eq. (3.31) has a part that formally depends only on the gauge fields but this dependence is complicated. Moreover, while the gauge

action is ultra-local, the fermion effective action is non-local and the derivative required to compute the force in eq. (3.36) would result in computational costs that are too high due to the complexity of the operation. In ref. [23] the so called R algorithm was introduced, with a reduced cost thanks to a method that estimates the change in the effective action stochastically.

The alternative that nowadays has been almost universally adopted estimates the determinant with pseudo-fermions. As we noted in writing down eq. (3.10), the product of the determinants of the theory with two degenerate flavours can be expressed as a path integral over the pseudo-fermion field. The fermionic part of the effective action can then be expressed as a bosonic bilinear

$$S_{\mathrm{PF}} = \chi^\dagger (D^\dagger D)^{-1} \chi = \xi^\dagger \xi \,, \quad \text{where} \quad \xi = (D[U])^{-1} \chi \,. \tag{3.41}$$

The pseudo-fermions could in principle be simulated by adding to the Hamiltonian a new set of conjugate momenta but this, to our knowledge, has never been done. Instead the field χ is generated with a "perfect" heat-bath by first generating the Gaussian field ξ and subsequently computing $\chi = D^\dagger[U]\xi$. In this way one obtains a configuration for the pseudo-fermionic variable extracted with the correct ensemble density given by the gauge field at the beginning of each the trajectory and $\propto \mathrm{e}^{-\chi^\dagger (DD^\dagger)^{-1}\chi}$. The usual approach is then to evolve the gauge field in the background of the pseudo-fermionic field that remains constant throughout the whole molecular dynamics trajectory.

The full Hamiltonian of the two flavour theory reads

$$H[\Pi, U, \chi] = T[\Pi] + S_{\mathrm{G}}[U] + \chi^\dagger (D^\dagger D)^{-1} \chi \,, \tag{3.42}$$

where the pseudo-fermions χ do not actively participate in the dynamics. For this particular form of the Hamiltonian, the explicit computation of the force, eq. (3.35), can be split in two terms. The pure gauge part is

$$F_{\mathrm{G}}(x; \mu) = -i \frac{\beta}{12} (U(x; \mu) V(x; \mu) - [U(x; \mu) V(x; \mu)]^\dagger) \tag{3.43}$$

with

$$V(x; \mu) = \sum_{\nu \neq \mu} (U(x + a\hat{\mu}; \nu) U(x + a\hat{\nu}; \mu)^\dagger U(x; \nu)^\dagger +$$
$$U(x + a\hat{\mu}; -\nu) U(x - a\hat{\nu}; \mu)^\dagger U(x; -\nu)^\dagger) \,, \quad \tag{3.44}$$

while for the fermionic part we use the matrix identity

$$\partial M^{-1} / \partial \omega = -M^{-1} (\partial M / \partial \omega) M^{-1} \tag{3.45}$$

and write

$$\frac{\partial(\chi^\dagger(DD^\dagger)^{-1}\chi)}{\partial\omega} = -\chi^\dagger(DD^\dagger)^{-1}\frac{\partial(DD^\dagger)}{\partial\omega}(DD^\dagger)^{-1}\chi \tag{3.46}$$

$$= -\chi^\dagger(DD^\dagger)^{-1}\left(\frac{\partial D}{\partial\omega}D^\dagger + D\frac{\partial D^\dagger}{\partial\omega}\right)(DD^\dagger)^{-1}\chi \tag{3.47}$$

where the ω dependence of the Wilson-Dirac operator is introduced through the definition of the derivative over a Lie manifold in eq. (3.35). Since we need the result for a later section we also write the full expression of the derivative of the Wilson-Dirac operator of eq. (2.34), with respect to a single color component c in direction μ at the space-time point x

$$\frac{\partial D_\mathrm{W}(y;z)}{\partial\omega(x,\mu,c)} = i\frac{\mathbb{1}+\gamma_\mu}{2a}U(x,\mu)^\dagger T_c\,\delta_{y-a\hat{\mu},z}\delta_{y,x} - i\frac{\mathbb{1}-\gamma_\mu}{2a}T_c\,U(x,\mu)\delta_{y+a\hat{\mu},z}\delta_{y,x} \tag{3.48}$$

where we do not specify the action of the operator in color space since it is trivial. The HMC algorithm can thus be summarized by the following steps

1. Setup

   - Pseudo-fermion heat-bath $\chi = D^\dagger[U]\xi$, where ξ is a Gaussian field.
   - Canonical momentum Π_0 refreshment with probability
     density $\propto \mathrm{e}^{-T[\Pi]}$

2. Hybrid Molecular Dynamics trajectory of length τ_traj as in eq. (3.39). After the last step of the integrator the starting fields are mapped in the new fields: $(\Pi, U) \to (\Pi', U')$

3. Conjugated momentum reversal (formal step needed for the proof of detailed balance)

4. Metropolis acceptance test

   - draw a uniformly distributed random number $r \in [0,1]$
   - accept the new gauge configuration U' if $\mathrm{e}^{H[\Pi,U]-H[\Pi',U']} > r$.

The HMC algorithm has been successfully used in lattice QCD computations at large volume and small lattice spacing, and its computational cost can be partly predicted starting from some basic observations. The Hamiltonian is an extensive quantity, as a consequence also the fluctuations $\delta H = H[\Pi',U'] - H[\Pi,U]$ are extensive quantities and maintaining constant acceptance rate as the volume increases can be done only by reducing the integration step size . In ref. [25, 8] it has been estimated that in lattice QCD the cost of the HMC algorithm, while keeping the acceptance rate fixed, scales $\propto (V/a^4)^{5/4}$. With dynamical fermions the cost of the algorithm is also a function of the sea quark mass the reason being that the condition number of the fermion matrix squared increases $\propto 1/M_f^2$, resulting in an increased cost of the inversions needed. Another related problem is the increase of the magnitude of the force originating from the fermionic

action. This problem can be addressed by preconditioning and using integration schemes with multiple time scales. One of the most widely used preconditioner of the determinant is mass preconditioning introduced in ref. [28], a second one presented in ref. [43] will be discussed in the next section.

A few comments on the two flavour approximation

The two degenerate flavours approximation is generally used to account for the effect of the two lightest sea quarks (up and down). For most of the physical observables computed this approximation has up to now given results compatible with the experimental expectations [7].

The fact that within this approximation we manage to obtain results close to experiment can be understood from chiral perturbation theory [20] where hadronic observables are expressed as a power series in the quark masses M_q (with also additional logarithmic terms)

$$O(M_q) = O_0 + (M_q/\Lambda_{\text{QCD}}) \, O_1 + \ldots \tag{3.49}$$

where the next terms in the expansion can in some cases be $M_q^{3/2}$ (e.g. in the case of some barionic quantities). In general the leading term $O_0 \neq 0$ and the leading corrections, besides typically being small, do not depend on the quark mass splitting but only on the value of the masses. For those quantities, like the pion mass M_π, where $O_0 = 0$, what happens is that the first non-zero term is O_1 and one can expect that the "correct" M_π is also obtained with two degenerate quarks whose mass is $\widehat{M} \approx (M_u + M_d)/2$ (independently on the relative size of the two individual masses). If lattice computations were to become so precise, with both systematic and statistical errors under control, that the effect of the mass splitting was to become relevant, then the contribution of electromagnetism would have to be kept also into account since the typical size of electromagnetic corrections is of the same order as the quark mass splitting.

The two flavour approximation does not include heavier quarks, the strange with $M_s \sim \text{O}(100\text{MeV})$ and the charm with $M_c \sim \text{O}(1\text{GeV})$. To include them in a MC simulation with Wilson-Dirac fermions one must estimate the determinant of the Dirac matrix. One issue that must be addressed is that the determinant of the Wilson-Dirac operator (real as a consequence of γ_5-Hermiticity eq. (3.7)), in general it is not positive. If the partition function is the sum of a positive and a negative contribution, the conceptual foundations of our numerical methods (MCMC) are invalidated and importance sampling can not be applied.

When the regions in field space where the determinant is negative have a negligible weight in the functional integral, it is possible to include the strange quark in the simulation (e.g. with the methods presented in ref. [6, 19]), by replacing the Wilson-Dirac operator with

$$|\det D_f| = \sqrt{\det D_f D_f^\dagger} \, , \tag{3.50}$$

effectively simulating the theory with the wrong action. Correct results can still be obtained by reweighting the expectation values with the correct action. In this formulation the modified determinant is again a positive weight in the path integral, and the HMC

method can be applied.

As we have discussed, the determinant with Wilson fermions could change sign: in this particular case the procedure is justified by the observation that with a heavy strange quark, the Wilson-Dirac operator estimated on the background of the gauge configurations that dominate the path integral, has been shown to have a spectral gap. This gap has been analyzed in ref. [10], where it is shown that the distribution of the lowest lying eigenvalue is well separated from zero, making it very unlikely that negative eigenvalues could occur in the course of the average-length Monte Carlo simulation.

As already pointed out a possible solution for the case in which some configurations contribute with a negative determinant is to incorporate the sign in the evaluation of the observable through a reweighting technique similar to the one presented in ref. [48]. An often cited limitation of reweighting techniques is that the width of the fluctuations of the determinant grows with the lattice volume, making the method practically unusable. In ref. [48] it is argued that if the determinant is factorized and the low modes (responsible for sign changes) are separated from the rest, it is possible to use reweighting also in the large volume limit, since the fluctuations of factorized low modes do not show volume dependence.

3.3.3. HMC with Domain Decomposition preconditioning

The term preconditioning is generally used in association to iterative linear solvers, where it is typically understood as a method that reduces the condition number of a problem [69]. In the context of the HMC algorithm we refer to algorithm or determinant preconditioning. This generically refers to a method that reformulates the computation of the pseudo-fermionic force contribution in a way that is more suitable for numerical computations. The aim of these techniques is to avoid large quark forces associated to large computational costs (when large forces are cheap to compute it is not a problem since the associated integrator step size can be made suitably small without increasing algorithmic costs beyond current computational capacity). The first step is the factorization of the quark determinant, leading to the introduction of multiple pseudo-fermions. Each one of these factors will then lead to a separate term in the action

$$\det D = \operatorname{sign} D \det R_1 \ldots \det R_n \to S_{\mathrm{PF}} = \sum_{k=1}^{n} (\chi_k, R_k^{-1} \chi_k) \, ,$$

where each factor R_k has to be a positive matrix.

As was pointed out in ref. [42, 43] the Schwarz procedure of domain decomposing the operator can be used both as a preconditioner for the solution of the Wilson-Dirac equation and to precondition the HMC algorithm itself. In particular we can cover the lattice with a regular grid of non-overlapping rectangular blocks Λ. The assumption here is that the number of blocks per direction is even. The union of black blocks is then denoted by Ω and the union of white blocks by Ω^*. With respect to an ordering of the lattice points where those in Ω come first, the Wilson-Dirac operator D assumes the

block form

$$D = \begin{pmatrix} D_\Omega & D_{\partial\Omega} \\ D_{\partial\Omega^*} & D_{\Omega^*} \end{pmatrix} \qquad (3.51)$$

where the operator D_Ω coincides with the Wilson operator acting on the domain Ω with Dirichlet boundary conditions, while $D_{\partial\Omega}$ is the sum of the hopping terms from the exterior boundary $\partial\Omega$ of the black blocks Ω to the exterior boundary $\partial\Omega^*$ of the white blocks Ω^*.

It is convenient to let these operators act on quark fields that are defined on the whole lattice, rather than on Ω or Ω^* only. The extension is done in the obvious way by padding with zeros so that we can write

$$D = D_\Omega + D_{\Omega^*} + D_{\partial\Omega} + D_{\partial\Omega^*} \ .$$

Similarly we can further decompose into operators acting on single blocks

$$D_\Omega + D_{\Omega^*} = \sum_\Lambda \hat{D}_\Lambda \qquad (3.52)$$

$$D_{\partial\Omega} = \sum_{\text{black } \Lambda} D_{\partial\Lambda}, \quad D_{\partial\Omega^*} = \sum_{\text{white } \Lambda} D_{\partial\Lambda} \qquad (3.53)$$

where $\hat{D}_\Lambda$ denotes the Wilson-Dirac operator acting on the block Λ with Dirichlet b.c. and $D_{\partial\Lambda}$ is the sum of the hopping terms that move the field components on the exterior boundary $\partial\Lambda$ of the block Λ to the points that lie in its interior boundary.

Given these premises, the factorization

$$\det D = \det D_\Omega \det D_{\Omega^*} \det \left\{ 1 - D_\Omega^{-1} D_{\partial\Omega} D_{\Omega^*}^{-1} D_{\partial\Omega^*} \right\} \qquad (3.54)$$

is deduced from the given block structure (3.51). An observation now is that the operator in curly brackets acts non trivially only on those components of the quark fields that reside on the exterior boundary of the white blocks $\partial\Omega^*$. Its determinant can therefore be reduced to the space of all fields supported on this subset of points. A reduction to an even smaller subspace $V_{\partial\Omega^*}$ of fields is in fact possible when the detailed properties of the boundary operator $D_{\partial\Omega^*}$ are taken into account.

Boundary fields subspace

We now explicitly specify the space $V_{\partial\Omega^*} \subset \partial\Omega^*$. The choice of this space is not unique, but is chosen such that the associated orthogonal projector $P_{\partial\Omega^*}$ satisfies

$$D_{\partial\Omega^*} P_{\partial\Omega^*} = D_{\partial\Omega^*} \ . \qquad (3.55)$$

This property guarantees that the determinant of the Schur complement eq. (3.54) coincides with the determinant of the projected operator R_2

$$R_2 = 1 - P_{\partial\Omega^*} D_\Omega^{-1} D_{\partial\Omega} D_{\Omega^*}^{-1} D_{\partial\Omega^*} \ . \qquad (3.56)$$

The action of the operator $D_{\partial\Omega^*}$ on an arbitrary quark field $\chi(x)$ is given by

$$D_{\partial\Omega^*}\chi(x) = -\,\theta_{\Omega^*}(x) \sum_\mu \left\{ \frac{1}{2}(1-\gamma_\mu)\theta_\Omega(x+\hat{\mu})U(x,\mu)\chi(x+\hat{\mu}) \right.$$

$$\left. +\,\frac{1}{2}(1+\gamma_\mu)\theta_\Omega(x-\hat{\mu})U(x-\hat{\mu},\mu)^{-1}\chi(x-\hat{\mu}) \right\}.$$

where $\theta_\Omega(x)$ and $\theta_{\Omega^*}(x)$ are the characteristic functions of the block domains Ω and Ω^*. The terms on the r.h.s. of this equation parallel transport the Dirac spinors from the external boundary $\partial\Omega^*$ to the external boundary $\partial\Omega$, and multiply them with projectors $\frac{1}{2}(1\pm\gamma_\mu)$ and link variables. This means that two components of the spinors residing on the subset

$$[\partial\Omega^*] = \left\{ x \in \partial\Omega^* \mid \forall\mu,\ (x+\hat{\mu}\in\partial\Omega)\ \oplus\ (x-\hat{\mu}\in\partial\Omega) \right\}$$

are lost irretrievably through the application of the projectors.

It is now straightforward to show that the operator

$$P_{\partial\Omega^*}\chi(x) = \begin{cases} 0 & \text{if } x \notin \partial\Omega^*, \\ \frac{1}{2}(1+\gamma_\mu)\chi(x) & \text{if } x \in [\partial\Omega^*] \text{ and } x+\hat{\mu}\in\partial\Omega, \\ \frac{1}{2}(1-\gamma_\mu)\chi(x) & \text{if } x \in [\partial\Omega^*] \text{ and } x-\hat{\mu}\in\partial\Omega, \\ \chi(x) & \text{otherwise.} \end{cases} \tag{3.57}$$

satisfies eq. (3.55). Moreover this choice excludes the trivial null space of $D_{\partial\Omega^*}$, minimizing the dimension of the space $V_{\partial\Omega^*}$ of boundary quark fields.

3.4. Lattice correlators from MC simulations

The estimate of spectral properties for hadron spectroscopy requires the computation of two-point functions. We have already seen how one can generate an ensemble of lattice configurations with the Monte Carlo method and how to compute gauge invariant pure SU(3) observables by taking the trace of products of links that form a closed loop (the simplest example being the plaquette variable eq. (2.24)). We now see how to compute a correlator as the one defined in eq. (2.53), on the background of a lattice configuration.

3.4.1. Meson two-point functions

The value of the pion correlator in eq. (2.53) projected to zero momentum is

$$C_{\mathrm{PS}}(t) = \frac{a^3}{V} \sum_{\vec{x}} \langle P^+(t,\vec{x})\, \overline{P}^+(0,\vec{y}) \rangle$$

$$= \frac{a^3}{V} \sum_{\vec{x}} \frac{1}{Z} \int \mathcal{D}U \int \mathcal{D}\overline{\psi}\mathcal{D}\psi\; P^+(t,\vec{x})\, \overline{P}^+(0,\vec{y})\; \mathrm{e}^{-S_{\mathrm{G}}-S_{\mathrm{F}}}\,, \tag{3.58}$$

where the choice of the $\vec{y}$ point is irrelevant due to periodic boundary conditions and to translation invariance. Analogously to the case of eq. (3.6), the fermionic fields in the path integral can be integrated out. The integral can be performed after the ψ and $\overline{\psi}$ have been reordered (taking into account the signs, that come from anti-commutation relations, and the order of the gamma matrices) in such a way that pairs with the same flavour content are next to each other. The ensemble expectation value w.r.t. the fermionic degrees of freedom alone $\langle\cdot\rangle_{\mathrm{F}}$ of a pair is then called Wick contraction and corresponds to a matrix element of the inverse Wilson Dirac operator, with definite flavour

$$\left\langle\psi^{(f)}_{\alpha_i,c_i}(x_i)\overline{\psi}^{(f)}_{\alpha_j,c_j}(x_j)\right\rangle_{\mathrm{F}} = D_f^{-1}(i,j) \equiv S_f(t_i,\vec{x}_i,\alpha_i,c_i;t_j,\vec{x}_j,\alpha_j,c_j) \ , \qquad (3.59)$$

where in $D_f^{-1}(i,j)$ i and j are a shorthand for the space-time, Dirac and color indices that appear on the l.h.s. and where S_f is the quark propagator for flavour f which is shown with all indices but later will be also expressed with a shortened notation that hides all but the indices relevant for the discussion. Our example with the pion correlator of eq. (3.58) is thus given by

$$
\begin{aligned}
C_{\mathrm{PS}}(t) = \\
-\frac{a^3}{V}\sum_{\vec{x}}&\left\langle\overline{\psi}^d_{\alpha_1,c_1}(t,\vec{x})[\gamma_5]_{\alpha_1\beta_1}\psi^u_{\beta_1,c_1}(t,\vec{x})\overline{\psi}^u_{\alpha_2,c_2}(0,\vec{y})[\gamma_5]_{\alpha_2\beta_2}\psi^d_{\beta_2,c_2}(0,\vec{y})\right\rangle \\
=\frac{a^3}{V}\sum_{\vec{x}}&[\gamma_5]_{\alpha_1\beta_1}[\gamma_5]_{\alpha_2\beta_2}\left\langle\psi^d_{\beta_2}(0,\vec{y})\overline{\psi}^d_{\alpha_1}(t,\vec{x})\psi^u_{\beta_1}(t,\vec{x})\overline{\psi}^u_{\alpha_2}(0,\vec{y})\right\rangle \\
=\frac{a^3}{V}\sum_{\vec{x}}&\left\langle\mathrm{Tr}\left(S_{\mathrm{d}}(0,\vec{y};t,\vec{x})\ \gamma_5 S_{\mathrm{u}}(t,\vec{x};0,\vec{y})\gamma_5\right)\right\rangle_{\mathrm{G}} \\
=\frac{a^3}{V}\sum_{\vec{x}}&\left\langle\mathrm{Tr}\left(S_{\mathrm{d}}(0,\vec{y};t,\vec{x})\ S_{\mathrm{u}}^\dagger(0,\vec{y};t,\vec{x})\right)\right\rangle_{\mathrm{G}} \ ,
\end{aligned}
\qquad (3.60)
$$

where we adopt Einstein's convention for the indices, in the second line we drop the color indices, the trace in the third line runs on both color and Dirac indices and where with $\langle\cdot\rangle_{\mathrm{G}}$ we denote the ensemble average over the gauge degrees of freedom given by an action where the fermions have been integrated out as in eq. (3.9). In the last line we have used the γ_5-Hermiticity of the Wilson Dirac operator. From eq. (3.60) it is clear that for the pion correlator it is necessary to compute only one of the two propagators (in case of two degenerate quarks).

For each point $\vec{y}$ the propagator can then be calculated by solving the linear system for S:

$$D(i,j)S(j,k) = \delta_{ik} \ , \qquad (3.61)$$

where the indices should be interpreted as above, the delta is a shorthand for a product of Kronecker deltas, one for each separate index, and where $\vec{x}_j = \vec{y}$.

Variance reduction

Because of translation invariance the value of the correlator computed through eq. (3.61) does not change if averaged over any number N_s of source points $\vec{y}$. If the distance of the sources is larger than the correlation distance (typically of the order of the inverse of the pion mass in a simulation with dynamical fermions) the estimates will be practically independent thus reducing the variance by a factor proportional to the number of sources employed. The cost of the computation would on the other hand increase by a quantity that is also proportional to the number of sources since the Dirac equation eq. (3.61) must be solved for each source point (this estimate of the cost is additional to the cost of producing a statistically independent configuration and ignores e.g. an eventual preconditioner as the one in ref. [44] that adds a cost to the inversions that does not depend on the number of inversions performed).

A method that uses extended random sources as the one proposed in ref. [57, 76] performs the average over a selected set of source points stochastically. Given an observable a method is favored if at fixed computational cost, the variance of the estimate is smaller (keeping also into account possible biases). The total benefit of a method can be quantified only if the cost of producing two statistically independent configurations is known, but this is typically much larger than the cost of a single measurement. A possibility is to compute the combined propagator

$$\overline{S}(t, \vec{x}) = \sum_{\vec{y}} S(t, \vec{x}; 0, \vec{y})\rho(\vec{y}) \tag{3.62}$$

where $\rho(\vec{y})$ is a random field of $U(1)$ variables. From this definition one constructs a second estimator of the correlator

$$C_\mathrm{PS}(t) = \frac{a^3}{V} \sum_{\vec{x}} \left\langle \mathrm{Tr}\left(\overline{S}(t, \vec{x})\,\overline{S}^\dagger(t, \vec{x})\right)\right\rangle_\mathrm{G} , \tag{3.63}$$

that as shown also in ref. [46] has a reduced variance w.r.t. the point source estimator.

4. Error analysis

In a LQCD computation one is typically interested in estimates of quantities $H^{s,\eta}$ computed on N_E different ensembles (where η labels the ensemble and s labels different quantities estimated on the same ensemble). The quantities $H^{s,\eta}$ can be either **primary** or **derived**. Primary quantities are expectation values of measurements performed configuration-wise, where by measurement we mean an arbitrarily complicated function of the state variables $q \in \mathcal{Q}$. Derived quantities are functions of primary quantities. The values $H^{s,\eta}$ are usually combined in order to compute some interesting physical quantity

$$P = p(\mathbf{H}^1, \mathbf{H}^2, \ldots, \mathbf{H}^{N_\mathrm{E}}), \quad \text{with} \quad \mathbf{H}^\eta = \{H^{1,\eta}, H^{2,\eta}, \ldots\} \tag{4.1}$$

where P is expressed as a function of the $\mathbf{H}^\eta$.

All estimates $\overline{H}^{s,\eta}$ computed with the Monte Carlo method are random variables and they come with a statistical error

$$H^{s,\eta} = \overline{H}^{s,\eta} + \mathrm{O}\left(\delta\overline{H}^{s,\eta}\right) \tag{4.2}$$

so the error of the estimate of P can be obtained by means of the known formula for the propagation of uncertainty

$$(\delta\overline{P})^2 = \sum_{\eta=1}^{N_\mathrm{E}} \sum_{s,s'} \left.\frac{\partial p(\mathbf{X}^1, \ldots)}{\partial X^{s,\eta}}\right|_{\mathbf{X}=\mathbf{H}} \Sigma^\eta(H^s, H^{s'}) \left.\frac{\partial p(\mathbf{X}^1, \ldots)}{\partial X^{s',\eta}}\right|_{\mathbf{X}=\mathbf{H}} \tag{4.3}$$

where $\Sigma^\eta(H^s, H^{s'})$ is the covariance matrix for quantities computed on ensemble η. Since quantities computed on different ensembles are statistically independent, the covariance vanishes and the terms in the external sum (the one over the index η) can be computed independently one from the other.

The contribution coming from a single ensemble is generally computed from data points belonging to one or more Markov chains. If this is the case, points belonging to the same chain are correlated to each other (auto-correlation), therefore a correct treatment of $\Sigma^\eta(H^s, H^{s'})$ requires knowledge of time series analysis, that we will shortly introduce.

4.1. Auto-correlation functions

Let us consider a finite realization of a stationary stochastic process $\mathcal{R}_N^r$. In case of a Markov processes we assume that the weight of the first configuration in each replica q_0^i is sufficiently close to $W(q)$, the one at equilibrium (this can always be accomplished by discarding a sufficient number of configurations prior to q_0^i). Following ref. [88] let us

first restrict our attention to primary observables A_α namely functions $a_\alpha(q)$ on $\mathcal{Q}$ that have values in $\mathbb{R}$. The Greek index enumerates different observables and the capitalized symbol A_α stands for the ensemble expectation value (EEV) of the primary observable (i.e. the path integral expectation value of QCD, we do not use brackets here to keep notation light and to conform to the notation used in eq. (4.1)

$$A_\alpha = \sum_{q \in \mathcal{Q}} a_\alpha(q) W(q) \,. \tag{4.4}$$

The estimates of A_α on a given realization $\mathcal{R}_N^r$ are denoted by $a_\alpha^{t,r}$ where t is a discrete time index that runs up to N. This notation is redundant since $a_\alpha^{t,r} \equiv a_\alpha(q_t^r)$, but such redundancy is necessary to keep notation compact. In the space of all replicas of finite length N we define an ensemble average

$$\langle\!\langle A_\alpha^t \rangle\!\rangle = \lim_{R \to \infty} \frac{1}{R} \sum_{r=1}^{R} a_\alpha^{t,r} \equiv A_\alpha \,, \tag{4.5}$$

where the double brackets will be used from here on to denote the ensemble average in the different replicas "direction" and the superscript t is there to remind that the average is taken at fixed MC time. The equivalence in eq. (4.5) is generally valid even though when treating asymptotically stochastic processes one has to keep in mind the possible presence of thermalization effects, that can anyhow still be made arbitrarily small by taking larger values of t. We remind that with ergodic algorithms (virtually all LQCD algorithms in use) a further equivalence holds, namely

$$A_\alpha = \lim_{N \to \infty} \frac{1}{N} \sum_{t=1}^{N} a_\alpha^{t,r} \tag{4.6}$$

independently on the choice of replica r.

Let us here introduce the deviations of primary quantity estimates from their EEV

$$\delta_\alpha^{t,r} = a_\alpha^{t,r} - A_\alpha \quad \text{and} \quad \overline{\delta}_\alpha^r = \frac{1}{N} \sum_{t=1}^{N} \delta_\alpha^{t,r} \,, \tag{4.7}$$

with which we define the *auto-correlation* function

$$\Gamma_{\alpha\beta}(\tau) = \langle\!\langle \delta_\alpha^t \delta_\beta^{t+\tau} \rangle\!\rangle \,, \tag{4.8}$$

namely the covariance between measurements separated by a MC time interval τ (the lag). $\Gamma_{\alpha\beta}(\tau)$ is only a function of the lag because of translation invariance in the MC time direction. The auto-correlation function satisfies some general properties

- $\Gamma_{\alpha\beta}(0)$ is the standard covariance $\sigma_{\alpha\beta}^2$

- $\Gamma_{\alpha\beta}(\tau) = \Gamma_{\beta\alpha}(\tau) = \Gamma_{\alpha\beta}(-\tau)$

- $|\Gamma_{\alpha\alpha}(\tau)| \leq \Gamma_{\alpha\alpha}(0)$.

A second related quantity is the normalized auto-correlation function

$$\rho_{\alpha\beta}(\tau) = \frac{\Gamma_{\alpha\beta}(\tau)}{\sqrt{\Gamma_\alpha(0)\Gamma_\beta(0)}} \,. \tag{4.9}$$

The function $\rho_{\alpha\beta}(\tau)$ is the correlation coefficient between pairs of values of the time series separated by an interval of length τ. As τ increases we would expect the correlation between $a_\alpha^{t,r}$ and $a_\beta^{t+\tau,r}$ to decrease, since if τ is large the stochastic process will in general have "forgotten" at MC time $t + \tau$ the state in which it was at time t. The rate at which the auto-correlation function decays to zero can thus be interpreted as a measure of the "memory" of the process.

In the case of ergodic Markov chains it is possible to further characterize the asymptotic behaviour of the auto-correlation function

$$|\Gamma_{\alpha\alpha}(\tau)| \overset{\tau\to\infty}{\sim} e^{-\tau/\tau_{\exp}} \tag{4.10}$$

where $\tau_{\exp}$ is the exponential auto-correlation time. The quantity $\tau_{\exp}$ is defined observable independent and characterizes the relaxation time of the slowest mode of the system. It can be shown [75] that this is the same quantity that characterizes the rate of convergence to equilibrium from an initial arbitrary distribution as discussed at the end of sec. 3.2.2, in particular convergence can be bounded from above in a way similar to eq. (4.10).

4.1.1. Average estimator and its error

In typical LQCD applications the number of replicas available for a single measurement are of the order of one (rarely one has more than two replicas and most often measurements all belong to the same realization). So data available typically consists of a finite number of recorded values obtained in a single run. The estimator of the EEV for each single replica $\mathcal{R}_N^r$ is given by the standard sample mean

$$\overline{A}_\alpha^r = \frac{1}{N}\sum_{t=1}^{N} a_\alpha^{t,r}\,, \tag{4.11}$$

where $\overline{A}_\alpha^r$ is an (unbiased) estimator of A_α in view of eq. (4.6). The covariance of this estimator is given by

$$\mathrm{cov}[\overline{A}_\alpha \overline{A}_\beta] = \frac{1}{N^2}\sum_{t=1}^{N}\sum_{s=1}^{N}\Gamma_{\alpha\beta}(t-s) = \frac{1}{N^2}\sum_{\tau=-(N-1)}^{N-1}(N-|\tau|)\,\Gamma_{\alpha\beta}(\tau)\,, \tag{4.12}$$

where the covariance between two estimates at some definite MC time is given by the auto-correlation function of eq. (4.8). From this expression one easily writes the variance

$\mathcal{Q}$	State space of a Markov chain, its elements are $q \in \mathcal{Q}$.
$\mathcal{R}_N^r$	r-th realization of a Markov chain of length N. It is an ordered set $\mathcal{R}_N^r \equiv \{q_0^r, q_1^r, \ldots, q_N^r\}$ of N states.
A_α	Expectation value of a primary observable (see eq. (4.4)). A set of primary quantities is denoted with the boldface symbol $\mathbf{A} = \{A_\alpha\}$.
$\langle\!\langle A_\alpha^t \rangle\!\rangle$	Expectation value of a primary observable in the replicas space (see eq. (4.5)). The average is performed at fixed MC time t. In general we will speak of stationary processes, namely $\langle\!\langle A_\alpha^t \rangle\!\rangle = A_\alpha$.
$a_\alpha(q)$	Function $a_\alpha : \mathcal{Q} \to \mathbb{R}$ that estimates A_α on configuration $q \in \mathcal{Q}$.
$a_\alpha^{t,r}$	Estimate of A_α on q_t^r, it is a synonym of $a_\alpha(q_t^r)$.
$\overline{A}_\alpha^r$	Estimator of A_α from a single chain r (see eq. (4.11)).
$\overline{\overline{A}}_\alpha$	Average of the estimator $\overline{A}_\alpha^r$ over multiple chains (see eq. (4.18).
$\delta_\alpha^{t,r}$	Deviations $\delta_\alpha^{t,r} = a_\alpha^{t,r} - A_\alpha$ (see eq. (4.7)).
$f(\cdot)$	$f : \mathbb{R}^n \to \mathbb{R}$ is a function of n primary quantities $\mathbf{A}$ and for this reason is called a **first-level-derived** quantity.
F	Value of the function $F = f(\mathbf{A})$ (typical examples in LQCD are hadron masses or decay constants).
F_α, $F_{\alpha\beta}$	First and second derivative of $f(\cdot)$ w.r.t. the α (or β) -th argument evaluated at $\mathbf{A}$ (see eq. (4.38))
$\overline{F}_\alpha^r$, $\overline{\overline{F}}_\alpha$	Estimates of F_α evaluated at $\overline{\mathbf{A}}$ (or $\overline{\overline{\mathbf{A}}}$) (see eq. (4.38))
$f^{t,r}$	First-level reduced quantity defined in eq. (4.44).
$\overline{F}^r$	Estimator of F from a single chain r (see eq. (4.35)).
$\overline{\overline{F}}$, $\widehat{F}$	Unbiased and biased estimator of F over multiple chains (see eq. (4.36)).
$\overline{f}^{t,r}, \overline{\overline{f}}^{t,r}$	Estimators of first-level reduced quantities that have been defined in eq. (4.51).

Table 4.1.: Summary table of symbols commonly used throughout this section

of the estimator given in eq. (4.11)

$$\text{var}[\overline{A}_\alpha] = \frac{1}{N^2} \sum_{\tau=-(N-1)}^{N-1} (N - |\tau|)\, \Gamma_{\alpha\alpha}(\tau) \tag{4.13}$$

$$= \frac{\sigma_\alpha^2}{N} \sum_{\tau=-(N-1)}^{N-1} \left(1 - \frac{|\tau|}{N}\right)\, \rho_{\alpha\alpha}(\tau)\,, \tag{4.14}$$

and the square root of the variance in the large N limit (by the central limit theorem) is then the statistical error of the estimate $\overline{A}_\alpha^r$

$$\delta\overline{A}_\alpha = \sqrt{\text{var}[\overline{A}_\alpha]} \tag{4.15}$$

with the usual statistical meaning of width of a Gaussian distribution.

Introducing the integrated auto-correlation time

$$\tau_{\text{int}}(A_\alpha) = \frac{1}{2} + \sum_{k=1}^{\infty} \rho_{\alpha\alpha}(k)\,, \tag{4.16}$$

we give the approximation that is used throughout the literature

$$(\delta\overline{A}_\alpha)^2 \simeq \frac{1}{N} \sum_{\tau=-\infty}^{\infty} \Gamma_{\alpha\alpha}(\tau) = \sigma_\alpha^2 \frac{2\,\tau_{\text{int}}(A_\alpha)}{N}\,, \tag{4.17}$$

that differs from the expression in eq. (4.13) by terms that are $O((\tau_{\text{exp}}/N)^2)$.

Since different replicas are assumed to be statistically independent, the covariance of the estimator

$$\overline{\overline{A}}_\alpha = \frac{1}{R} \sum_{r=1}^{R} \overline{A}_\alpha^r \tag{4.18}$$

that averages over a finite number of them is simply given by

$$\text{cov}[\overline{\overline{A}}_\alpha \overline{\overline{A}}_\beta] = \frac{1}{RN^2} \sum_{\tau=-(N-1)}^{N-1} (N - |\tau|)\, \Gamma_{\alpha\beta}(\tau)\,, \tag{4.19}$$

applying again the approximation in eq. (4.17) the expression

$$(\delta\overline{\overline{A}}_\alpha)^2 \simeq \sigma_\alpha^2 \frac{2\,\tau_{\text{int}}(A_\alpha)}{RN} \tag{4.20}$$

given also in ref. [88] is recovered. The estimator $\overline{\overline{A}}_\alpha$ is unbiased and in the limit of large R, $\overline{\overline{A}}$ values are normally distributed, independently of whether individual $\overline{A}^r$ are.

4.1.2. Estimation of the auto-correlation function and its error

In a way analogous to how we estimate the expectation value of an observable from an average in MC time, it is also possible to estimate the auto-correlation function itself:

$$\overline{\Gamma}^r_{\alpha\beta}(\tau) = \frac{1}{N - |\tau|} \sum_{t=1}^{N-|\tau|} (a^{t,r}_\alpha - \overline{A}^r_\alpha)(a^{t+|\tau|,r}_\beta - \overline{A}^r_\beta) \tag{4.21}$$

and

$$\overline{\overline{\Gamma}}_{\alpha\beta}(\tau) = \frac{1}{R(N - |\tau|)} \sum_{r=1}^{R} \sum_{t=1}^{N-|\tau|} (a^{t,r}_\alpha - \overline{\overline{A}}_\alpha)(a^{t+|\tau|,r}_\beta - \overline{\overline{A}}_\beta) \, . \tag{4.22}$$

The estimators in the two equations (4.21 and 4.22) are biased by the fact that we use $\overline{A}^r_\alpha$ (or $\overline{\overline{A}}_\alpha$) instead of A_α. The bias can be evaluated through

$$\sum_{t=1}^{N-|\tau|} (a^{t,r}_\alpha - \overline{A}^r_\alpha + (\overline{A}^r_\alpha - A_\alpha))(a^{t+|\tau|,r}_\beta - \overline{A}^r_\beta + (\overline{A}^r_\beta - A_\beta)) =$$

$$(N - |\tau|)(\overline{A}^r_\alpha - A_\alpha)(\overline{A}^r_\beta - A_\beta) + \sum_{t=1}^{N-|\tau|} (a^{t,r}_\alpha - \overline{A}^r_\alpha)(a^{t+|\tau|,r}_\beta - \overline{A}^r_\beta) \tag{4.23}$$

that together with eq. (4.21) gives the following EEV

$$\langle\!\langle \overline{\Gamma}_{\alpha\beta}(\tau) \rangle\!\rangle = \Gamma_{\alpha\beta}(\tau) - \mathrm{cov}[\overline{A}_\alpha \overline{A}_\beta] \tag{4.24}$$

where the expression for the covariance is the one in eq. (4.12). The bias in eq. (4.22) is obtained by simply replacing bars with double bars in eq. (4.24). This bias is an $O(1/RN)$ effect and for most applications it can be neglected (compared to the statistical fluctuations of $\overline{\overline{\Gamma}}$ that, as we discuss next, are of $O(1/\sqrt{RN})$).

The computation of second order statistical properties of the estimate $\overline{\Gamma}$ of the auto-correlation function is done by considering EEV of products, e.g. $\overline{\Gamma}^r(t)\overline{\Gamma}^r(t+s)$, that means fourth order properties in terms of the primary observables, namely EEVs in the form $\langle\!\langle \delta^t_\alpha \delta^{t+s}_\beta \delta^{t+u}_\gamma \delta^{t+v}_\eta \rangle\!\rangle$. For this quantity we use the identity

$$\langle\!\langle \delta^t_\alpha \delta^{t+s}_\beta \delta^{t+u}_\gamma \delta^{t+v}_\eta \rangle\!\rangle =$$

$$\langle\!\langle \delta^t_\alpha \delta^{t+s}_\beta \rangle\!\rangle \langle\!\langle \delta^{t+u}_\gamma \delta^{t+v}_\eta \rangle\!\rangle + \langle\!\langle \delta^t_\alpha \delta^{t+u}_\gamma \rangle\!\rangle \langle\!\langle \delta^{t+s}_\beta \delta^{t+v}_\eta \rangle\!\rangle +$$

$$\langle\!\langle \delta^t_\alpha \delta^{t+v}_\eta \rangle\!\rangle \langle\!\langle \delta^{t+s}_\beta \delta^{t+u}_\gamma \rangle\!\rangle + \kappa_4 \tag{4.25}$$

where κ_4 is the fully connected four point function. If we look at the very special case of $t = s = u = v = 0$ the expression is reduced to a quantum field theory identity and the fully connected term, as a consequence of locality, is known to vanish rapidly as the separation in space-time of the primary observables is increased. In more general cases

and at MC time $\neq 0$ not much can be said about the relative size of κ_4 and, as far as we know, a thorough discussion can not be found in the literature. In section 4.5 we look at this particular issue in the case of the three dimensional ϕ^4 lattice model.

Since we do not wish to further discuss the bias in the estimate of second order properties (that is the systematics of the error of the error), to simplify the discussion we will assume that $\langle A_\alpha \rangle$ is known so that we can express the (now unbiased) estimator of the auto-correlation function as

$$\overline{\Gamma}^r_{\alpha\beta}(\tau) = \frac{1}{N - |\tau|} \sum_{t=1}^{N-|\tau|} \delta_\alpha^{t,r} \delta_\beta^{t+\tau,r} \; , \qquad (4.26)$$

we do not introduce a new symbol here, but it will be clear from the context whether we mean eq. (4.21) or eq. (4.26).

The quantity needed for computing the statistical error of this estimator of $\Gamma(\tau)$ is the following covariance matrix

$$\mathrm{cov}\left[\overline{\Gamma}_{\alpha\beta}(\tau_1)\overline{\Gamma}_{\alpha\beta}(\tau_2)\right] = \langle\!\langle \overline{\Gamma}_{\alpha\beta}(\tau_1)\overline{\Gamma}_{\alpha\beta}(\tau_2)\rangle\!\rangle - \langle\!\langle \overline{\Gamma}_{\alpha\beta}(\tau_1)\rangle\!\rangle\langle\!\langle \overline{\Gamma}_{\alpha\beta}(\tau_2)\rangle\!\rangle \qquad (4.27)$$

where the first quantity on the r.h.s. is

$$\langle\!\langle \overline{\Gamma}_{\alpha\beta}(\tau_1)\overline{\Gamma}_{\alpha\beta}(\tau_2)\rangle\!\rangle = \frac{1}{(N-\tau_1)(N-\tau_2)} \sum_{t=1}^{N-\tau_1} \sum_{s=1}^{N-\tau_2} \langle\!\langle \delta_\alpha^t \delta_\beta^{t+\tau_1} \delta_\alpha^s \delta_\beta^{s+\tau_2}\rangle\!\rangle \qquad (4.28)$$

with the assumption $\tau_1 \geq 0$ and $\tau_2 \geq 0$. Using the identity in eq. (4.25), the MC time invariance of stationary processes and the definition of $\Gamma_{\alpha\beta}(\tau)$ we derive

$$\mathrm{cov}\left[\overline{\Gamma}_{\alpha\beta}(\tau_1)\overline{\Gamma}_{\alpha\beta}(\tau_2)\right] \simeq$$

$$\frac{1}{(N-\tau_1)(N-\tau_2)} \sum_{t=1}^{N-\tau_1} \sum_{s=1}^{N-\tau_2} \Gamma_{\alpha\alpha}(s-t)\Gamma_{\beta\beta}(s-t+\tau_2-\tau_1)$$

$$+ \Gamma_{\alpha\beta}(s-t+\tau_2)\Gamma_{\alpha\beta}(s-t-\tau_1) \quad (4.29)$$

where the approximation comes from the fact that we drop κ_4. Neglecting κ_4 introduces an uncontrolled systematic effect in the determination of the error of the estimated auto-correlation function that could in principle be studied by looking at a large number of replicas. In this respect the study that we have performed for the ϕ^4 model (see e.g. fig. (4.7)) shows that the $\kappa_4 = 0$ approximation allows a computation of the error of $\overline{\rho}^r_{\alpha\alpha}(\tau)$ close to the unbiased estimate, even in the the case of processes that show large values of κ_4.

If in eq. (4.29) one repeats the sum over the diagonals used to derive eq. (4.13), we get a quite complicated formula that can be found in ref. [68]. A simpler expression that can

be used to derive the approximations to be used in practical error analysis is

$$\text{cov}\left[\overline{\Gamma}_{\alpha\beta}(\tau_1)\overline{\Gamma}_{\alpha\beta}(\tau_2)\right] \simeq$$

$$\frac{N}{(N-\tau_1)(N-\tau_2)} \sum_{k=-\infty}^{\infty} \Gamma_{\alpha\alpha}(k)\Gamma_{\beta\beta}(k+\tau_2-\tau_1)+$$

$$\Gamma_{\alpha\beta}(k+\tau_2)\Gamma_{\alpha\beta}(k-\tau_1) \quad (4.30)$$

that for large N is equivalent to the expression in eq. (4.29) up to terms that are exponentially suppressed.

From this last formula the variance of $\overline{\Gamma}_{\alpha\alpha}$ can be quickly derived and is given by

$$\text{var}\left[\overline{\Gamma}_{\alpha\alpha}(\tau)\right] \simeq \frac{1}{N-\tau} \sum_{k=-\infty}^{\infty} \Gamma_{\alpha\alpha}^2(k) + \Gamma_{\alpha\alpha}(k+\tau)\Gamma_{\alpha\alpha}(k-\tau) , \quad (4.31)$$

that is a particularly useful expression since, as we will see in the next section, there is almost no situation in which the full covariance matrix needs to be computed (unless one is specifically interested in the analysis of the auto-correlation function itself).

We finally define the estimators of the normalized auto-correlation function as

$$\overline{\rho}_{\alpha\alpha}^r(\tau) = \frac{\overline{\Gamma}_{\alpha\alpha}^r(\tau)}{\overline{\Gamma}_{\alpha\alpha}^r(0)} \quad \text{and} \quad \overline{\overline{\rho}}_{\alpha\alpha}(\tau) = \frac{\overline{\overline{\Gamma}}_{\alpha\alpha}(\tau)}{\overline{\overline{\Gamma}}_{\alpha\alpha}(0)} \quad (4.32)$$

whose error (that can be propagated by using the covariance given in eq. (4.29)) is approximated, up to $\text{O}(1/\tau_{\text{int}})$ terms, by

$$\text{var}[\overline{\rho}_{\alpha\alpha}(\tau)] \simeq \frac{1}{N-\tau} \sum_{k=1}^{\infty} \left\{\rho_{\alpha\alpha}(k+\tau) + \rho_{\alpha\alpha}(k-\tau) - 2\rho_{\alpha\alpha}(k)\rho_{\alpha\alpha}(\tau)\right\}^2 \quad (4.33)$$

with this last formula for the first time given in ref. [43].

All the expressions involving infinite sums must be evaluated keeping in mind that we do not have access to the auto-correlation function at all times, but only at its approximated value over a finite interval. One of the quantities that we will actually compute is $\overline{\rho}(\tau)$ and its error, for which we use eq. (4.33) evaluated with $\overline{\rho}(\tau)$ truncated at a suitable (large enough) MC time. The second quantity that we extensively use is τ_{int} but we leave the discussion of methods for estimating it to a later section.

4.1.3. Functions of primary observables

Let us now consider the set of *primary* quantities $\mathbf{A} = \{A_\alpha\}$. As before with $\overline{\mathbf{A}}^r$ we denote the random variable corresponding to the estimate over a single realization and with $\overline{\overline{\mathbf{A}}}$ the one corresponding to averages over multiple realizations.

In subsequent steps of the analysis it often becomes necessary to compute functions of EEVs and their errors, $f : \mathbb{R}^n \to \mathbb{R}$. We call these *first-level-derived* quantities. We

define the value of a derived quantity computed on the EEV of primary quantities with

$$F \equiv f(\mathbf{A}) \tag{4.34}$$

and estimates over single replicas with

$$\overline{F}^r = f(\overline{\mathbf{A}}^r) \tag{4.35}$$

while for averages over a finite number of replicas we use

$$\overline{\overline{F}} = f(\overline{\overline{\mathbf{A}}}) \quad \text{and} \quad \widehat{F} = \frac{1}{R}\sum_{r=1}^{R} \overline{F}^r \,, \tag{4.36}$$

where conventions here differ from those in ref. [88]. Typical derived quantities in LQCD are smooth functions in a neighborhood of $\mathbf{A}$ and for this reason, without loss of generality, we assume that the function $f(\cdot)$ is differentiable in $\mathbf{A}$. If now with $\mathbf{F}$ we denote a set of first-level-derived quantities, it is possible to construct second-level-derived quantities through the relation $H = h(\mathbf{F})$ this definition can be arbitrarily extended by recursion. The notion of first-, second-, ..., n^{th}-level-derived quantity is here introduced as a useful distinction for the sole purpose of the error analysis, and it is only procedural.

The error analysis of derived quantities like F (or H) can be carried on by noting that since the variance of $\overline{\mathbf{A}}^r \propto N^{-1}$, the Taylor expansion of $f(\cdot)$ in the deviations $\overline{\delta}_\alpha^r$, (see eq. (4.7)), in the large N limit is justified

$$\overline{F}^r = F + \sum_\alpha F_\alpha \overline{\delta}_\alpha^r + \frac{1}{2}\sum_{\alpha\beta} F_{\alpha\beta}\overline{\delta}_\alpha^r\overline{\delta}_\beta^r + \ldots \tag{4.37}$$

where F_α are the derivatives

$$F_\alpha = \left.\frac{\partial f(\mathbf{X})}{\partial X_\alpha}\right|_{\mathbf{X}=\mathbf{A}} , \quad F_{\alpha\beta} = \left.\frac{\partial^2 f(\mathbf{X})}{\partial X_\alpha \partial X_\beta}\right|_{\mathbf{X}=\mathbf{A}} . \tag{4.38}$$

From the expansion one can see that both $\overline{F}$ and $\widehat{F}$ are biased by

$$\lang\!\langle\, \overline{F} - F \,\rangle\!\rangle = \lang\!\langle\, \widehat{F} - F \,\rangle\!\rangle \simeq \frac{1}{2}\sum_{\alpha\beta} F_{\alpha\beta}\, \text{cov}[\overline{A}_\alpha \overline{A}_\beta] \propto N^{-1} \tag{4.39}$$

where the bias goes away for large N. The bias of $\overline{\overline{F}}$ is further reduced by a factor R^{-1}

$$\lang\!\langle\, \overline{\overline{F}} - F \,\rangle\!\rangle = \frac{1}{R}\lang\!\langle\, \overline{F} - F \,\rangle\!\rangle . \tag{4.40}$$

These biases can often be neglected compared to the leading $\mathrm{O}(1/\sqrt{N})$ size of the statistical error. When the quantity of interest is highly non linear w.r.t. the estimated

size of the statistical error, i.e.

$$\left| \left. \frac{\partial f(\mathbf{X})}{\partial X_\alpha} \right|_{\mathbf{X}=\overline{A}_\alpha+\delta\overline{A}_\alpha} - \left. \frac{\partial f(\mathbf{X})}{\partial X_\alpha} \right|_{\mathbf{X}=\overline{A}_\alpha-\delta\overline{A}_\alpha} \right| \gg \overline{F}\, \delta\overline{A}_\alpha \,, \tag{4.41}$$

it can be advisable to try to estimate the size of the bias (e.g. with the method suggested in ref. [88] or with a jack-knife analysis as explained in ref. [46]). It is also interesting to note that if $R \gtrsim N/\tau_{\mathrm{int}}$, a non-zero bias of $\widehat{F}$ eventually becomes of the same order of the statistical error (since the statistical error gets an extra $1/\sqrt{R}$ factor that the bias does not have). To prevent this it is always advisable to use $\overline{\overline{F}}$ as a better estimate.

The expression for the variance at leading order in the Taylor expansion is

$$\mathrm{var}\left[\overline{F}\right] = \left\langle\!\!\left\langle (\overline{F}-F)^2 \right\rangle\!\!\right\rangle = \sum_{\alpha,\beta} F_\alpha F_\beta \, \mathrm{cov}\left[\overline{A}_\alpha \overline{A}_\beta\right] \tag{4.42}$$

$$\simeq \sum_{\alpha,\beta} \frac{F_\alpha F_\beta}{N} \sum_{\tau=-\infty}^{\infty} \left\langle\!\!\left\langle \delta_\alpha^t \delta_\beta^{t+\tau} \right\rangle\!\!\right\rangle \,, \tag{4.43}$$

whose square root can again be interpreted as the statistical error $\delta\overline{F}$ of the quantity $\overline{F}^r$ in the large N limit. The approximation in eq. (4.43) is done neglecting terms that are exponentially small in N (see e.g. eq. (4.17)). In ref. [88] the practical method proposed to construct $\mathrm{var}\left[\overline{F}\right]$, consists in exchanging the order of the sums in eq. (4.43), postponing to the last step of the analysis the sum over Monte Carlo time. We now generalize that method to the error analysis of n-th level derived observables.

We begin by introducing the reduced quantities

$$f^{t,r} = F + \sum_\alpha F_\alpha \delta_\alpha^{t,r} \,, \tag{4.44}$$

for which $\left\langle\!\!\left\langle f^t \right\rangle\!\!\right\rangle = F$ holds. The variance in eq. (4.43) can then be expressed as

$$\mathrm{var}\left[\overline{F}\right] \simeq \frac{1}{N} \sum_{\tau=-\infty}^{\infty} \left\langle\!\!\left\langle (f^t - F)(f^{t+\tau} - F) \right\rangle\!\!\right\rangle = \frac{1}{N} \sum_{\tau=-\infty}^{\infty} \Gamma_{\mathrm{f}}(\tau) \,, \tag{4.45}$$

where we introduce the auto-correlation function of the first-level-derived observable $\Gamma_{\mathrm{f}}(\tau)$. In a way analogous to what we have done for primary observables in eq. (4.16), we define the integrated auto-correlation time of a first-level-derived observable as

$$\tau_{\mathrm{int}}(F) = \frac{1}{2} + \sum_{\tau=1}^{\infty} \rho_{\mathrm{f}}(\tau) \,, \tag{4.46}$$

with $\rho_{\mathrm{f}}(\tau) = \Gamma_{\mathrm{f}}(\tau)/\Gamma_{\mathrm{f}}(0)$. It should be clear by now how the same reasoning can be extended to the error analysis of second or higher level derived observables.

In the case of the observable P defined in eq. (4.1), the error is computed via the

ensemble-wise reduced quantities

$$p^{\eta;t,r} = P + \sum_s P_{s,\eta}(h^{s,\eta;t,r} - H^{s,\eta}) \tag{4.47}$$

that are the analogue of the ones defined in eq. (4.44), with

$$P_{s,\eta} = \left.\frac{\partial f(\mathbf{X}^\eta)}{\partial X^{s,\eta}}\right|_{\mathbf{X}^\eta = \mathbf{H}^\eta}, \tag{4.48}$$

and where $h^{s,\eta;t,r}$ can represent either an n-th-level-reduced or a primary quantity (in this sense reduced observables can be treated the same way as primary observables), with the first two indices labelling the observable and the second two labelling the MC time. The contribution to the statistical error of $\overline{P}$ coming from the MC computation is then given by (see also eq. (4.3))

$$(\delta\overline{P})^2 \simeq \sum_{\eta=1}^{N_{\mathrm{E}}} \frac{1}{N_\eta} \sum_{\tau=-\infty}^{\infty} \Gamma_{\mathrm{p}^\eta}(\tau) \tag{4.49}$$

where N_η is the extent of the MC simulation on ensemble η, and

$$\Gamma_{\mathrm{p}^\eta}(\tau) = \left\langle\!\!\left\langle (p^{\eta;t} - P)(p^{\eta;t+\tau} - P) \right\rangle\!\!\right\rangle \tag{4.50}$$

is an auto-correlation function analogue to the one defined in eq. (4.45). If the quantity P has an additional dependence on quantities that do not come from a Monte Carlo computation (or, in case they do, quantities for which only the statistical error is known) one can sum additional contributions in quadrature to eq. (4.49) and in this way obtain the complete statistical error.

The quantities we have defined so far all involve exact EEVs, but in practice the auto-correlation function of the reduced quantities can be estimated introducing (here we show the case of F that can easily be extended to P)

$$\overline{f}^{t,r} = \overline{F}^r + \sum_\alpha \overline{F}^r_\alpha(a^{t,r}_\alpha - \overline{a}^r_\alpha) \tag{4.51}$$

and

$$\overline{\overline{f}}^{t,r} = \overline{\overline{F}} + \sum_\alpha \overline{\overline{F}}_\alpha(a^{t,r}_\alpha - \overline{\overline{A}}_\alpha) \tag{4.52}$$

where $\overline{F}^r_\alpha$ (or $\overline{\overline{F}}_\alpha$) is an estimate of the derivative obtained by evaluating eq. (4.38) at $\mathbf{X} = \overline{\mathbf{A}}^r$ (or $\overline{\overline{\mathbf{A}}}$): this approximation is a secondary source of bias in the estimator of the variance (besides the one in eq. (4.24)) and as also stated in ref. [88] we will ignore this

$O(1/N)$ bias altogether. We finally define the estimator

$$\overline{\Gamma}_{\mathrm{f}}^{r}(\tau) = \frac{1}{N - |\tau|} \sum_{t=1}^{N-|\tau|} (\overline{f}^{t,r} - \overline{F}^r)(\overline{f}^{t+|\tau|,r} - \overline{F}^r) \tag{4.53}$$

while we do not write explicitly the $\overline{\overline{\Gamma}}_{\mathrm{f}}(\tau)$ estimator but we refer to eq. (4.22). For the discussion of the statistical properties of the estimators $\overline{\Gamma}_{\mathrm{f}}^{r}(\tau)$ and $\overline{\overline{\Gamma}}_{\mathrm{f}}(\tau)$ we refer back to the discussion in the preceding section.

4.1.4. Estimate of τ_{int} and its error

The actual quantity that one is going to compute in numerical calculations of lattice QCD, besides the EEV estimator, is the statistical error. The expressions in eq. (4.17) require knowledge of the integrated auto-correlation time, a secondary quantity that must be estimated from $\overline{\Gamma}$.

Since the auto-correlation function typically goes to zero exponentially with τ while $\delta\overline{\Gamma}(\tau)$ and $\delta\overline{\rho}(\tau)$ tend to a constant (this can be checked explicitly from eq. (4.31) and eq. (4.33), neglecting the $1/(N-\tau)$ factor that diverges when $\tau \to N$), the signal to noise ratio decreases exponentially making $\Gamma(\tau)$ difficult to determine at large values of τ. Reliable estimates of τ_{int} can nevertheless be obtained since also the contributions to the sum in eq. (4.16) become exponentially negligible at increasing lag. In refs. [88, 53] the proposed estimate

$$\overline{\tau}_{\mathrm{int}}(F, W) = \frac{1}{2} + \sum_{\tau=1}^{W} \overline{\rho}_{\mathrm{f}}(\tau) \tag{4.54}$$

(here F can be either a primary or an n-th-level derived observable) involves a window W to be chosen to balance the systematic error due to truncation

$$\Delta_{\mathrm{f}}(W) = \sum_{\tau=1}^{\infty} \rho_{\mathrm{f}}(W + \tau) \tag{4.55}$$

with the statistical error given by the square root of the variance

$$\mathrm{var}\left[\overline{\tau}_{\mathrm{int}}(F, W)\right] \simeq \frac{4W + 2 - \overline{\tau}_{\mathrm{int}}(F, W)}{N} \overline{\tau}_{\mathrm{int}}^2(F, W) \tag{4.56}$$

whose approximate formula was given for the first time in ref. [53] and subsequently refined in ref. [88].

The value of W should balance between the size of statistical and systematic errors.

The choice that ref. [88] advocates is the one that minimizes an estimate[1]

$$E(W) = e^{-W/\tau_W} + 2\sqrt{W/N} \quad \text{where} \quad \tau_W \approx S\,\overline{\tau}_{\text{int}}(F, W) \tag{4.58}$$

for the sum of statistical and systematic relative error of τ_{int}. S is a parameter that can be tweaked in order to change the value of W (larger values of S generally result in larger values of W). In the publicly available code presented in ref. [88] it has a default value of 1.5, but it must be adjusted by hand if relevant time scales much larger than τ_{int} are present. In other words, a proper choice of S requires an inspection of the particular shape of the auto-correlation function. In some cases the shape may be determined according to some general properties of the underlying Markov process.

4.2. Properties of $\Gamma(t)$ in algorithms with detailed balance

When discussing an ergodic algorithm with detailed balance it is convenient to introduce the symmetric matrix

$$T(q, q') = [W(q')]^{-1/2} P(q' \leftarrow q)[W(q)]^{1/2} \tag{4.59}$$

which has real eigenvalues λ_n, $n \geq 0$, with $\lambda_0 = 1$ and $|\lambda_n| < 1$ for $n \geq 1$. We order the eigenvalues as $\lambda_n \leq \lambda_{n-1}$. There is a complete set of eigenfunctions $\chi_n(q)$ with $\chi_0(q) = [W(q)]^{1/2}$. Starting from the representation that assumes a thermalized chain (as we have done up to now),

$$\Gamma_{\alpha\beta}(\tau) = \sum_{q,q' \in \mathcal{Q}} [a_\beta(q') - A_\beta]\, P^\tau(q' \leftarrow q)\, [a_\alpha(q) - A_\alpha]\, W(q) \tag{4.60}$$

we then have for the auto-correlation function of a derived quantity F

$$\Gamma_{\text{f}}(\tau) =$$
$$\sum_{\alpha\beta} F_\alpha F_\beta \sum_{q,q' \in \mathcal{Q}} [a_\alpha(q) - A_\alpha]\, \chi_0(q)\, T^\tau(q, q')\, \chi_0(q')\, [a_\beta(q') - A_\beta]$$
$$= \sum_{n \geq 1} (\lambda_n)^\tau\, [\eta_n(F)]^2 \tag{4.61}$$

in terms of the "matrix elements"

$$\eta_n(F) = \sum_\alpha F_\alpha \sum_{q \in \mathcal{Q}} \chi_n(q)\chi_0(q)\, [a_\alpha(q) - A_\alpha]. \tag{4.62}$$

---

[1]The exact formula applied in ref. [88] is

$$\tau_W^{-1} = \log\left(\frac{1 + 1/(2\overline{\tau}_{\text{int}}(F, W))}{1 - 1/(2\overline{\tau}_{\text{int}}(F, W))}\right) \Big/ S. \tag{4.57}$$

In the spectral decomposition of eq. (4.61) we can identify the slowest mode with $\tau_{\exp} = -1/\log(\lambda_1)$, provided that $\lambda_1 > 0$. In general all eigenmodes of the matrix T contribute to the above sum over n. However, exact symmetries may entail selection rules with $\eta_n(F)$ vanishing for some n. As an example let us consider a parity symmetry. Parity is a unitary self-adjoint operator that acts on (Euclidean) space-time coordinates as a spatial inversion

$$\mathcal{P} = \mathcal{P}^\dagger = \mathcal{P}^{-1} \,, \quad \mathcal{P}(x_0, \vec{x}) = (x_0, -\vec{x}) \,. \tag{4.63}$$

A representation of the parity operator can be defined to act on states (gauge configurations of lattice QCD), as $q \to \mathcal{P}q$. Parity is defined to be a symmetry of the algorithm if

$$T(\mathcal{P}q, \mathcal{P}q') = T(q, q') \,. \tag{4.64}$$

With respect to the action of $\mathcal{P}$, the eigenfunctions $\chi_n(q)$ of T can then be divided into even ones, $\chi_{n_+}(\mathcal{P}q) = \chi_{n_+}(q)$ and odd ones, $\chi_{n_-}(\mathcal{P}q) = -\chi_{n_-}(q)$. Primary observables can then also be split into even O^+ and odd O^- such that

$$O^p(\mathcal{P}q) = p\,O^p(q) \,, \quad \text{with} \quad p = \pm \tag{4.65}$$

and have an auto-correlation function

$$\Gamma^p(\tau) = \sum_{n_p \geq 1} (\lambda_{n_p})^\tau \left[\eta_{n_p}(O^p)\right]^2 \tag{4.66}$$

with only even or odd contributions. If the ensemble average of odd observables vanishes, one can restrict the attention to $p = +1$. This is the case when the action is parity invariant.

4.2.1. Parity invariance of the HMC with Wilson Dirac fermions

In a lattice QCD computation that uses the HMC algorithm with Wilson-Dirac fermions, the states in eq. (4.64) are given by $q = \{\Pi, U\}$, where U are gauge field variables and Π are the conjugated momenta. It can be shown that the HMC Hamiltonian in eq. (3.42) is invariant under the action of the parity operator. This implies that the statistical weight in the path integral $W(\Pi, U)$ given in eq. (3.33) is also parity invariant. To prove the invariance of eq. (4.64) we are thus left to show that the transition probability $P(q' \leftarrow q)$ is parity invariant.

Since the HMC is a Metropolis algorithm its transition matrix has the form given in eq. (3.23). The probability of acceptance $P_A(q' \leftarrow q)$ depends exclusively on the Hamiltonian, and is parity invariant. The probability of generating a new configuration is a delta function

$$P_G(q' \leftarrow q) = \delta(\{\Pi', U'\} - \mathfrak{I}[\Pi, U; \epsilon, \tau_{\text{traj}}]) \tag{4.67}$$

up to the momentum reversal step that is a global change of sign of the momentum field

and for this reason trivially parity invariant and the generation of the random Gaussian fields that is also trivially parity invariant.

The step $P_\mathrm{G}(q' \leftarrow q)$ is parity invariant if the parity operator factorizes outside of the integrator, that is if the integrator preserves parity

$$\mathfrak{I}[\mathcal{P}\Pi, \mathcal{P}U; \epsilon, \tau_\mathrm{traj}] = \mathcal{P}\,\mathfrak{I}[\Pi, U; \epsilon, \tau_\mathrm{traj}] \,. \tag{4.68}$$

Parity is a symmetry that is preserved by Hamilton equations (the parity operator commutes with the Hamiltonian), but it seems to us that the validity of this property is not automatically guaranteed for an approximated integrator, and for this reason must be explicitly checked, by showing that that the leapfrog integration scheme commutes with the parity operator. The integrator is defined by chaining the two transformations of eq. (3.36) and of eq. (3.37). The transformation T_U involves only local algebraic relations of fields, and for this reason preserves parity (i.e. $[\mathcal{P}U]^n = \mathcal{P}U^n$ with $n \in \mathbb{N}$). The transformation T_P involves the derivative of the action. Since the action is parity invariant the derivative with respect to the fields is covariant: this fact can be also explicitly checked starting from the expression of the force in eq. (3.43) and in eq. (3.47). The leapfrog integrator thus preserves parity.

In the case of DD-HMC since the boundaries of lattice domains are frozen along a MD trajectory (non active links), to ensure ergodicity, at the beginning of each new trajectory one has to globally shift the domain grid. This shift could in principle be completely random, ensuring parity invariance, but in the implementation that can be found in ref. [40] the shifts alternate random to a series of directed steps that partly break an otherwise perfectly parity invariant algorithm.

4.3. Improved error estimates

For algorithms with detailed balance we are thus able to predict the general formula of the auto-correlation function as a sum of decaying exponentials. This picture does not change even when the spectrum of the Markov matrix contains real negative eigenvalues, since it is always possible to consider the auto-correlation function only at even MD time. Defining $\tau_n = -1/\log(\lambda_n)$ one can see that

$$\sum_{\tau=0}^\infty \mathrm{e}^{-\tau/\tau_n} \leq \tau_n + 1 \leq \tau_\mathrm{exp} + 1 \tag{4.69}$$

with which we define the following upper bound for the truncation bias of eq. (4.55)

$$\Delta_\mathrm{f}(W) \leq (\tau_\mathrm{exp} + 1) \sum_{n \geq 1} \mathrm{e}^{-W/\tau_n} [\eta_n(F)]^2 \simeq \tau_\mathrm{exp}\,\Gamma_\mathrm{f}(W) \,, \tag{4.70}$$

where the approximation is valid when $\tau_\mathrm{exp} \gg 1$. We expect these bounds to hold quite generically, also for algorithms which do not satisfy detailed balance. Certainly MC experiments that we have seen so far in lattice QCD are in agreement with such a behaviour.
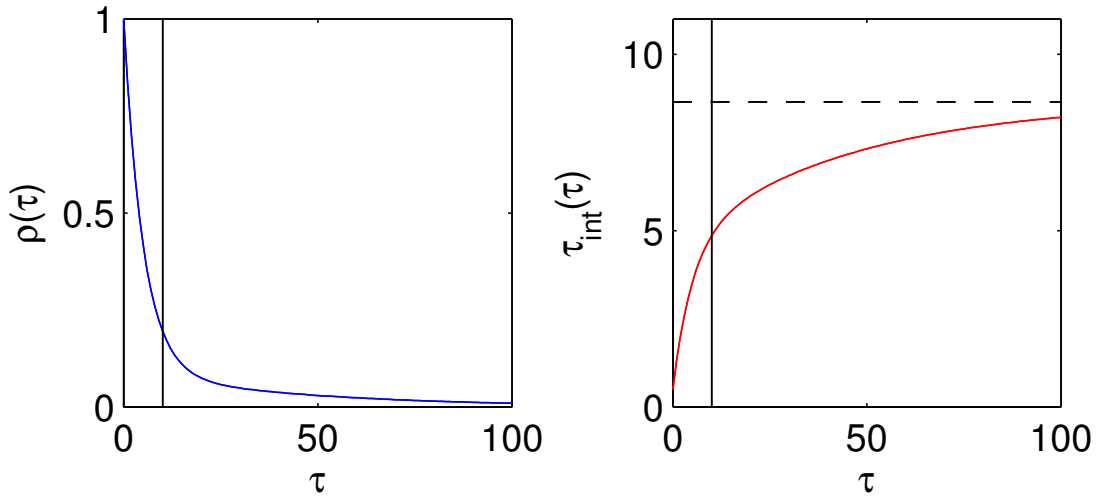
Figure 4.1.: **Left:** sketch of an auto-correlation function with a long tail. **Right:** its integrated auto-correlation time. If $\rho(\tau)$ is known with a 15% accuracy, a window that cuts the tail as the one shown by the solid black line is not uncommon: this would translate in a 50% underestimate of τ_{int}.

Let us now *assume* that we are in *a situation* where the following is true

1. There is some knowledge about τ_{exp} from previous MC runs or an extrapolation from other parameters of the simulated theory.

2. The considered MC run is still long compared to τ_{exp} itself,

$$N \gg \tau_{\mathrm{exp}} , \tag{4.71}$$

   but not so long that one can just sum up the auto-correlation function with a window $W \sim \tau_{\mathrm{exp}}$.

3. We are interested in an error estimate which safely includes the contribution represented by the slow mode corresponding to τ_{exp} or slow modes n with $\tau_n \approx \tau_{\mathrm{exp}}$.

We propose to choose a window W_{l}, according to the criterion of ref. [88], eq. (4.58) and the associated

$$\tau_{\mathrm{int}}^{\mathrm{l}}(F) = \overline{\tau}_{\mathrm{int}}(F, W_{\mathrm{l}}) \tag{4.72}$$

as well as a second window W_{u} where the auto-correlation function is still significant by (say) three standard deviations and add an estimate of the tail giving

$$\tau_{\mathrm{int}}^{\mathrm{u}}(F) = \overline{\tau}_{\mathrm{int}}(F, W_{\mathrm{u}}) + \tau_{\mathrm{exp}}\overline{\rho}_{\mathrm{f}}(W_{\mathrm{u}}) . \tag{4.73}$$

In cases where ρ_{f} falls very quickly and is either compatible with zero at short time

$t = W_0$, say $W_0 = 5$, or it is negative due to statistical fluctuations we replace this estimate by

$$\tau_{\text{int}}^{\text{u}}(F) = \overline{\tau}_{\text{int}}(F, W_0) + 2\tau_{\text{exp}}\delta[\overline{\rho}_{\text{f}}(W_0)] \quad \text{for} \quad \delta[\overline{\rho}_{\text{f}}(W_0)] > \overline{\rho}_{\text{f}}(W_0) \,, \tag{4.74}$$

where $\delta[\overline{\rho}]$ is the estimated error of $\overline{\rho}$ and W is either W_{u} or $W_{\text{u}} + 1$, whichever gives the smallest value of $\tau_{\text{int}}^{\text{u}}(F)$. When one is interested in $\tau_{\text{int}}(F)$ itself, e.g. for the investigation of algorithms, one should choose an interval covering $\tau_{\text{int}}^{\text{l}}(F)$ and $\tau_{\text{int}}^{\text{u}}(F)$ together with their statistical errors. If on the other hand one just wants a safe estimate of the error of the observable we propose to use $\tau_{\text{int}}^{\text{u}}(F)$.

An objection to the above formulae is that from a real world Monte Carlo simulation it is virtually impossible to obtain a definite knowledge about the longest time constant(s) involved ($\tau_n \simeq \tau_{\text{exp}}$). For this reason it is useful sometimes to distinguish by introducing the time constant τ_* defined as our best estimate of the dominant time constant, which can either be taken from a model or by investigating a large number of observables and take the largest observed value. All formulae can then be re-expressed in terms of τ_* and, also in case the identified mode is not the real τ_{exp}, the proposed method actually provides a more conservative estimate of the contributions up to the lower threshold, and can therefore improve the analysis.

4.4. Decoupling and dynamical correlation coefficient

In general the auto-correlation function of an observable will couple to all algorithmic modes that are not forbidden by symmetry.[2] In particular in algorithms with detailed balance the asymptotic relation

$$\rho_{\text{f}}(\tau) \overset{\tau \to \infty}{\sim} C_F \, \text{e}^{-\tau/\tau_{\text{exp}}} \tag{4.75}$$

holds. Larger values of the amplitude $C_F = [\eta_1(F)]^2/\Gamma_{\text{f}}(0)$ mean a stronger coupling (at a given lattice spacing) between the observable F and the slow mode of the simulation. This representation is useful if τ_{exp} is already known rather precisely, but this rarely happens to be the case. A more practical representation replaces τ_{exp} by an effective one. To this end, we take observables A_α (not necessarily primary) which couple relatively strongly to the slow MC mode. We will see in the next chapters that in QCD possible choices are the square of the topological charge, the smeared plaquette or observables along the Wilson flow line.

We can use

$$\tau_{\text{exp}}^{\text{eff}}(t) = \frac{\tau}{2 \log \left\{ \text{Max}_\alpha \frac{\rho_{\alpha\alpha}(\tau/2)}{\rho_{\alpha\alpha}(\tau)} \right\}} \,, \tag{4.76}$$

but clearly other choices are possible. The effective coefficient

$$C_F^{\text{eff}}(\tau) = \rho_{\text{f}}(\tau)\text{e}^{\tau/\tau_{\text{exp}}^{\text{eff}}(\tau)} \,. \tag{4.77}$$

---

[2]We remind the reader that in QCD with parity conserved, the whole discussion is to be restricted to parity even observables.
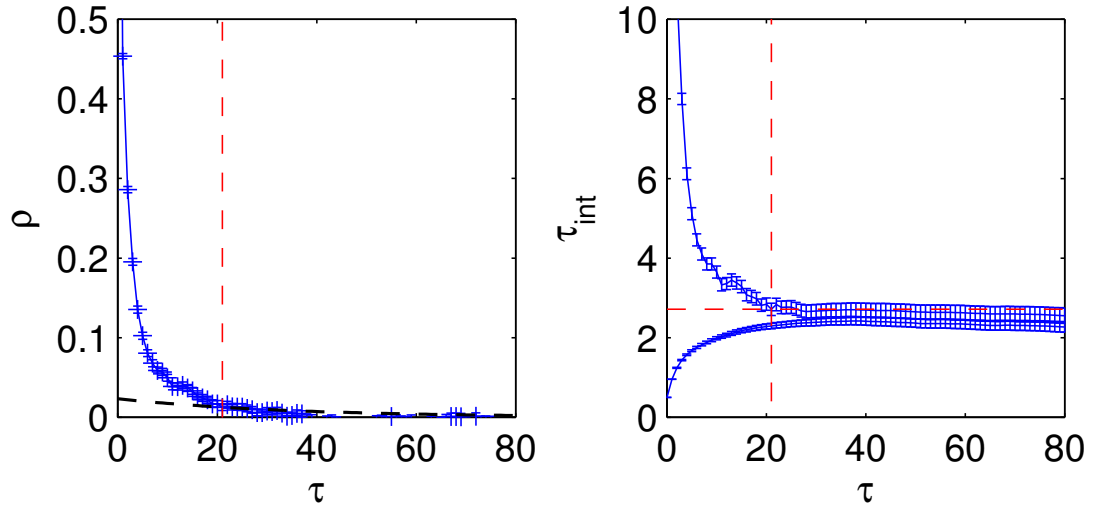
Figure 4.2.: **Left:** Auto-correlation function of an observable with a tail: the exponential mode corresponding to τ_* is also shown. The coupling to the slow mode, in this particular case, is small ($\sim 3\%$). **Right:** its integrated auto-correlation time. The upper bound is also shown at different sizes of the window. The vertical line is W_{u}.

then suggests itself. When detailed balance is guaranteed, a further effective estimator is

$$\widetilde{C}_F^{\mathrm{eff}}(\tau) = \frac{[\Gamma_{\mathrm{ff'}}(\tau)]^2}{\Gamma_{\mathrm{f}}(0)\Gamma_{\mathrm{f'}}(\tau)} \mathrm{e}^{\tau/\tau_{\mathrm{exp}}^{\mathrm{eff}}(\tau)} \tag{4.78}$$

where we have assumed that F' is an observable with a strong coupling to the slow mode. In other words $C_{F'}$ is large. This representation will be valid (at large τ) if λ_1 is an isolated eigenvalue and in practice if indeed the critical slowing down is dominated by the single mode $n = 1$. It simply follows from the mode decomposition $\Gamma_{\mathrm{ff'}}(\tau) = \sum_{n\geq 1}(\lambda_n)^\tau \, \eta_n(F)\eta_n(F')$.

Clearly eq. (4.77) is more generic and even expected to be useful when detailed balance is not satisfied, but the advantage of eq. (4.78) is that it can possibly be used at much larger τ, showing smaller statistical errors in that region.

We can now define what we mean by decoupling of an observable from the slow mode $n = 1$: in practice it means $C_F \ll 1$ while in terms of critical slowing down, it should be defined as a significant decrease of C_F as the correlation length and τ_{exp} grow, e.g. $C_F \sim (\text{correlation length})^{-\gamma}$ with some positive γ. In MC runs this decoupling is expected to be visible in the behaviour of $\widetilde{C}_F^{\mathrm{eff}}(\tau)$ at moderate time τ. Given the inherent problems in seeing asymptotic behaviour in numerical simulations, it is useful to go further and define the time scale τ_* through

$$\tau_{\mathrm{exp}}^{\mathrm{eff}}(r\,\tau_*) = \tau_* \tag{4.79}$$

and

$$C_F^*(r) = C_F^{\text{eff}}(r\tau_*) , \quad \text{where} \quad \lim_{r \to \infty} C_F^*(r) = C_F \text{ holds} . \tag{4.80}$$

In the same way, C_F^{eff} may be replaced by $\widetilde{C}_F^{\text{eff}}$. Using τ_* is similar in spirit to the original Sokal proposal for fixing the window of summation for the τ_{int} by the point at which the summation window W exceeds a multiple of $\tau_{\text{int}}(W)$. A choice of r significantly smaller than one is necessary when the overall statistics is moderate. We emphasize again our condition eq. (4.71), however. The advantage of eq. (4.80) is that we do not have to consider asymptotically large τ with their associated systematics. Decoupling can be studied at a fixed (not unreasonably small) value of r. If $C_F^*(r)$ shows decoupling it will usually also be the case in C_F.

4.5. Error of the error in a simple model

The estimates of statistical error of the auto-correlation function and related quantities (i.e. τ_{int} and $\rho(\tau)$) are based on the approximation where in eq. (4.25) one neglects the κ_4 term. We investigate now the validity of this approximation in an HMC simulation of the three dimensional ϕ^4 model. This model has been chosen since lattices of moderate size can be simulated without too much computational effort. With larger lattices we can study the HMC in a regime that is of physical relevance, and since the model presents a second order phase transition we can simulate in the vicinity of the critical line and have long range correlations on the lattice.

4.5.1. The model

The ϕ^4 model is a lattice discretization of scalar quantum field theory with quartic self-interactions. The discretization that we use is

$$S = \sum_x -2\kappa \left(\sum_{\mu=1}^{3} \phi(x)\phi(x + a\hat{\mu}) \right) + \phi(x)^2 + \lambda(\phi(x)^2 - 1)^2 \tag{4.81}$$

that is the same as the one used in ref. [27, 26]. We simulate the model on a cubic lattice of size $L = 20$, at the value of the parameters $\kappa = 0.18$ and $\lambda = 1.1$, where at the same λ in ref. [26] we read a value of $\kappa_c = 0.1875483(2)$. We use an HMC algorithm of ref. [70] with trajectory length $\tau_{\text{traj}} = 1$ and step size $\epsilon = 1/20$. We have generated 900 replicas each of length 160000 MD time. The starting configuration is a field of random noise in the $\phi(x) \in [0, 1]$ interval and we have discarded 2000 trajectories to ensure thermalization.

In the ϕ^4 theory we introduce the fourier transformed fields

$$\widetilde{\phi}(p) = \sum_x e^{ipx}\phi(x) \tag{4.82}$$

with which we define the propagator in momentum space as

$$S(p) = \sum_{x,y} e^{ip(x-y)} \langle \phi(x)\phi(y) \rangle = \left\langle |\widetilde{\phi}(p)|^2 \right\rangle. \tag{4.83}$$

Through the momentum space propagator we introduce a renormalized mass M_{R}

$$S(p) = \frac{Z}{p^2 + M_{\mathrm{R}}^2}, \tag{4.84}$$

this mass is an off-shell quantity but is nonetheless a well-defined physical quantity to compute.

The observables that we consider are thus the magnetization $m = \widetilde{\phi}(0)$, the magnetic susceptibility $\chi_m = \langle m^2 \rangle /V$ (where $V = L^3$), the action density $s = S/V$ and an estimator of M_{R}, namely

$$M_{\mathrm{R}}^{\mathrm{eff}}(p) = \sqrt{\frac{p^2 \left\langle |\widetilde{\phi}(p)|^2 \right\rangle}{\left\langle \widetilde{\phi}(0)^2 \right\rangle - \left\langle |\widetilde{\phi}(p)|^2 \right\rangle}}, \tag{4.85}$$

computed for the value of the momentum $p = (\frac{2\pi}{L}, 0, 0)$ and averaged over permutations.

4.5.2. Measurements

We will study the expression in eq. (4.25) restricted to a single observable A_α and for the special arguments

$$\kappa_4(\tau; \alpha) = \left\langle\!\left\langle \delta_\alpha^t \delta_\alpha^t \delta_\alpha^{t+\tau} \delta_\alpha^{t+\tau} \right\rangle\!\right\rangle - \left\{ 2\Gamma_{\alpha\alpha}(\tau)^2 + \Gamma_{\alpha\alpha}(0)^2 \right\} \tag{4.86}$$

we will investigate the relative size of $\kappa_4(\tau; \alpha)$ through a quantity analog to the Binder cumulant of statistical mechanics

$$V_\alpha(\tau) = 1 - \frac{\left\langle\!\left\langle \delta_\alpha^t \delta_\alpha^t \delta_\alpha^{t+\tau} \delta_\alpha^{t+\tau} \right\rangle\!\right\rangle}{2\Gamma_{\alpha\alpha}(\tau)^2 + \Gamma_{\alpha\alpha}(0)^2} \tag{4.87}$$

that is exactly zero when $\kappa_4(\tau; \alpha) = 0$. An interesting quantity to compute is the point estimate of the variance as a function of the Monte Carlo time

$$\mathrm{var}(A_\alpha^\tau) = \frac{1}{R} \sum_{r=1}^{R} (a_\alpha^{\tau,r} - \overline{\overline{A}}_\alpha)^2, \tag{4.88}$$

to be used in the analysis of the approach to thermalization. With many replicas the variance of the estimate $\overline{\rho}_{\alpha\alpha}(\tau)$ can be directly evaluated,

$$\mathrm{var}[\overline{\rho}_{\alpha\alpha}(\tau)] = \frac{1}{R} \sum_{r=1}^{R} (\overline{\rho}_{\alpha\alpha}^r(\tau) - \overline{\overline{\rho}}_{\alpha\alpha}(\tau))^2, \tag{4.89}$$
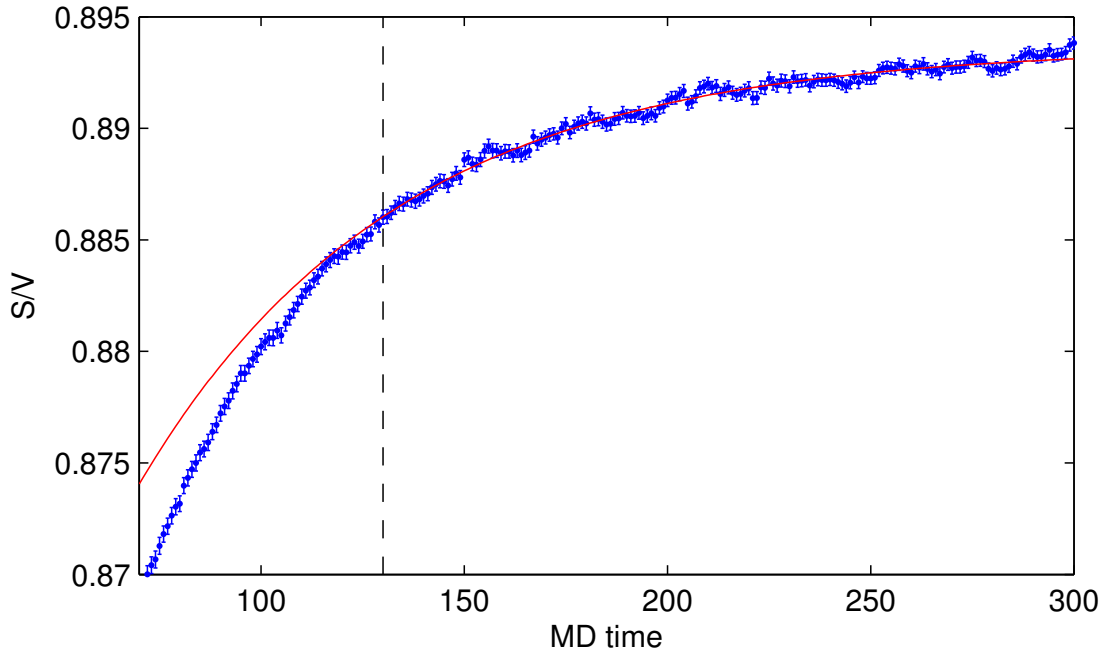
Figure 4.3.: Thermalization history of the action density. The red line is a single exponential fit with a characteristic time of $\tau_* \simeq 60$. The dashed vertical line marks the first point of the fit range $\tau_{\min} = 130$.

as well as the variance of other estimates of interest (e.g. $\tau_{\text{int}}(W)$).

Thermalization and exponential auto-correlation time

The approach to thermalization of an observable averaged over several Monte Carlo chains is exponential with the characteristic times given by the spectrum of the Markov transition matrix. Close to equilibrium the dominant mode is given by τ_{exp} (for a proof see e.g. ref. [74]). In fig. (4.3) we show the thermalization of the action density fitted to a single exponential. The starting time for the fit is chosen such that the fitted exponential decay does not change too much. Moreover the same analysis performed for the observables χ_m and $S(p)$ gives similar results. In fig. (4.4) we show that in approaching the equilibrium the variance thermalizes at the same rate as (or even faster than) the observable under study. This in practice means that for some observables that thermalize slowly, it is reasonable to think about estimating τ_{exp} from a single realization of a chain.

Connected four point function

We study here the connected part of the four point function (eq. (4.87)). In fig. (4.6) we show that magnetization and action density have a very small value of $V_\alpha(0)$. This
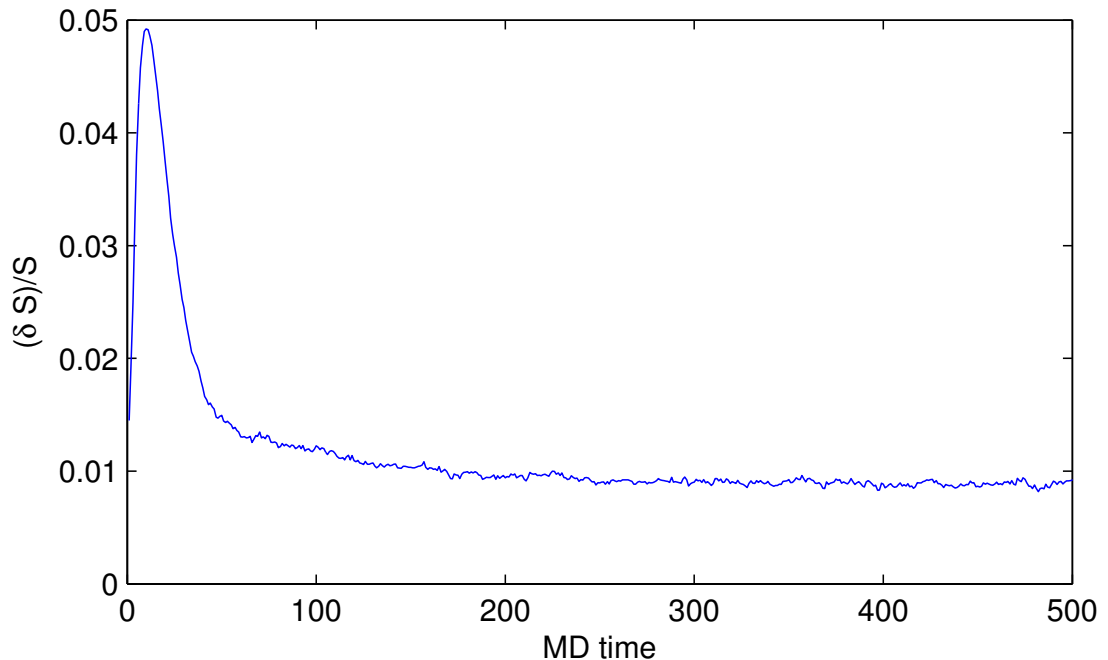
Figure 4.4.: The relative error of the action density as a function on the Monte Carlo time.

corresponds to the physical setup of an observable that is quasi-Gaussian since it is formed by summation of a large number of independent contributions. What is interesting to observe is that $V_\alpha(\tau > 0)$ is at first pushed away from zero. This is particularly visible in the case of the action density. In both cases deviations from Gaussianity are small, $O(5\%)$. In fig. (4.5) we show the same plot but for the magnetic susceptibility and the effective mass. In this case the connected contribution is larger. This is of no surprise, at least for the case of χ_m: in the symmetric phase $\langle m \rangle = 0$, therefore the distribution of m^2 is very asymmetrical. Indeed since we have seen that the magnetization is quasi-Gaussian, one expects m^2 to roughly follow a χ^2 distribution. In all cases of fig. (4.5) the connected contribution goes to zero smoothly and monotonically with a half-bell shaped curve. This situation is to be expected also in QCD where $\langle Q_{\text{top}} \rangle = 0$. With a large contribution from the connected four point function the approximation behind the error-of-the-error formulae (e.g. eq. (4.33)) ceases to be valid, but even with a contribution as large as the one shown in fig. (4.5), we can see from fig. (4.7) that the error formula given by neglecting κ_4 still gives a reasonable estimate of $\delta\bar{\rho}_{\alpha\alpha}(\tau)$. In fig. (4.8) we also compare the approximation that we use for computing the error of τ_{int} with the error computed from the full covariance. The approximation gives results that are close to the true error for all observables. The observed differences are due to a combined effect of neglecting κ_4 and truncating the full covariance (this last approximation is the one that enables us to express the error in the elegant formula of eq. (4.56), and neglects terms that are
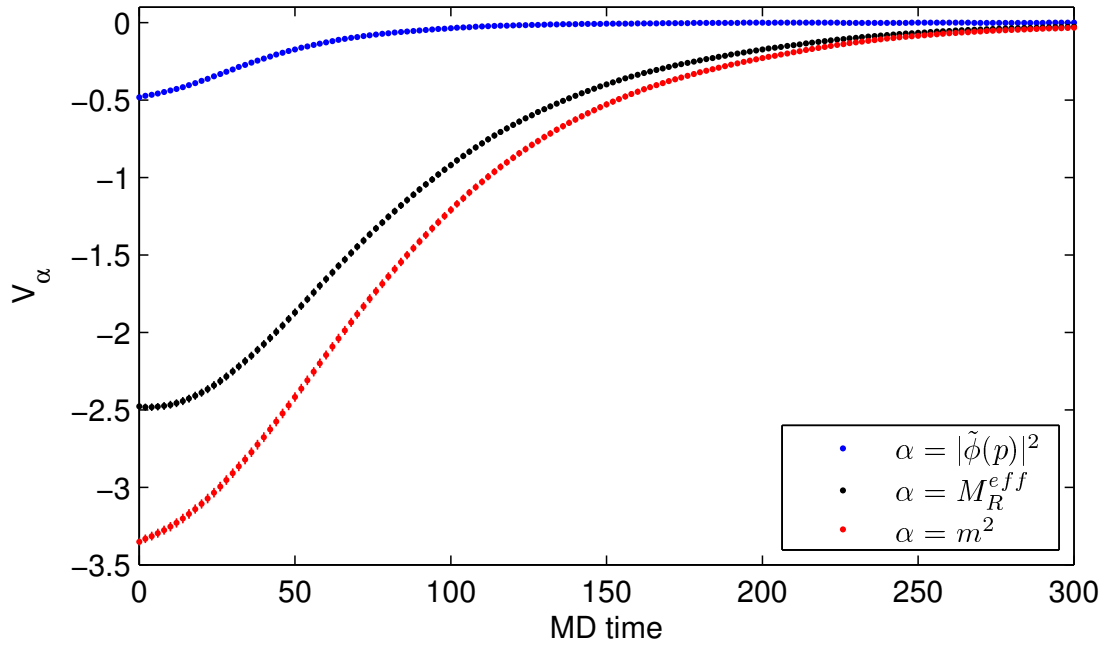
Figure 4.5.: The quantity V_α of eq. (4.87), the observables α are the magnetic suscepti-bility, the effective mass and the propagator at momentum $p = (\frac{2\pi}{L}, 0, 0)$, in this order from bottom to the top (note that the error bars are shown!).
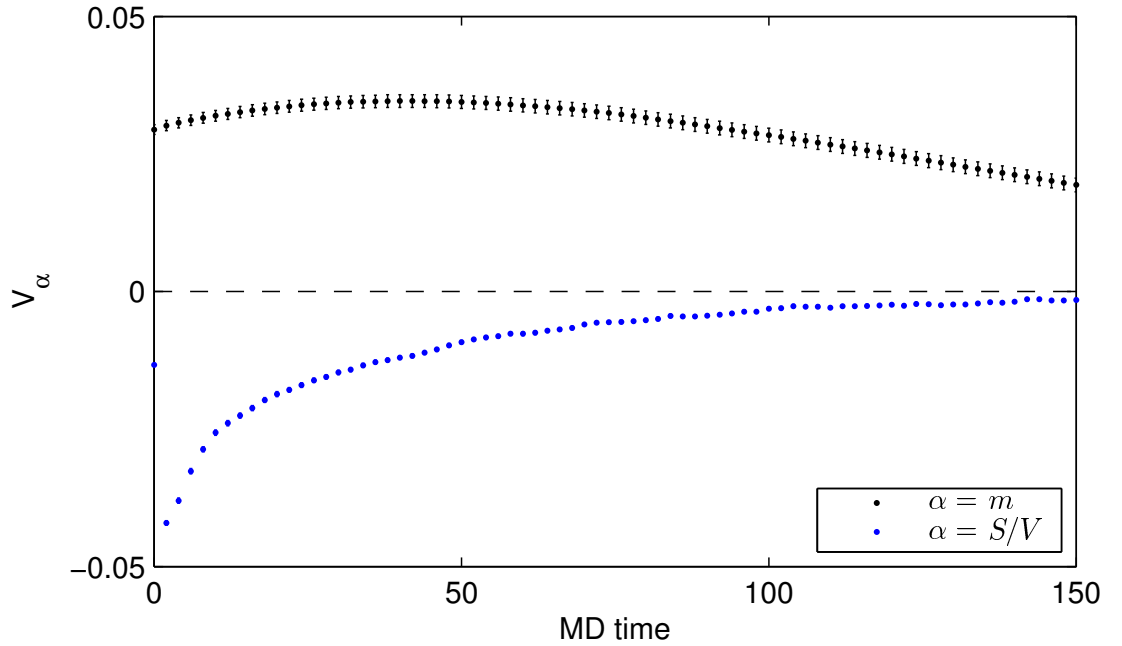
Figure 4.6.: The quantity V_α of eq. (4.87), the observables here are the magnetization m and the action density (from top to bottom).

proportional to $\tau_{\text{int}}(W)$).

Correlation coefficient and symmetries of the action

The ϕ^4 action is invariant under the $\mathbb{Z}^2$ transformation $\phi(x) \to -\phi(x)$, and so is M_{R} and χ_m that are $\mathbb{Z}^2$-even while m is $\mathbb{Z}^2$-odd. It is trivial to prove that the algorithm preserves the $\mathbb{Z}^2$ symmetry and for this reason the even and odd sectors are orthogonal (we show only a numerical example of this fact in fig. (4.9)).

An advantage of having a very large statistics is that we can investigate to high accuracy both estimators of the dynamical coefficient defined in eq. (4.75) (we have not been able to do so in a completely satisfactory way in our pure gauge analysis). In fig. (4.10) we directly compare estimators of C_S for the action density and the correlation function at nonzero lattice momentum. From the plot one can see that $\widehat{C}_F^{\text{eff}}(\tau)$ at larger values of τ has smaller statistical errors, and for the two observables shown it converges faster to a plateau.
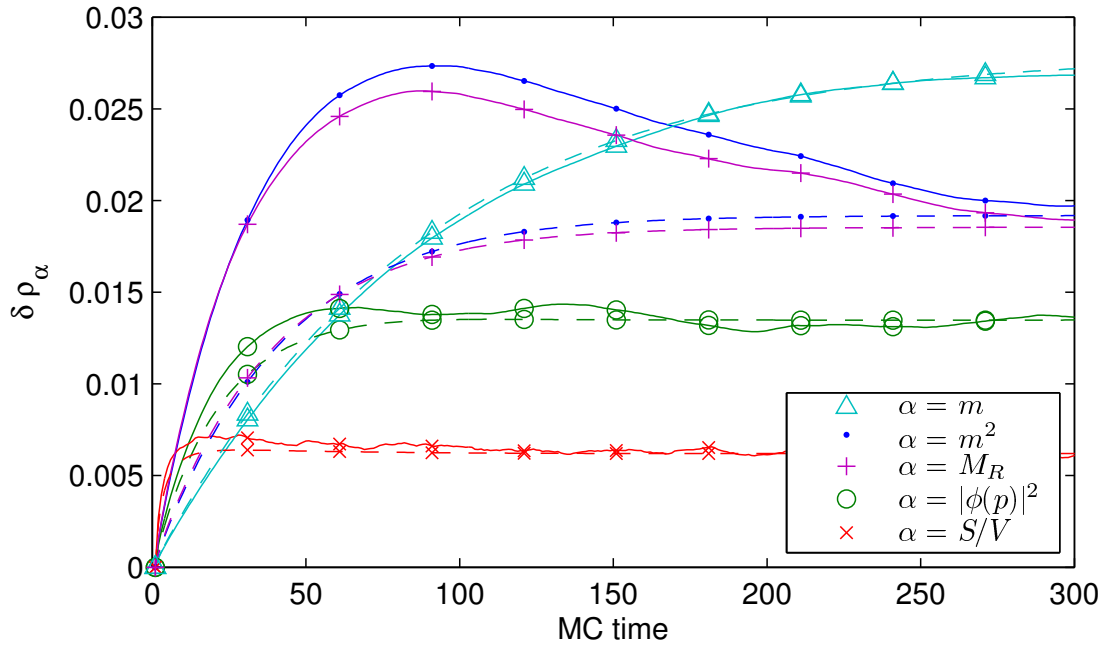
Figure 4.7.: Comparison of the estimated error of the normalized auto-correlation function computed with eq. (4.33) (dashed lines) and estimated with the full covariance, computed over 900 chains (solid line).
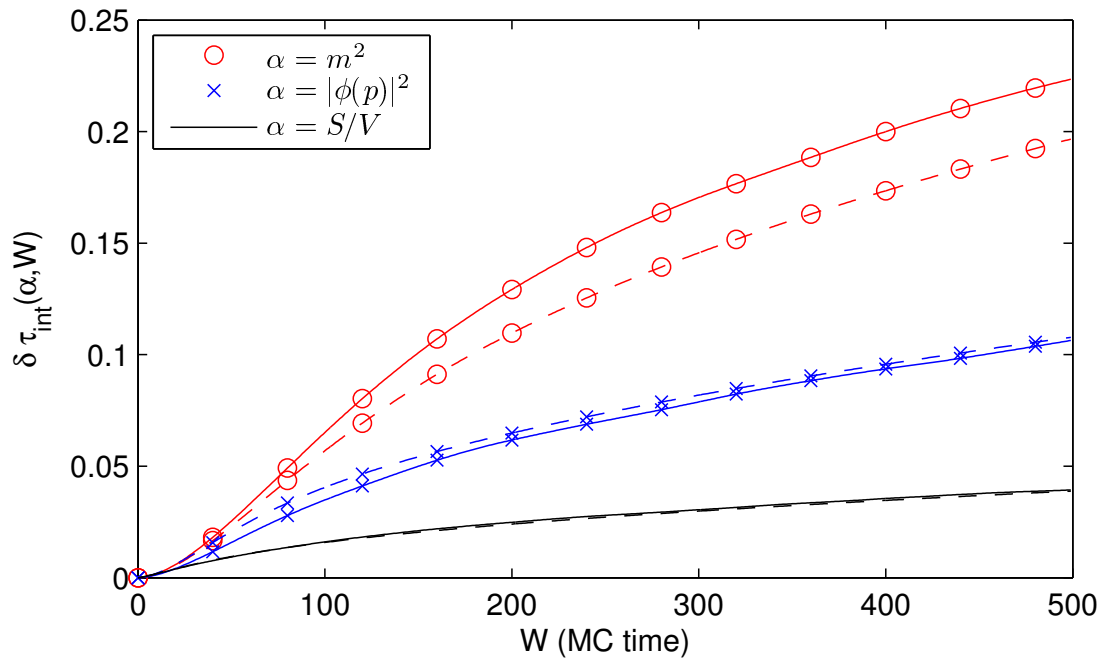
Figure 4.8.: Comparison of the estimated error of the integrated auto-correlation time computed with eq. (4.56) (dashed lines) and estimated with the standard variance computed over 900 chains (solid line)
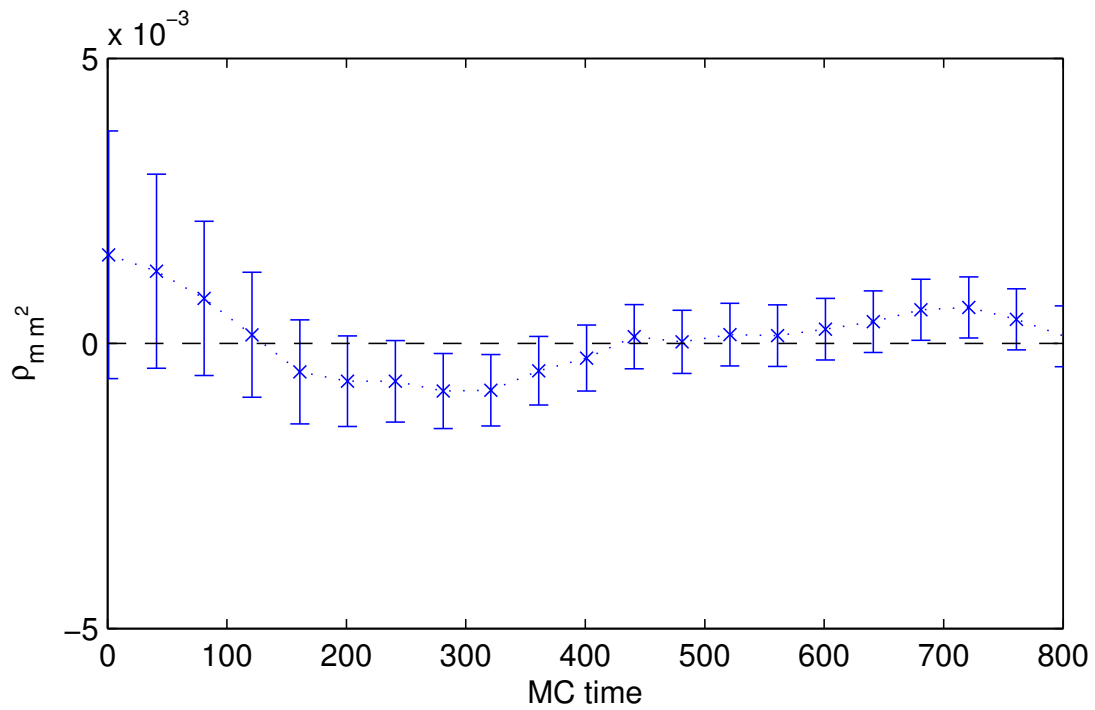
Figure 4.9.: Cross-auto-correlation function between the magnetization and the suscepti-
bility. For this plot we have used a larger statistics of 1600 chains.
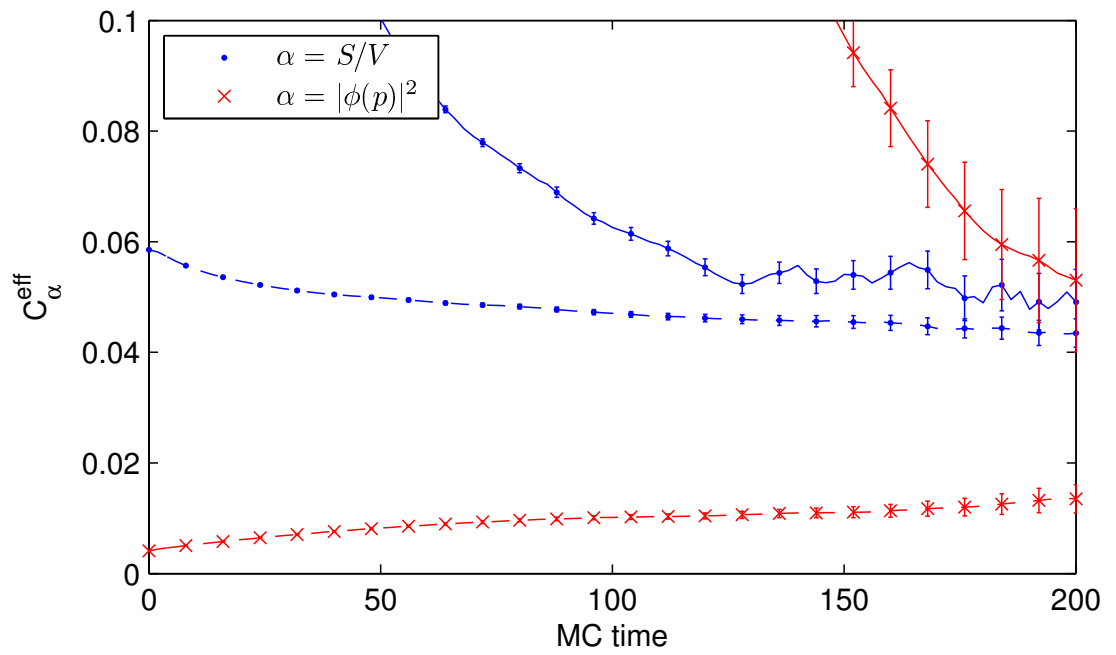
Figure 4.10.: Effective correlation coefficient of two observables. The role of the slow mode is played by the magnetic susceptibility. The solid lines corresponds to the estimator given by eq. (4.77) while the dashed lines corresponds to eq. (4.78).

5. Critical slowing down: quenched analysis

All lattice QCD simulations are performed at finite lattice spacing a and need an extrapolation to the continuum in order to be used for computing values of physical quantities. More reliable extrapolations can be done by simulating the theory at increasingly smaller lattice spacing. The picture that results when the lattice spacing is reduced and physics is kept constant, is that all finite physical quantities of negative mass dimension diverge if measured in lattice units. In statistical mechanics language this states that the continuum limit is a critical point of the theory since correlation lengths diverge (taking the two dimensional Ising model as an example, larger blocks of contiguous spins align in the same direction when approaching the critical temperature). MC algorithms are known to encounter difficulties when used for simulating theories close to a critical point, and this known fact is usually called *critical slowing down* of the algorithm.

Critical slowing down is usually encoded by a quantity z called the dynamical critical exponent. The exponent z describes the asymptotic behaviour of correlation lengths in MC time as the lattice spacing decreases

$$\xi(a) \overset{a\to0}{\sim} a^{-z} \tag{5.1}$$

where $\xi(a)$ is a typical length scale and is usually taken to be the integrated auto-correlation time of an observable of interest. It is generally thought that quantities to be used in a scaling analysis should be physical observables (in the sense of having a well defined continuum limit, possibly a smooth monotonic function of a). For the length scale used in the analysis of critical slowing down, instead of the observable dependent τ_{int} it is possible to use τ_{exp} itself. Since τ_{exp} is notoriously difficult to determine, in our analysis we will instead use τ_* defined by eq. (4.79). It is expected that the two quantities have a similar asymptotic behaviour.

A study of critical slowing down requires computing the auto-correlation function of quantities close to the continuum limit to high accuracy. Since pure gauge simulations are much cheaper than simulations with dynamical fermions, we first perform the critical slowing down analysis of quenched observables in the pure SU(3) algorithm setup. The knowledge that we gain from this analysis will then be carried over to a simulation in full QCD.

5.1. Algorithmic setup

Our analysis will focus on a single algorithm, namely the HMC. This is justified since our main worry is reliability of error estimate in QCD computations with dynamical fermions and in this context the Hybrid Monte Carlo algorithm is nowadays the only

viable choice. Besides standard HMC (in particular we have used the code of ref. [23]) we have also used a Domain Decomposed HMC algorithm for pure gauge theory. This second algorithm is based on the so called DD-HMC for two flavours (a simplified version, with the fermion forces stripped off, of the code presented in ref. [40]). Larger lattices have been simulated with a domain decomposed algorithm with block-wise acceptance step. Since energy violations in the Hamiltonian scale with the volume, an algorithm with block-wise acceptance can achieve with a comparatively larger step size the same acceptance rate as an algorithm with global acceptance (i.e. reduced computational cost). As we show in fig. (5.2) these two flavours of the algorithm show similar auto-correlation times (this actually happens for all pure gauge observables that we have measured).

In algorithms that implement domain decomposition there is a distinction between active and frozen links. Links that don't have both endpoint in the interior of a block are frozen, this means that they do not actively participate the updating process. If we denote the length of the edges of a domain with B_i, the ratio of active to total number of links is

$$R = \frac{\prod_{i=0}^{3}(B_i - 2) + \frac{1}{4}\sum_{i=0}^{3}\prod_{i \neq j}(B_j - 2)}{\prod_{i=0}^{3} B_i} \ . \tag{5.2}$$

In case of large (in physical units) block sizes, the efficiency of the algorithm is then expected to scale proportionally to R and as we show in fig. (5.1) this seems to actually be the case. As we will see later, when the blocks are small this need not to be the case anymore.

The presence of separate domains entails that in order to update all links and restore ergodicity the block grid has to be shifted at the beginning of each trajectory. The drawback of purely random shifts is that single links can remain frozen for many trajectories before becoming active. For this reason in ref. [40] a mixed scheme that alternates random to directed shifts was proposed. We have kept this scheme even though it breaks exact detail balance. In our numerical experiments we have seen no evident consequence of this breaking, namely we have not been able to detect clear signals, in the shape of observed auto-correlation functions, of modes associated with complex eigenvalues (either these contributions are very small or are altogether absent). For this reason even though the spectral decomposition of the auto-correlation function is not expected anymore to be a sum of decaying exponentials, we still think that an estimate of the upper bound of τ_{int} based on eq. (4.73) is a useful quantity.

5.1.1. Simulations

In this analysis we have simulated a range of lattice spacings going from 0.14 fm down to 0.047 fm, with the scale determined fixing $r_0 = 0.5$ fm [62]. We have performed simulations at constant physical volume of $(2.2 \text{ fm})^4$. The list of chains that we have simulated is presented in table 5.1. As one can see we have always kept acceptance rates above 90%. Within the C series we have performed runs with three different values of β. The explanation for this is that $\beta = 6.179$ is in the constant volume series, $\beta = 6.2$ was simulated in order to reproduce results of ref. [31] while $\beta = 6.136$ was done in order to
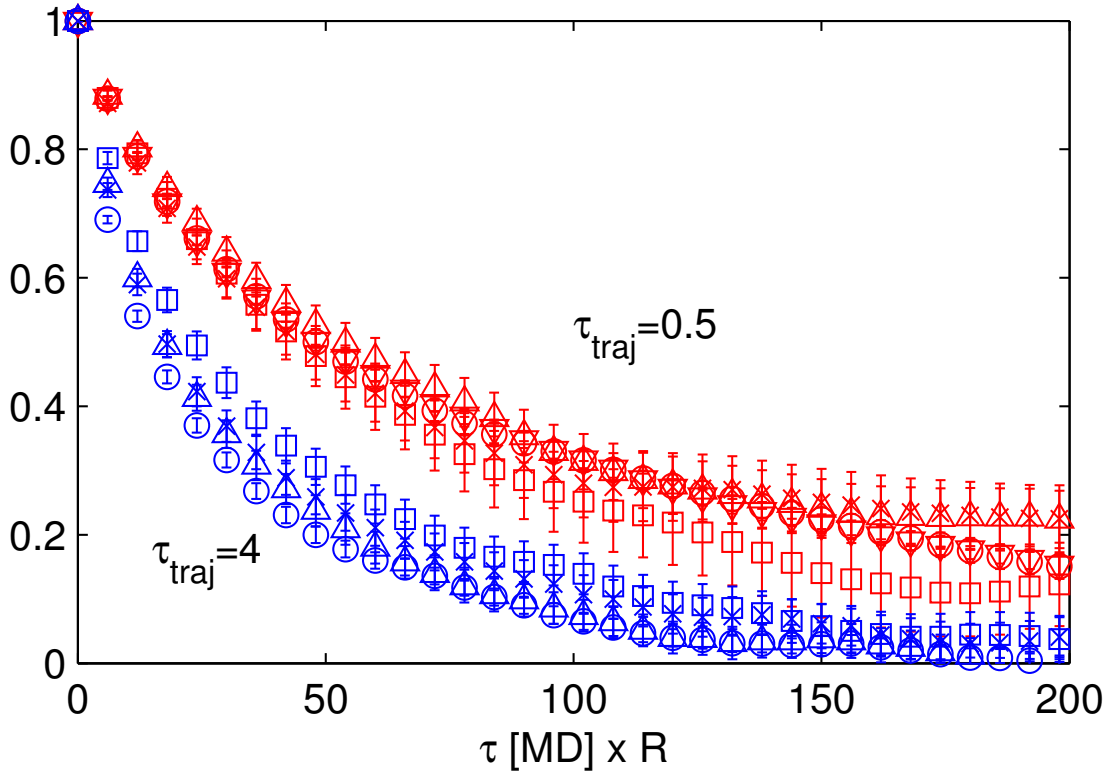
Figure 5.1.: Normalized auto-correlation functions of the smeared topological suscep-
tibility χ_1 (eq. (5.3)) at $\beta = 6$. The MC time units on the x-axis have
been rescaled by the ratio of active links R. The plot shows auto-correlation
functions corresponding to chains with trajectory length $\tau_{\text{traj}} = 0.5$ and
$\tau_{\text{traj}} = 4$ (see also table 5.1). The values of R that are plotted here vary
between 1 and ~ 0.25.
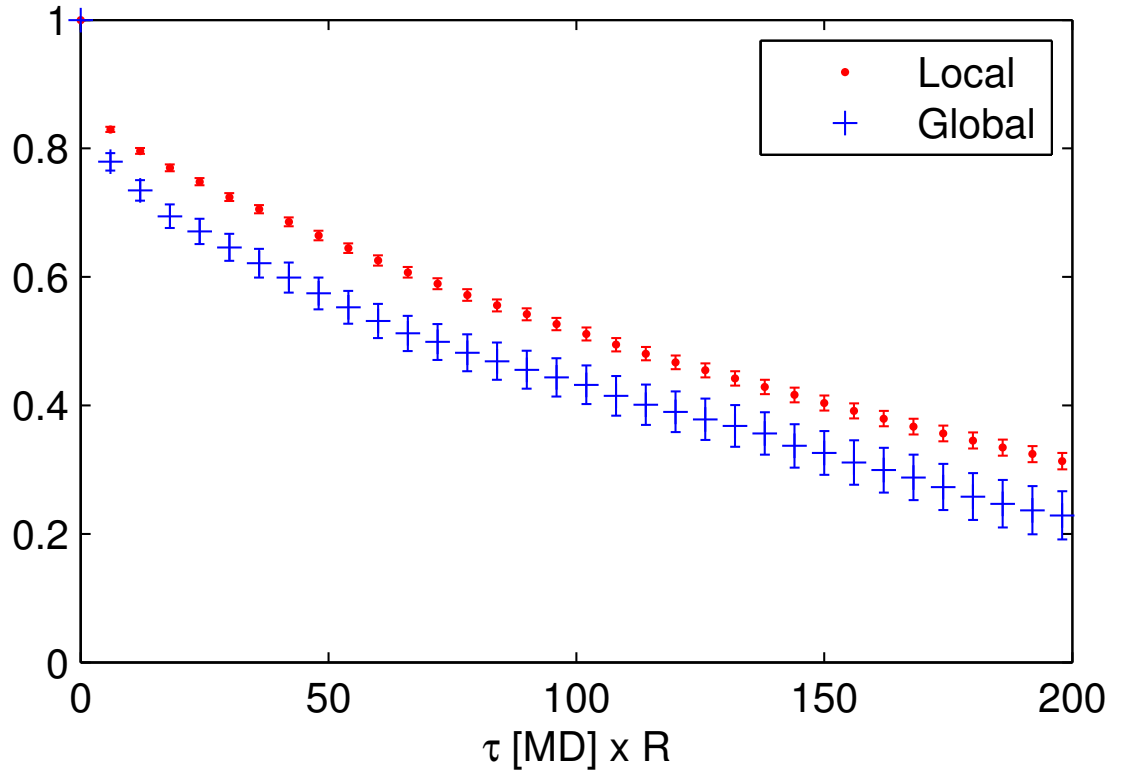
Figure 5.2.: Normalized auto-correlation functions of χ_1 at $\beta = 6.179$. The MC time units on the x-axis have been rescaled by the ratio of active links R. The plot shows auto-correlation functions corresponding to chains with trajectory length $\tau_{\text{traj}} = 4$. Local and global refer to the acceptance strategy of the pure SU(3) DD-HMC algorithm.

have a quenched chain at the same r_0/a as some $N_f = 2$ runs performed inside CLS[1] (enabling us to bridge our results to dynamical fermions simulations, as we will see in the next chapter).

5.2. Observables

In the pure gauge sector of the theory we have measured both the topological charge and Wilson loops. Wilson loops are the lattice analogue of path ordered exponentials along loops. They are built by forming traces of ordered products of link variables in the same way as we did for the plaquette defined in eq. (2.24), that is indeed the 1×1 Wilson loop. A Wilson loop $W^{r \times t}$ is defined as the average over the whole lattice of products of links along $r \times t$ rectangles where r denotes the space extent and t the time. The topological charge Q_{top} has been computed from a discretized form of the continuum expression given in eq. (2.69). Further pure SU(3) observables are the topological susceptibility

$$\chi_{\text{top}} = \frac{\left\langle Q_{\text{top}}^2 \right\rangle}{TL^3} \, , \tag{5.3}$$

and the plaquette P that as already noted is the same as $W^{1 \times 1}$.

In some cases the pure gauge observables have also been measured after having removed some of the UV physical modes with a smoothing technique known as HYPercubic smearing described in ref. [30]. The smearing parameters we use in our setup are the same as the ones found in ref. [32]. HYP smearing can be recursively applied, and the total number of iterations is called smearing level. In this study we considered up to five smearing levels, marked by an index α attached to either one of the observables under consideration, namely Q_α, χ_α, $W_\alpha^{r \times t}$ and P_α. Since the computation of Wilson loops is more demanding we have measured them only at one smearing level. The reason for measuring smeared quantities can be intuitively explained by saying that smearing exposes coherent features of the single gauge configuration: these can be thought as long range structures that an updating algorithm must destroy in order to generate a completely independent configuration . In the present chapter, the approach that we have used to study critical slowing down is to keep the smearing radius fixed in units of lattice spacing (i.e. the number of smearing levels independent of β), so that in the continuum limit one recovers the original (unsmeared) observable (this indeed holds only if the observable has a continuum limit at all). In an alternative approach, that has for instance been used in ref. [47], one keeps the smoothing radius fixed in physical units: this requires to relate smearing radii at different lattice spacings in a way that is not always known (this is for instance the case of HYP smearing). In ref. [47] the smoothing technique used is the numerical integration of the Wilson flow, that allows a rigorous definition of physical scaling.

On two ensembles we have measured also quenched observables, namely hadronic observables with only valence quarks (this amounts to set $\det D_f = \text{const.}$ in the Monte

---

[1]https://twiki.cern.ch/twiki/bin/view/CLS/WebHome

Carlo process). We took the values of the hopping parameters from ref. [31] and computed the correlators used in the quenched study of the $D_{\rm s}$ meson. In particular we have computed the axial-pseudo-scalar and pseudo-scalar-pseudo-scalar correlators projected to zero momentum

$$C_{\rm PP}(t) = \frac{a^3}{V} \sum_{\vec{x}} \langle P(t, \vec{x}) P(0) \rangle \tag{5.4}$$

$$C_{\rm A_0P}(t) = \frac{a^3}{V} \sum_{\vec{x}} \langle A_0(t, \vec{x}) P(0) \rangle \ . \tag{5.5}$$

To reduce the variance of the estimated correlators, propagators have been computed using the source described in eq. (3.62), with 5 stochastic sources per configuration.

Interesting derived quenched observables are the effective meson mass $M_{\rm eff}(t)$ defined as the solution of

$$\frac{C_{\rm PP}(t + a)}{C_{\rm PP}(t - a)} = \frac{\cosh\left((t + a - T/2) M_{\rm eff}(t)\right)}{\cosh\left((t - a - T/2) M_{\rm eff}(t)\right)} \ , \tag{5.6}$$

and the PCAC bare quark mass defined through eq. (2.60) as

$$M_{\rm PCAC} = \frac{1}{T_2 - T_1 + 1} \sum_{t=T_1}^{T_2} \frac{\left(\partial_0^{\rm f} + \partial_0^{\rm b}\right) C_{\rm A_0P}(t) + 2a\, c_{\rm A} \partial_0^{\rm f} \partial_0^{\rm b}\, C_{\rm PP}(t)}{4 C_{\rm PP}(t)} \ , \tag{5.7}$$

where the expression is averaged over a suitable time range that excludes short time separations. The range is chosen such that $O(a^2)$ effects are small. The improvement coefficient for the axial current $c_{\rm A}$ has been taken from ref. [52]. Another derived quantity of interest is the effective pseudo-scalar decay constant

$$f_{\rm eff}(t) = \frac{2 M_{\rm PCAC}}{M_{\rm PS}^2} \sqrt{\frac{C_{\rm PP}(t)}{e^{-t\, M_{\rm PS}} + e^{-(T-t)\, M_{\rm PS}}}} \ , \tag{5.8}$$

where $M_{\rm PS}$ is the effective mass of eq. (5.6) averaged over a suitable plateau. Analogously we define $f_{\rm PS}$ as the plateau average of the estimator defined in eq. (5.8).

Exceptional configurations

When simulating the theory with dynamical fermions a repulsive force generated by the fermion determinant keeps the trajectories of molecular dynamics far from the region where the Wilson-Dirac matrix determinant becomes zero. This does not happen in quenched simulations: sampled configurations might occasionally be such that eigenvalues of the Wilson-Dirac matrix $D_{\rm W}[U] + M_{\rm q}$, at small quark masses $M_{\rm q}$, become extremely small or even with a real negative part. When this happens we are simulating in a regime where the theory has no physical meaning and the quenched approximation breaks down. Configurations where this happens are said to be exceptional: this problem is most severe with lighter pion masses (since the lower end of the spectrum of the Wilson-Dirac operator

TAG	β	$T/a\ L/a$	a[fm]	block	R	τ_{traj}	$\Delta\tau$	A	stat
A1a	5.789	16 16	0.140	8^4	0.369	0.5	0.01	0.961	105280
A1b	5.789	16 16	0.140	8^4	0.369	1	0.01	0.971	70080
A1d	5.789	16 16	0.140	8^4	0.369	4	0.01	0.968	141120
B0a	6	24 24	0.093	HMC	1	0.5	0.0077	0.931	199600
B0b	6	24 24	0.093	HMC	1	1	0.0077	0.954	110000
B0c	6	24 24	0.093	HMC	1	2	0.0077	0.943	210000
B0d	6	24 24	0.093	HMC	1	4	0.0077	0.946	130000
B0e	6	24 24	0.093	HMC	1	8	0.0077	0.945	116000
B1a	6	24 24	0.093	12^4	0.53	0.5	0.0077	0.932	52640
B1b	6	24 24	0.093	12^4	0.53	1	0.0077	0.951	55520
B1c	6	24 24	0.093	12^4	0.53	2	0.0077	0.945	61280
B1d	6	24 24	0.093	12^4	0.53	4	0.0077	0.945	65440
B2a	6	24 24	0.093	$12^2{\times}6^2$	0.363	0.5	0.0077	0.945	113800
B2b	6	24 24	0.093	$12^2{\times}6^2$	0.363	1	0.0077	0.958	116400
B2c	6	24 24	0.093	$12^2{\times}6^2$	0.363	2	0.0077	0.956	119200
B2d	6	24 24	0.093	$12^2{\times}6^2$	0.363	4	0.0077	0.954	110400
B3a	6	24 24	0.093	6^4	0.247	0.5	0.0077	0.956	61000
B3b	6	24 24	0.093	6^4	0.247	1	0.0077	0.966	128000
B3c	6	24 24	0.093	6^4	0.247	2	0.0077	0.963	138000
B3d	6	24 24	0.093	6^4	0.247	4	0.0077	0.962	147000
B4a	6	24 24	0.093	$12{\times}6^3$	0.3	0.5	0.019*	0.97	1008000
B4b	6	24 24	0.093	$12{\times}6^3$	0.3	1	0.02*	0.97	1584000
B4c	6	24 24	0.093	$12{\times}6^3$	0.3	2	0.02*	0.98	780000
C1d	6.136	64 32	0.075	$16{\times}8^3$	0.422	4	0.02*	0.946	175360
C2b	6.179	32 32	0.070	8^4	0.369	1	0.0059	0.956	393000
C2d	6.179	32 32	0.070	8^4	0.369	4	0.0222*	0.956	1568160
C3d	6.179	48 48	0.070	12^4	0.53	4	0.0182*	0.919	486560
C4d	6.179	32 32	0.070	4^4	0.09	4	0.065*	0.96	1374720
C5d	6.2	64 32	0.068	$16{\times}8^3$	0.422	4	0.0229*	0.928	684000
D1d	6.475	48 48	0.047	12^4	0.53	4	0.0167*	0.927	707680

Table 5.1.: Parameters of our runs. We give the bare coupling, the size of the lattice, the lattice spacing from $r_0 = 0.5$ fm, the block decompostion in the DD-HMC, the corresponding fraction of active links R, the trajectory length τ and the step size of the integration $\Delta\tau$ along with the acceptance rate A and the total statistics in molecular dynamics units. Runs with blockwise acceptance step are marked with an asterisk on the step size.

is proportional to the quark mass) but in our simulations (with a very high statistics of c.a. 40000 measurements) even at the strange quark mass we see many suspicious cases that we have decided to drop from the analysis. To decide whether to keep or not a configuration we adopted a criterion inspired by the one presented in ref. [60], and decided to discard a configuration when the fourth moment of the pseudo-scalar correlator $M_4 = \sum_t t^4 C_{\mathrm{PP}}(t)$ is more than ten standard deviations away from the average value (iterating until no configuration is discarded). The logic behind this method is that the correlator is a quantity that has mass dimension 3, and for this reason in perturbation theory $C_{\mathrm{PP}}(t) \underset{t \to 0}{\sim} t^{-3}$ up to logarithmic corrections. This means that the integral of the correlator along the euclidean time t is a divergent quantity in the continuum limit (even after multiplicative renormalization of the pseudo-scalar density), and it can be made finite by multiplying it with t^d, with $d \geq 3$. In particular we have chosen a larger value of $d = 4$ since this increases the weight of fluctuations at larger euclidean time (more relevant for the physics that we are typically interested to) w.r.t. those at shorter times.

In fig. (5.3) we show the M_{PCAC}, namely the derived observable corresponding to the PCAC mass, computed after removing the suspicious configurations. Large excursions away from the average are still present.

5.3. Critical slowing down

Following the proposal in ref. [71] the error estimate of physical observables is computed through the upper bound formula, eq. (4.73). The value of τ_* that is needed for estimating the upper bound of the statistical error, can in principle be obtained by looking the exponential decay of the auto-correlation function of some slow observables. An alternative is to compute it from a model. This avoids the cumbersome task of estimating τ_* directly from data on every ensemble that enters a lattice QCD computation, also because in some cases direct information about slow modes might either be not reliable or not available. The analysis of critical slowing down besides being a tool for theoretical understanding, can thus be used to suggest a way to easily improve the error analysis, namely to construct a reasonable model for τ_*.

We propose to model the lattice spacing dependence $\tau_*[a]$ according to two possible ansätze

$$\tau_*[a] = \left(\frac{a}{k_a} \right)^z \quad \text{and} \quad \tau_*[a] = k_e e^{\zeta/a} \, , \tag{5.9}$$

where the power law is what one usually considers when discussing critical slowing down (see eq. (5.1)) while the exponential law was advocated in ref. [12] in the context of two dimensional CP^{N-1} models. The observable that we choose for the analysis of critical slowing down is the topological susceptibility after one smearing step. On all lattice spacings that we have investigated, we observe $\chi_\alpha \simeq \chi_1$ (at least as long as $\alpha \neq 0$). In fig. (5.4) we show the resulting fits where one can see that both ansätze work reasonably well in the range $a \in [0.05, 0.09]$ fm. The computed fit parameters for the power law ansatz are $k_a = 0.18(1)$ fm and $z = -5.4(4)$, while in the case of the exponential ansatz we obtain $k_e = 0.5(1)$ and $\zeta = 0.41(3)$ fm. The quoted errors are only statistical and we
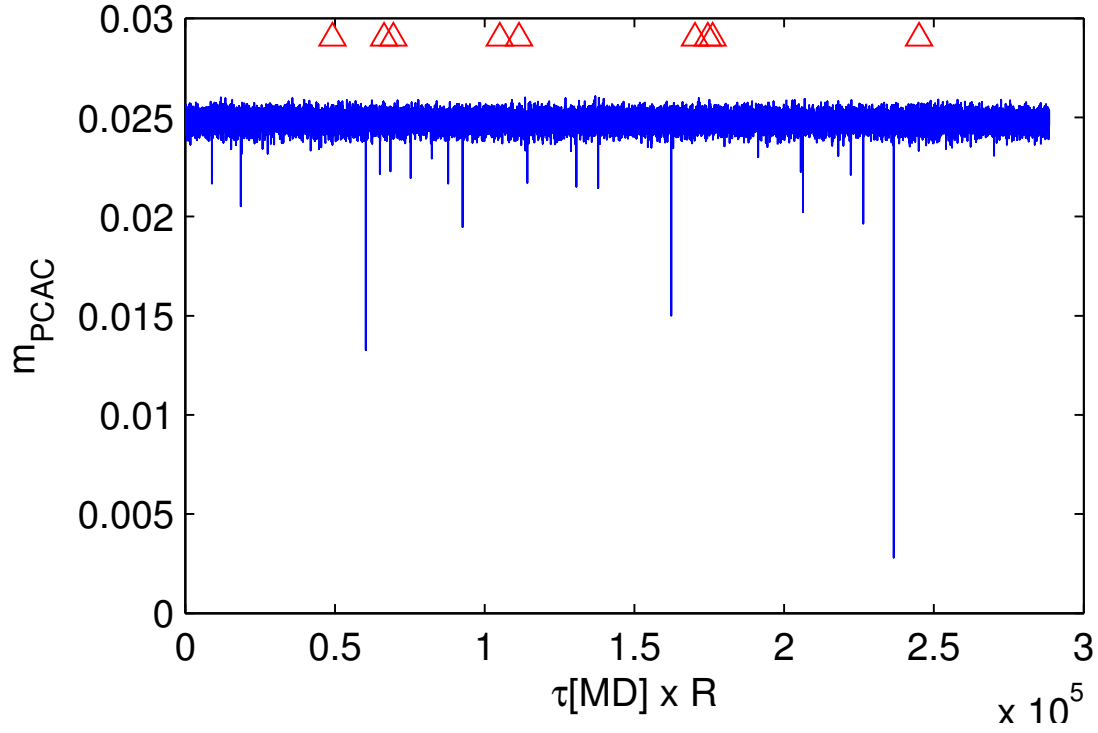
Figure 5.3.: C5d chain, the observable shown is the M_{PCAC} first-level-derived (bare strange quark mass) after having removed the suspicious configurations using the M_4 criterion (the configurations removed are 9 and their position is marked in the plot by an upper triangle symbol).
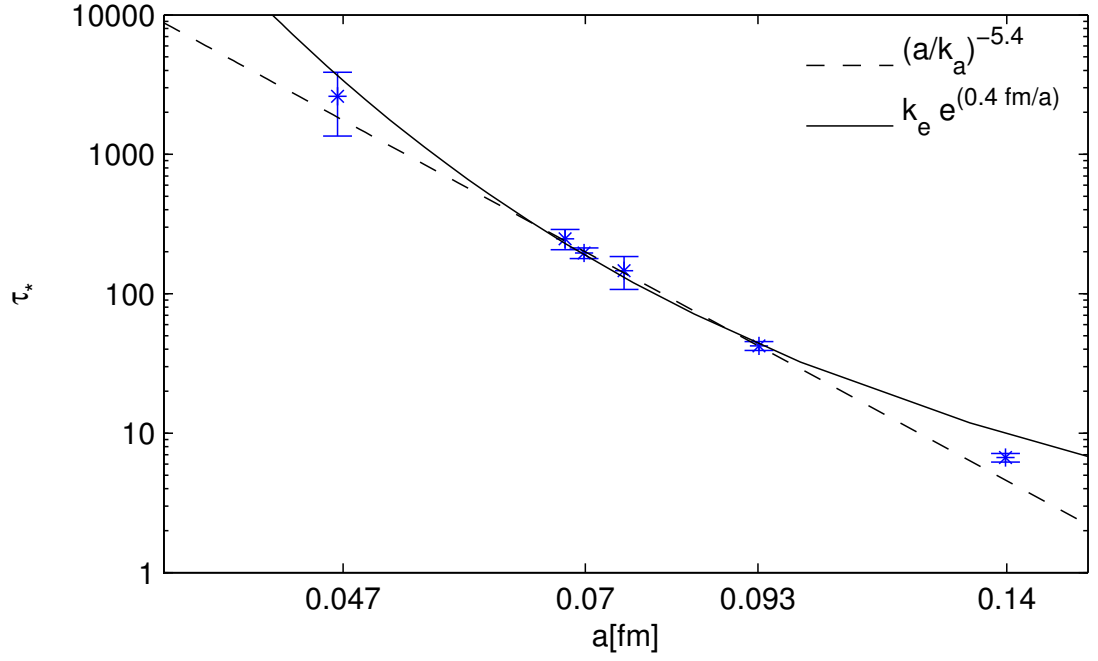
Figure 5.4.: Fit to the ansatz eq. (5.9). The observable is the smeared susceptibility χ_1 from the runs with trajectory length $\tau_{\mathrm{traj}} = 4$. The values of τ_*, eq. (4.79), are computed setting $r = 1$. In case of multiple runs at the same lattice spacing the plotted value is the corresponding average. The fits are performed over all but the rightmost point.

do not attempt to estimate any of the systematics. Even though the point at $a \sim 0.14$ fm does not enter the fit it is still reasonably well described. For all **practical** purposes we **choose** to use the more standard **power law ansatz** with a critical slowing down exponent $z = -5$ as proposed in ref. [71].

The trajectory length dependence of τ_{int}, visible in fig. (5.1), can also be modelled and taken into account. One possibility is to invoke the random walk hypothesis, stretching an analogy that sees the HMC algorithm as a random walker in configuration space that changes direction at the end of each trajectory: the distance covered would then scale with the square root of the number of steps taken. This behaviour is not expected to be universal and is expected to hold only in the case of observables for which $\tau_{\text{int}} \gg \tau$. For this reason it is plausible to think that the argument holds for τ_{exp}. Accordingly we will model the trajectory length dependence of τ_* with the following ansatz

$$\tau_*[\tau_{\text{traj}}] = \frac{k_{\text{traj}}}{\sqrt{\tau_{\text{traj}}}} + \frac{\tau_{\text{traj}}}{2} \ . \tag{5.10}$$

In fig. (5.5) we show the fit obtained from the runs at $\beta = 6$, where data appears to be represented reasonably well, especially given the qualitative nature of the random walk assumption.

Estimation of the exponential auto-correlation time

Estimating the exponential auto-correlation time from numerical data is not a simple task. The approach that we have used is to look at the decay of the auto-correlation function at large MC times. Even with the very large statistics that we manage to obtain in the quenched approximation we are still not able to estimate systematic effects. This should not be cause of great concern especially given the quite large statistical errors associated with typical estimates of τ_*.

In this phase we have looked at the estimator $\tau_{\text{exp}}^{\text{eff}}$ of eq. (4.76) for various observables (on the left of fig. (5.6) we show it for χ_1 of the C2d chain). We have in particular noted that an observable with a strong signal is the smeared topological susceptibility, and that for this observable the value of $\tau_{\text{exp}}^{\text{eff}}$ that we obtain is almost independent on the smearing level α. Not all observables behave as the topological charge w.r.t smearing, in the case of P_α, for example, we observe a sizable dependence on α.

As discussed when we introduced eq. (4.79), τ_* is defined through a relation that can be recursively solved for each value of the parameter r. As one can see from the plot on the right in fig. (5.6), τ_* is almost independent on the choice of r, signaling that the decay of the auto-correlation function could be well described by a single exponential on a wide interval starting from a lag of $\sim 0.5\tau_*$. Even though τ_* equals τ_{exp} only in the asymptotic limit

$$\lim_{r \to \infty} \tau_* = \tau_{\text{exp}} \tag{5.11}$$

we can see that at $r \sim 1$ the value of τ_* that we obtain is constant within errors. This gives support to the idea that the the mode that we identify with τ_* is indeed the one that contributes the most to the tail of other observables in the same parity sector (as
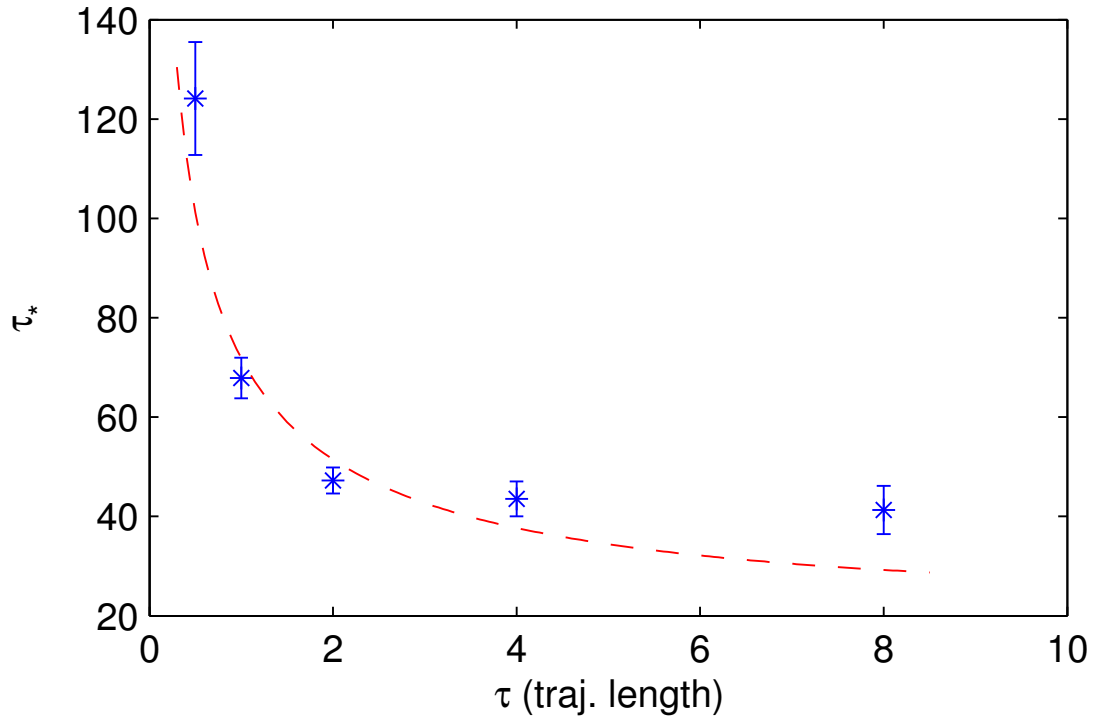
Figure 5.5.: Fit to the ansatz eq. (5.10), data comes from the runs at $\beta = 6$. The values of τ_* (multiplied by the appropriate ratio of active links factor R) at the same trajectory lengths τ_{traj} have been averaged. Errors are combined assuming statistical independence. The fit parameter is $k_{\mathrm{traj}} = 71$.
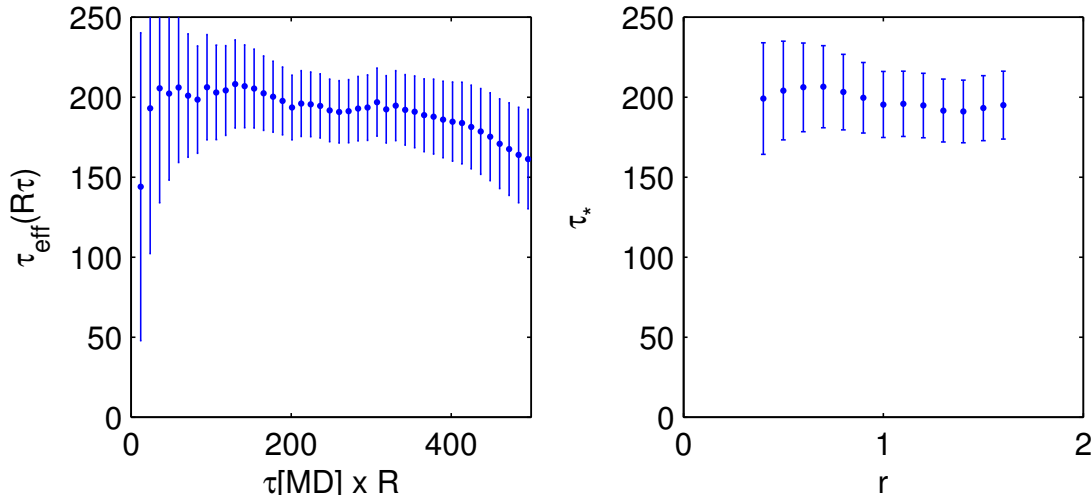
Figure 5.6.: Estimate, coming from the observable χ_1, of the effective exponential auto-correlation time $\tau_{\exp}^{\mathrm{eff}}$ and of the dependence of τ_* on r computed on the C2d chain.

discussed in section 4.2). This assumption is further backed with the quenched analysis that we will describe in the next section.

Dependence on volume and discretization

Most of the ensembles in table 5.1 have a fixed physical volume with $L \sim 2.2$ fm, for which finite size effects of typical expectation values are known to be small in the pure gauge theory. In order to check an eventual dependence of τ_{int} on volume, we simulated an ensemble with $L \simeq 3.3$ fm, at $\beta = 6.179$. In fig. (5.7) we demonstrate that the volume dependence for the smeared plaquette and for the susceptibility χ_1 is very weak.

Auto-correlation times and critical slowing down might as well depend on the choice of lattice discretization. Our analysis has mainly focused on the Wilson gauge action, but we have also generated an ensemble with the Iwasaki action (that is defined e.g. in ref. [61]) at $a \simeq 0.09$ fm, with the same volume we typically used and with the HMC algorithm. We observed larger auto-correlation times for the topological charge,

$$\tau_{\mathrm{int}}(\chi_5) = 34(4) \qquad \text{Wilson gauge action} \qquad (5.12)$$
$$\tau_{\mathrm{int}}(\chi_5) = 220(50) \qquad \text{Iwasaki action} \qquad (5.13)$$
$$(5.14)$$

however for the (smeared) plaquette we observed that auto-correlation times in both discretizations are roughly the same.
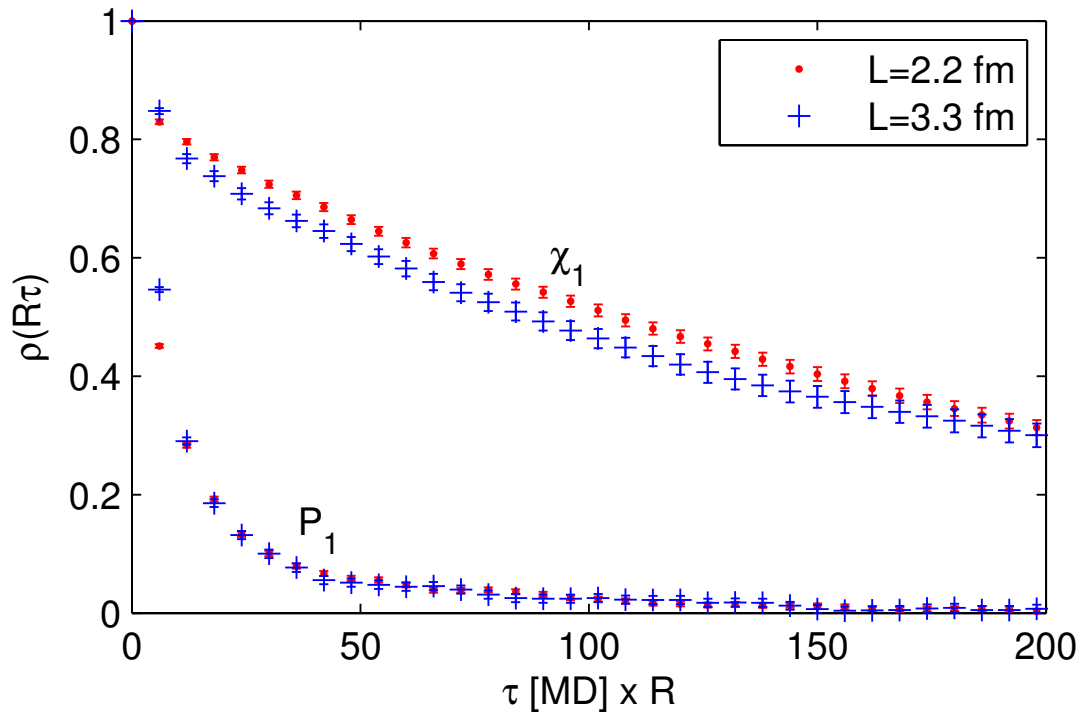
Figure 5.7.: Auto-correlation function of χ_1 and P_1 at two different volumes. The runs correspond to the tags C2d and C3d.
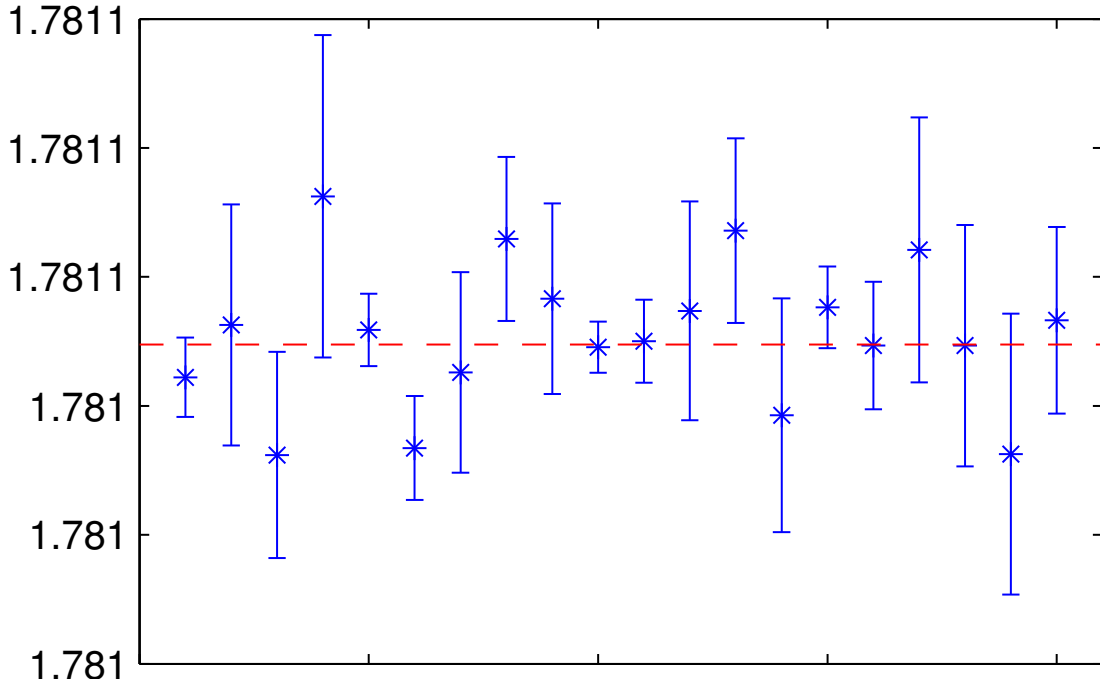
Figure 5.8.: Fit to a constant of plaquette values on the $\beta = 6$ lattices. With a $\chi^2/\text{d.o.f.} \simeq 0.7$ different simulations agree very well to the common average (dashed red line).

5.4. Applications to error analysis

At the lattice spacing corresponding to $\beta = 6$ we have performed twenty independent runs with two different algorithms and different setups. In fig. (5.8) we plot the values of the plaquette at this β together with their error: the χ^2 is compatible with the hypothesis that the expectation value of the plaquette is the same in all runs, confirming the consistency of our computations.

A result that we wish to discuss now in more detail is the scaling of auto-correlation times with the ratio of active links. Introducing blocks with frozen boundaries does not allow the propagation information across the boundaries during the time of a single trajectory. This in principle might reduce the efficiency of the algorithm by a factor that is larger than the ratio of active links R. If this were the case, the effect is expected to become stronger as the block size in physical units is reduced. In such limit the algorithm becomes ultra-local and large scale changes even more unlikely. A possible test is to look at τ_{int} of observables measured on configurations produced by HMC with and without domains, and with domains of different sizes, and compare their respective integrated auto-correlation times after rescaling by R (eventually repeating this experiment at different values of the trajectory length): perfect scaling would yield maximal decorrelation of links (namely the effect of having frozen boundaries is negligible), where maximal is w.r.t.

TAG	$\overline{P}$	$\tau_{\mathrm{int}}^{\mathrm{u}}(P_5)$	$\tau_{\mathrm{int}}^{\mathrm{u}}(Q_5^2)$
$\tau = 0.5$			
B0a	1.781044 (6)	100 (11)	130 (16)
B1a	1.781053 (19)	110 (30)	90 (18)
B2a	1.781032 (16)	130 (27)	110 (21)
B3a	1.781072 (26)	90 (25)	90 (20)
B4a	1.781052 (6)	95 (9)	110 (12)
$\tau = 1$			
B0b	1.781033 (8)	51 (6)	62 (8)
B1b	1.781045 (16)	55 (9)	70 (11)
B2b	1.781066 (13)	60 (11)	60 (11)
B3b	1.781057 (15)	60 (11)	60 (11)
B4b	1.781049 (4)	55 (3)	61 (4)
$\tau = 2$			
B0c	1.781050 (7)	38 (3)	45 (3)
B1c	1.781055 (17)	42 (7)	43 (7)
B2c	1.781067 (15)	44 (6)	48 (7)
B3c	1.781039 (19)	49 (9)	41 (6)
B4c	1.781055 (6)	40 (3)	49 (4)
$\tau = 4$			
B0d	1.781049 (10)	31 (3)	37 (3)
B1d	1.781064 (21)	38 (6)	46 (7)
B2d	1.781049 (19)	34 (5)	37 (5)
B3d	1.781033 (22)	44 (7)	43 (7)
$\tau = 8$			
B0e	1.781053 (15)	30 (3)	39 (4)

Table 5.2.: Integrated autocorrelation time and value of some observables on the $\beta = 6$ series of lattices
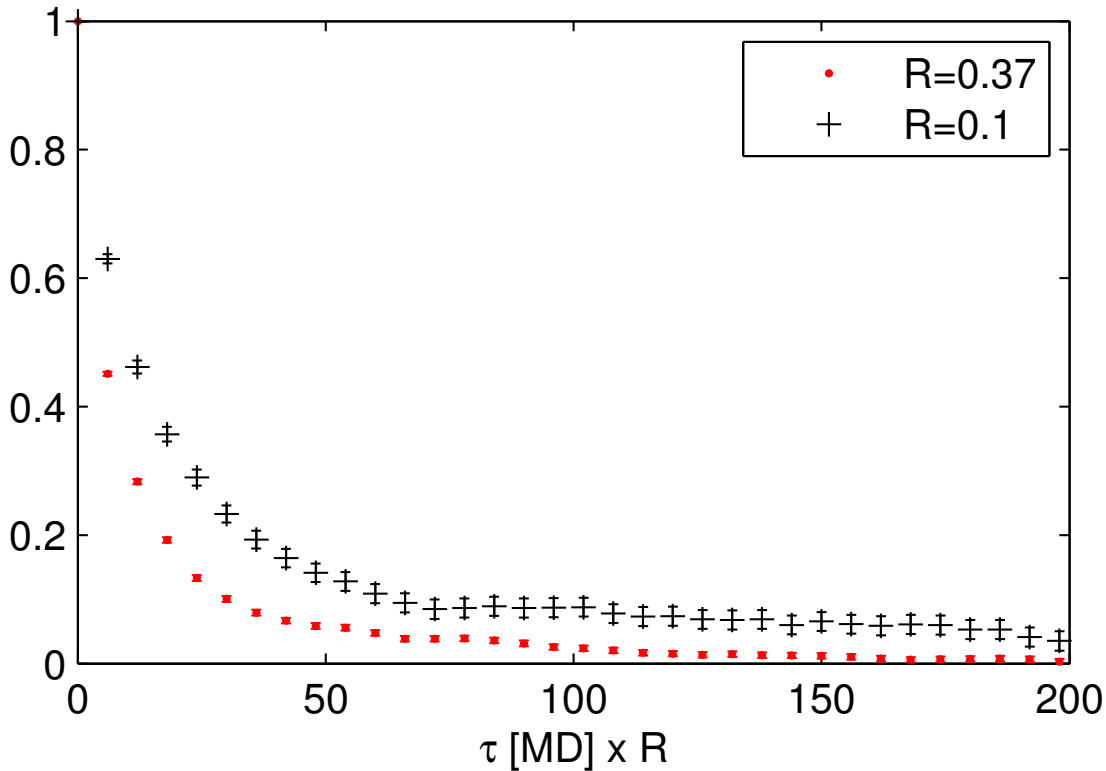
Figure 5.9.: Auto-correlation function of the smeared plaquette P_1 on the $\beta = 6.179$
lattices. The $\rho(\tau)$ shown is for two different values of the ratio of active links
R, corresponding to chain C2d and C4d.

the case without blocks.

If we look at the values of τ_{int} given in the table with the $\beta = 6$ results we see no
evidence of domain's boundary effects at any of the investigated trajectory length /
block size combinations. One still would expect to see effects from the blocking once the
block size becomes sufficiently small, for this reason we have performed a simulation at
$\beta = 6.179$ with the smallest block size possible, namely 4^4 (and a resulting ratio of active
links $R \simeq 0.1$). As is possible to see in fig. (5.9), where results for the once-smeared
plaquette are shown, the smaller block size shows a significantly larger auto-correlation
time. This difference does not come out if one instead looks at the unsmeared plaquette
(where the variance is dominated by short distance fluctuations).

5.4.1. Quenched observables

Quenched observables allow to test the ideas presented so far in a setup that resembles
the typical application in a lattice QCD computation. Moreover we can collect a large
sample of measurements that allows us to perform tests with a higher precision than on

a computation that involves dynamical fermions.

We have computed quenched observables only on the C1d and on the C5d chains. We have estimated the correlators for the pseudo-scalar and for the zero component of the axial current and we have combined them in order to compute C_{PP} and $C_{\mathrm{A_0P}}$. The valence quarks have been set at the strange and at the charm masses: in the C5d chain values of the hopping parameter were taken from ref. [31] (in particular we took the value corresponding to $\kappa_{\mathrm{c_1}}$ in the reference). In the case of C1d for the "strange" we have kept the same value of the hopping parameter as the one we have used for the finer lattice spacing (thus resulting in a slightly heavier quark mass in lattice units) while for the charm we used the value of $\kappa_{\mathrm{c_2}}$ in ref. [31] at $\beta = 6.2$. We would like to stress again that in this part of the analysis we were mostly interested in computing the auto-correlation function of some physically motivated correlators, with a sufficiently high statistics to investigate the possible contribution of slow modes.

The very high statistical accuracy of the computed effective M_{PCAC} lends itself to an analysis of the cutoff effects clearly visible in fig. 5.10. The deviations that we observe from a flat behaviour (the expected M_{PCAC} plateau) can be modelled as exponential contributions that, at fixed lattice spacing, vanish with $t \to \infty$ (the overall amplitude of these contributions must vanish in the continuum limit). The leading contribution to the cutoff effect should be given by one of the excited states of the underlying meson spectrum (since we are in quenched QCD the relevant degrees of freedom are given by the valence quarks used in the computation). We try to extract this information with the effective energy gap given by the continuum expression

$$\Delta E(t) = -\frac{\partial}{\partial t} \log \left(\frac{\partial}{\partial t} M_{\mathrm{PCAC}}(t) \right) \tag{5.15}$$

this should give a plateau when the effect seen in fig. 5.10, at large t, is described by a single exponential. We discretize eq. (5.15) in the following way

$$\Delta E_{\mathrm{eff}}(t) = -\frac{1}{4} \log \left\{ \left(\frac{M_{\mathrm{PCAC}}(t+2a) - M_{\mathrm{PCAC}}(t)}{M_{\mathrm{PCAC}}(t) - M_{\mathrm{PCAC}}(t-2a)} \right)^2 \right\} \tag{5.16}$$

namely with a symmetric discretization of the time derivative. The resulting plots are shown in fig. (5.12) and fig. (5.13) where we also put in evidence a possible plateau. The size of the gap shown in the plots is about 700 MeV, and that is about the same as the difference between charmonium mass and its first excited state.

We leave now the analysis of the systematic uncertainties (that are here so visible only because the statistical errors are tiny), and turn to the topic that is our main concern, namely the analysis of statistical errors of observables with long tails in the auto-correlation function. In particular the case where tails might go undetected due to a statistics that is too low. At first we would like to show that this worry is justified at least in some cases (especially when the lattice spacing becomes small). In figs. (5.11, 5.15 and 5.17) we show plots of the normalized auto-correlation function of some quenched observables, wile in table 5.3 we show their upper and lower bound of the integrated auto-correlation time, and the slow mode contribution to the upper bound of the error.
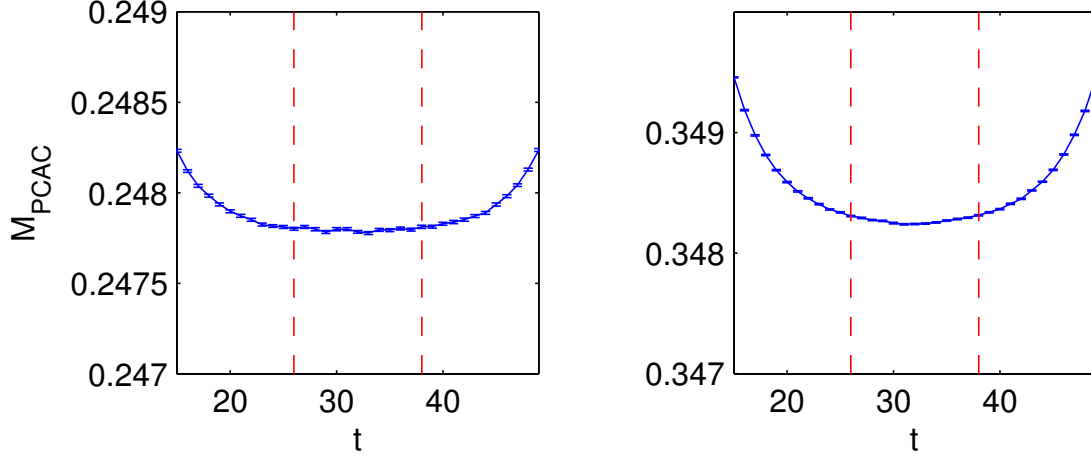
Figure 5.10.: PCAC mass of a valence "charm" quark. The vertical dashed lines represent the interval over which we averaged in order to compute the observable M_{PCAC}. **Left:** C1d chain with hopping parameter $\kappa \simeq 0.1275$. **Right:** C5d chain with hopping parameter $\kappa \simeq 0.1246$. Deviations from a plateau are visible at the level below 1 MeV.
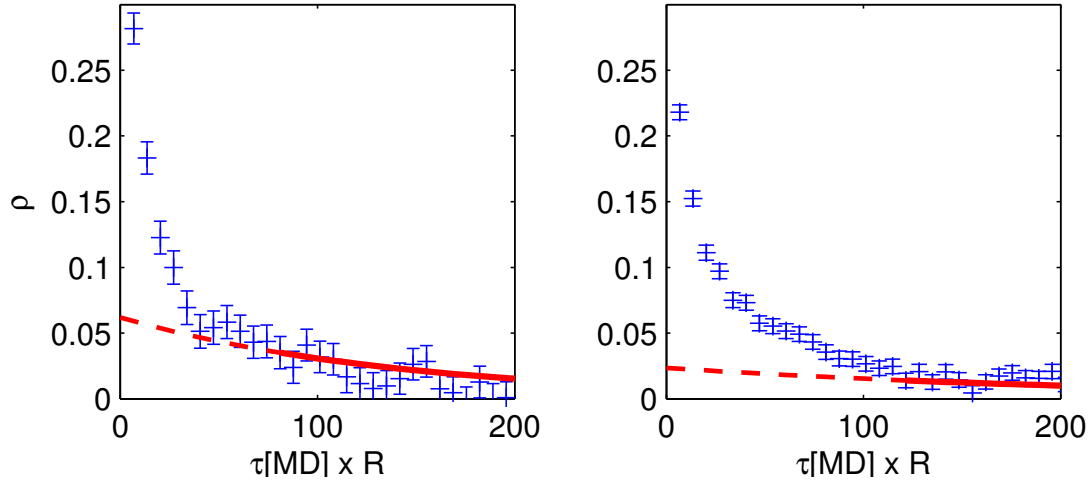

Figure 5.11.: Normalized auto-correlation function for the PCAC mass averaged over the plateau shown in fig. (5.10). The exponential tail used for computing the upper bound $\tau_{\text{int}}^{\text{u}}$ is also plotted. The solid line starts at W_{u}. **Left:** C1d chain with hopping parameter $\kappa \simeq 0.1275$. **Right:** C5d chain with hopping parameter $\kappa \simeq 0.1246$.
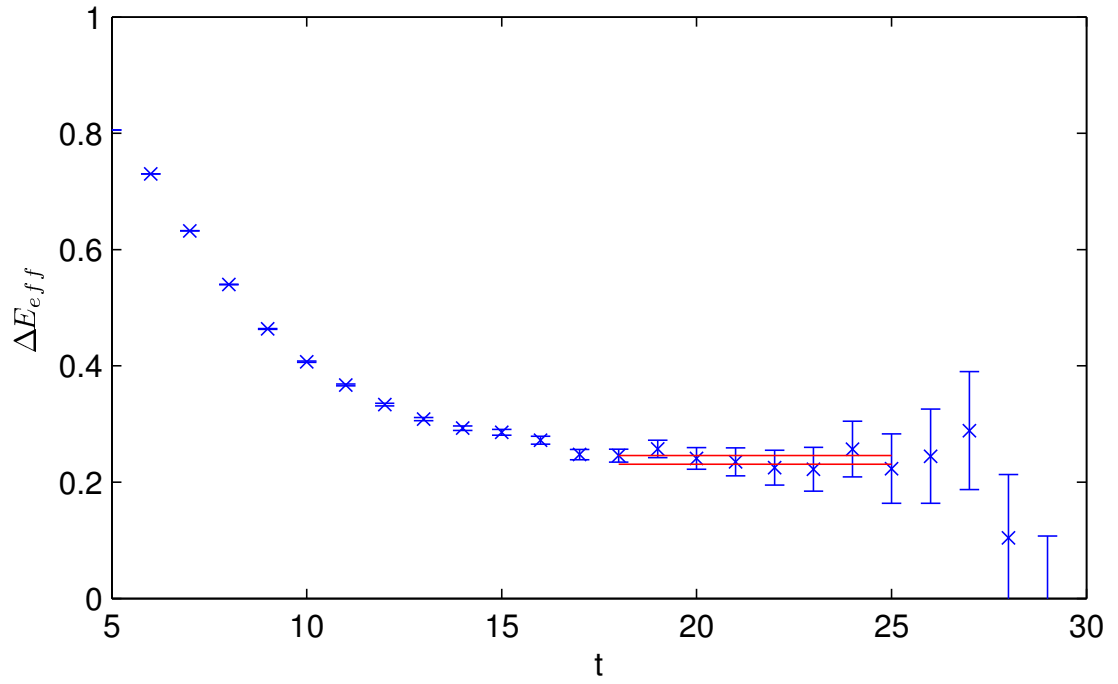
Figure 5.12.: Cutoff effects for M_{PCAC} of two degenerate valence "charm" quarks. We show the C5d chain with hopping parameter $\kappa \simeq 0.1246$. The two red lines mark a plateau average.
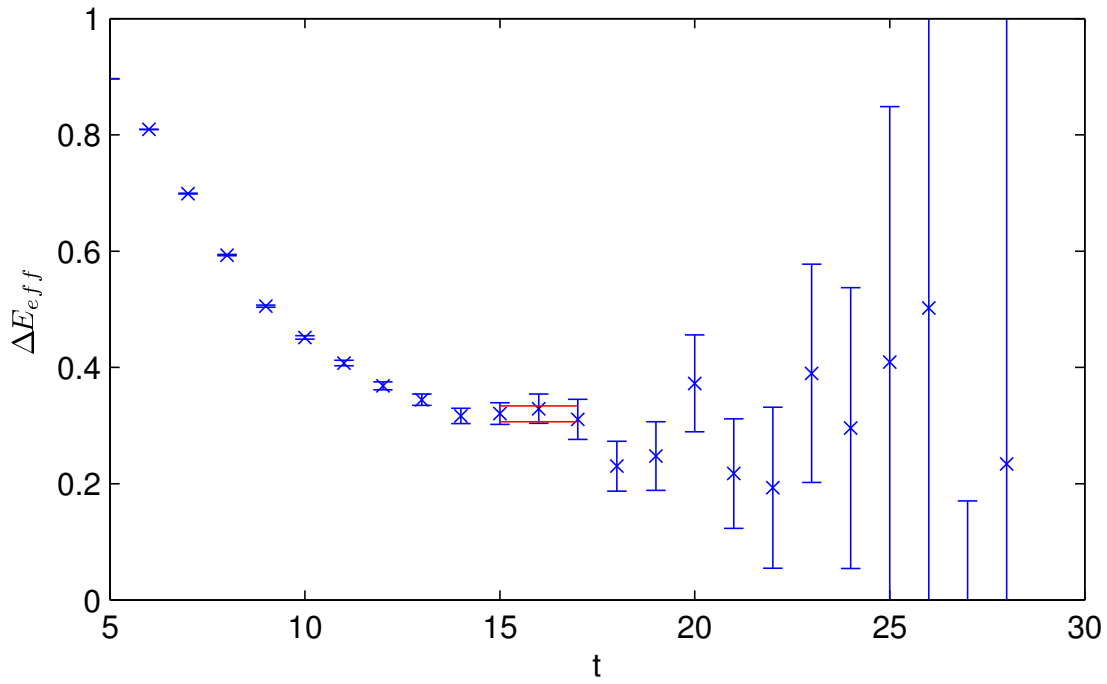
Figure 5.13.: Cutoff effects for M_{PCAC} of two degenerate valence "charm" quarks. We show the C1d chain with hopping parameter $\kappa \simeq 0.1275$. The two red lines mark a plateau average over the three central points.

β	O	κ_1	κ_2	$\overline{O}$	$\tau_{\mathrm{int}}^{\mathrm{l}}$	$\tau_{\mathrm{int}}^{\mathrm{u}}$	$C(W_{\mathrm{u}})\tau_*$
6.2							
	M_{PCAC}	0.1350	0.1350	0.024822(4)	0.73(2)	1.28(17)	0.55
	f_{PS}			0.10551(6)	0.65(1)	1.07(17)	0.39
	M_{PS}			0.23523(9)	1.07(3)	1.78(18)	0.53
	M_{PCAC}	0.1350	0.1246	0.172103(5)	0.64(1)	1.14(17)	0.50
	f_{PS}			0.07504(7)	0.55(1)	0.86(17)	0.34
	M_{PS}			0.67909(11)	0.65(1)	1.20(17)	0.51
	M_{PCAC}	0.1246	0.1246	0.348334(5)	1.87(7)	2.61(21)	0.61
	f_{PS}			0.09039(2)	0.71(2)	1.20(17)	0.48
	M_{PS}			1.03239(4)	2.16(8)	2.89(22)	0.59
6.14							
	M_{PCAC}	0.1350	0.1350	0.022334(7)	0.77(4)	1.21(23)	0.46
	f_{PS}			0.11222(11)	0.74(3)	1.35(24)	0.69
	M_{PS}			0.23547(17)	1.09(6)	1.82(24)	0.73
	M_{PCAC}	0.1350	0.1275	0.128179(7)	0.70(3)	1.14(23)	0.45
	f_{PS}			0.08625(12)	0.60(2)	1.10(23)	0.53
	M_{PS}			0.59422(21)	0.84(4)	1.84(23)	1.01
	M_{PCAC}	0.1275	0.1275	0.247815(7)	1.92(14)	2.75(31)	0.91
	f_{PS}			0.09625(4)	0.73(3)	1.23(23)	0.50
	M_{PS}			0.87048(8)	2.38(19)	3.23(35)	0.92

Table 5.3.: Expectation values and integrated auto-correlation time for the quenched observables on two different ensembles. $C(W_{\mathrm{u}}) = C_{\mathrm{O}} \exp(-W_{\mathrm{u}}/\tau_*)$, where C_{O} is the estimated amplitude of the slow mode.
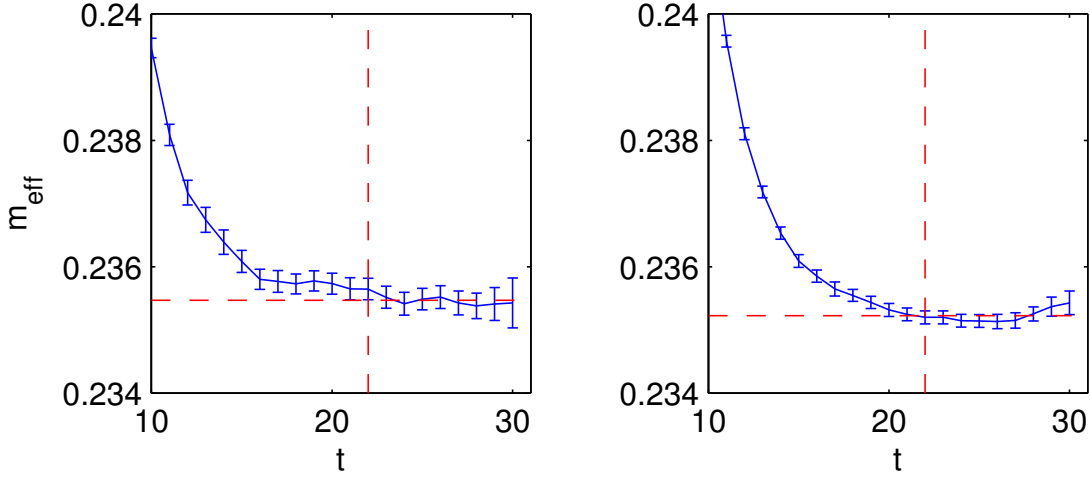
Figure 5.14.: Effective pseudo-scalar mass (eq. (5.6)) of a "heavy pion" where the up and down quark masses are $O(M_s)$. The vertical dashed line marks the start of the plateau over which we averaged in order to estimate M_{PS}. **Left:** C1d chain. **Right:** C5d chain.

From the plots we mainly draw the conclusion that in hadronic observables we do see a tail in the auto-correlation function, the tail appears to be well described by τ_* (the fitted value) and at this high precision the contribution coming from the tail is relatively small. This is also confirmed by the numbers in table 5.3, from which we conclude that the contribution coming from the tail is between 20% to 50% of the estimated τ_{int}^{l}. If one neglected the tail contribution the total error would come out up to 10–25% underestimated. Due the high precision of the measurements, in a case like the effective mass shown in fig. (5.14) this is much smaller than the systematic error.

The main lesson that we can gain is that as long as the statistical errors are well under control, with a chain that spans many τ_*'s (or τ_{exp}'s), it appears that the tails can either be reliably estimated or, in a case like the one shown in fig. (5.17), they can be safely neglected. This however need not to be the case when the chain is not sufficiently long, namely when its length is only a few τ_{exp}'s.

The case of a short chain

Let us now consider the case where we have an observable O computed on a chain of length N, assuming that

1. the chain is long w.r.t the typical MC scales of the observable O, namely $N \gg \tau_{\text{int}}(O)$

2. the chain does not sample the tail well $N \gtrsim \tau_{\text{exp}}$.

This case differs from the ones we have previously analyzed because the slow modes of the chain are not sampled very well, but if we assume that O is an observable that does not
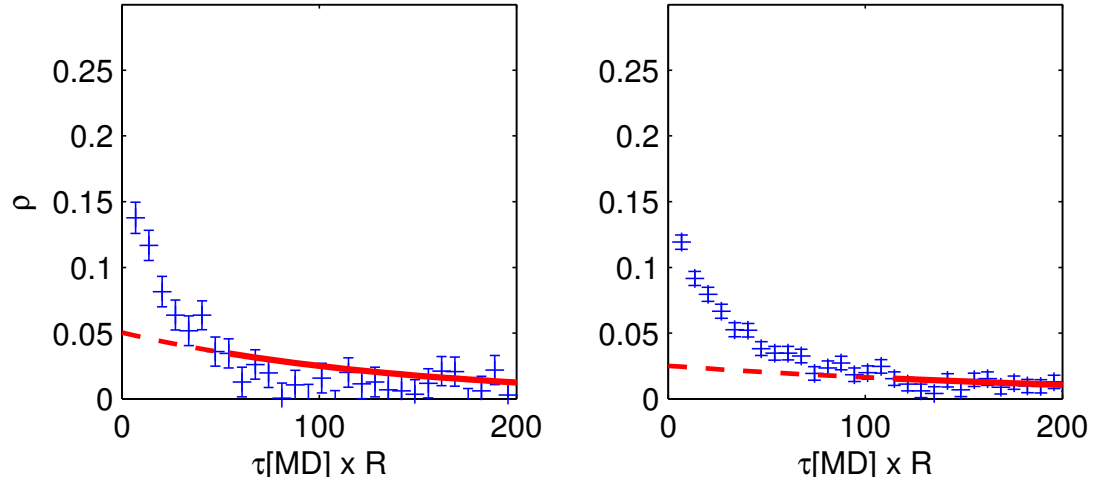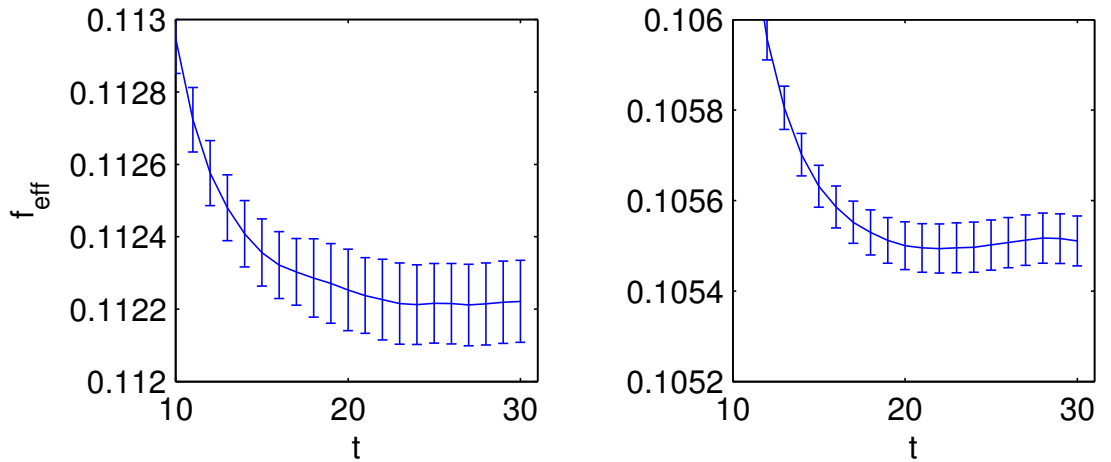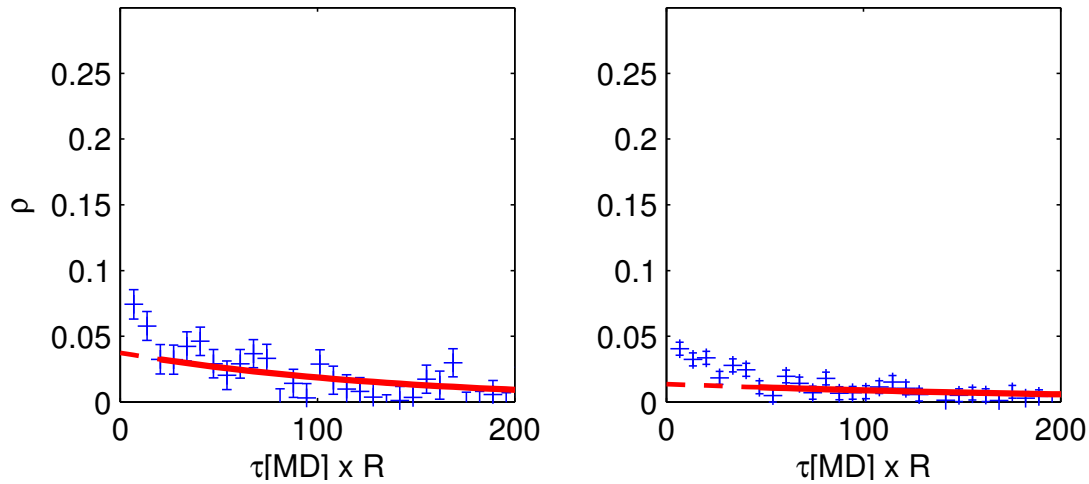
Figure 5.15.: Normalized auto-correlation function of M_{PS} with the plateau shown in fig. (5.14). The exponential tail used for computing the upper bound $\tau^{\mathrm{u}}_{\mathrm{int}}$ is also plotted (dashed line). **Left:** C1d chain. **Right:** C5d chain.

Figure 5.16.: Effective pseudo-scalar decay constant (eq. (5.8)) of a "heavy pion" where the up and down quark masses are $O(M_{\mathrm{s}})$. The vertical dashed line marks the start of the plateau over which we averaged in order to estimate f_{PS}. **Left:** C1d chain. **Right:** C5d chain.

Figure 5.17.: Normalized auto-correlation function of f_{PS} with the plateau shown in fig. (5.16). The exponential tail used for computing the upper bound $\tau_{\mathrm{int}}^{\mathrm{u}}$ is also plotted (dashed line). **Left:** C1d chain. **Right:** C5d chain.

couple strongly to the slow modes, we know that τ_{int} will still be estimated well. In case this is not true, namely if $\tau_{\mathrm{int}}(O)$ has non-negligible contributions from a tail that extends up to say 10 or 20 times $\tau_{\mathrm{int}}(O)$ then the tail contributions could be missed and $\tau_{\mathrm{int}}(O)$ would end up being underestimated. In fig. (5.18) we present a convincing example. The observable shown is the topological charge computed without smearing the gauge field. It is not very relevant for physics since it is parity odd and its expectation value is 0, but it provides an interesting example for the error analysis. The unsmeared Q_{top} couples strongly to UV modes (in MC time) that are most probably related to the short distance fluctuations of the gauge field. From the plot of the auto-correlation function in fig. (5.18) we can see that Q_{top} couples also to the slow mode $\tau_*^{\mathrm{odd}} = 2\tau_*$ (this is the empirical relation that we observe between the slow modes in the two different sectors): even though this coupling is weak (from eq. (4.80) we estimate it to be $C_{Q_{\mathrm{top}}}^* \simeq 0.03$), it still accounts for more than half of $\tau_{\mathrm{int}}(Q_{\mathrm{top}})$. If we were to estimate $\tau_{\mathrm{int}}(Q_{\mathrm{top}})$ from a single chain of length $N \simeq 4000\,\tau_{\mathrm{int}}(Q_{\mathrm{top}})$, as we show on the right of fig. (5.18), a large part of the tail would be overwhelmed by the noise and we would risk to miss up to 50% of τ_{int}. In fig. (5.19) a second example is shown. This is a histogram of errors computed breaking up a long chain in many smaller sub-chains. From the figure one can see that the estimate $\tau_{\mathrm{int}}^{\mathrm{u}}$ tends to give an overestimate of the statistical error that does not exceed a factor of 2, while $\tau_{\mathrm{int}}^{\mathrm{l}}$ is systematically underestimating the true error even though the effect is rarely as small as 50%.

We can conclude that estimating τ_{int} from a short chain (with for instance a length $O(10)\,\tau_{\mathrm{exp}}$, close to the ones that are typically found in the literature of QCD with dynamical fermions [34]) can be done reliably if a knowledge of τ_* is given. In the case of the more standard estimator $\tau_{\mathrm{int}}^{\mathrm{l}}$, the noise might indeed grow at the point that we would
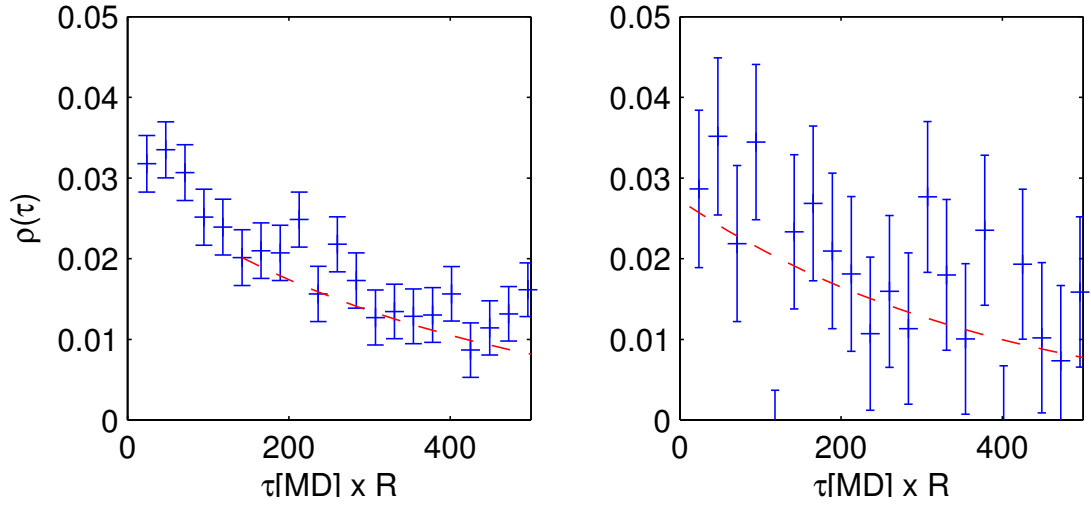
Figure 5.18.: Normalized auto-correlation function of the unsmeared Q_{top}. The exponential tail used for computing the upper bound $\tau_{\text{int}}^{\text{u}}$ is also plotted. **Left:** estimate from the whole chain. **Right:** estimate from a subset of the chain of length 4000 $\tau_{\text{int}}(Q_{\text{top}})$.

get an estimate up to 40% smaller than the real τ_{int} (but this figure will also depend on the relative size of τ_*). The estimator $\tau_{\text{int}}^{\text{u}}$ tends to give an error estimate that is more conservative but at the same time more reliable and therefore recommended.
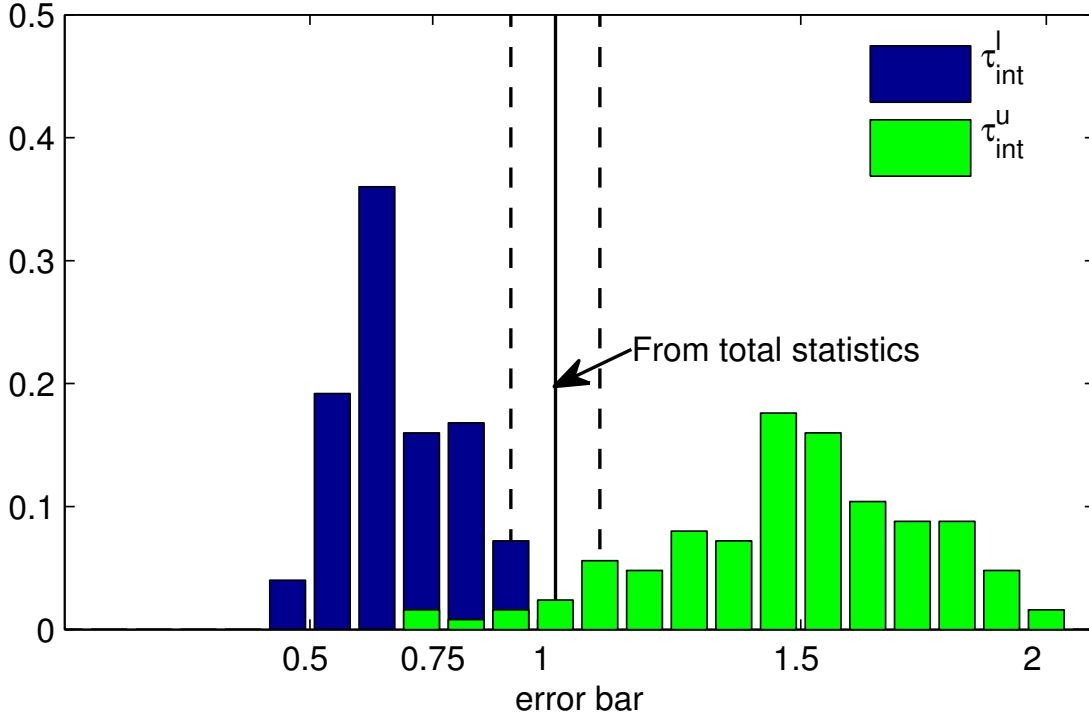
Figure 5.19.: Histogram of the values of $\tau_{\mathrm{int}}^{\mathrm{u}}$ and $\tau_{\mathrm{int}}^{\mathrm{l}}$ that we obtain when we compute them on subsets of the entire available data. The ensemble used is C5d and the observable is M_{PS} computed with $\kappa_1 = \kappa_2 = 0.1264$. Each subset has a size of 5500 MDU, that is a bit less than 1% of the total available statistics. The value of $\tau_* = 600MDU$ that we use is the one that comes from the complete run. The central line shows the normalization, that we chose to be the error computed from the total statistics available (properly normalized). The dashed lines indicate the error of the error.

6. Critical slowing down: $N_f = 2$ analysis

Given the much higher computational cost of numerical simulations that include the effects of light sea quarks, a scaling analysis as the one shown in fig. (5.4) would be prohibitively expensive on nowadays machines. Instead we tried to isolate the contribution from the slow mode at an intermediate lattice spacing and applied the scaling law that we have found in the pure gauge analysis to the dynamical fermions ensembles. In this way we are able to estimate the size of τ_* in a range of lattice spacings that covers all current simulations with two flavours of improved Wilson fermions.

Tag	Size	a [fm]	M_π [MeV]	N[MDU]	τ_* [MDU]
A2	64×32^3	0.074	630	8200	70
A3	64×32^3	0.074	500	8000	70
A4	64×32^3	0.074	390	8100	70
A5	64×32^3	0.074	330	8000	30
E4	64×32^3	0.065	590	2600	130
E5	64×32^3	0.065	440	16000	130
F6	96×48^3	0.065	310	4800	130
F7	96×48^3	0.065	270	10000	130
N4	96×48^3	0.048	550	3800	450
N5	96×48^3	0.048	440	3800	450
N6	96×48^3	0.048	340	2600	200
O7	128×64^3	0.048	270	3900	200

Table 6.1.: CLS ensembles

The chains that we have used in this analysis have been computed as part of the CLS[1] effort and they are listed in table 6.1. The configurations have been generated with the DD-HMC algorithm of ref. [40] and with the mass preconditioned HMC of ref. [54]. Units are not rescaled by the ratio of active links, this is reflected in the difference of τ_* in simulations performed at the same value of the lattice spacing.

6.1. Critical slowing down in full QCD

The main aim of this study was to bridge the scaling law that we derived in the pure gauge sector to the dynamical fermion sector. We did this by assuming that correlation times in simulations with dynamical fermions scale with a the same way as their quenched counterparts.

---

[1] https://twiki.cern.ch/twiki/bin/view/CLS/WebHome

TAG	Q_5^2					P_5		
	$\langle Q_5^2 \rangle$	$\langle a^4 \chi_t \rangle$	$\tau_{\mathrm{int}}^{\mathrm{l}}$	$\tau_{\mathrm{int}}^{\mathrm{u}}$	τ_*	$\tau_{\mathrm{int}}^{\mathrm{l}}$	$\tau_{\mathrm{int}}^{\mathrm{u}}$	τ_*
C1d	50(4)	$2.4(2) \times 10^{-5}$	137(25)	134(15)	140(18)	38(4)	43(5)	74(11)
E5f	17.3(1.8)	$0.82(9) \times 10^{-5}$	16(4)	23(5)	21(5)	84(31)	66(13)	66(19)
E5g	18.9(1.5)	$0.90(7) \times 10^{-5}$	10(2)	14(3)	15(4)	29(8)	29(5)	39(12)

Table 6.2.: Values of τ_{int} for some observables.

6.1.1. A comparison with quenched data

As part of the CLS effort we have carried out two long runs at the physical parameter of the E5 ensemble. Both runs consist of about 16000 MD units with a ratio of active links $R = 0.37$. The E5f chain was generated with $\tau_{\mathrm{traj}} = 1/2$ and E5g with $\tau_{\mathrm{traj}} = 4$. The quenched simulation that we use for comparison is the C1d. The lattice spacings have been matched with r_0/a from ref. [37], and the difference we see between the value of a from table 6.1 and the value of a in table 5.1 comes from the fact that in the former the scale setting was done with f_K as in ref. [55]. We would like to note that, compared to standard LQCD computations, the length of the two E5 chains is quite long, but compared to an integrated correlation time of a slow observable, e.g. P_5, we merely have $N \simeq 200 \, \tau_{\mathrm{int}}(P_5)$.

A first difference we noticed between the quenched and the full QCD ensembles is the shorter decorrelation time of the topological charge with dynamical fermions, as one can see also in fig. (6.1). This effect might be related to the suppression of the topological susceptibility in the chiral limit: with smaller pion masses large excursions of the topological charge become more unlikely, effectively reducing the "volume" of configuration space to be explored by the algorithm.

A second difference is the noticeable effect of smearing on $\tau_{\mathrm{int}}(\chi_\alpha)$. In the previous chapter we have said that in the pure gauge sector $\tau_{\mathrm{int}}(\chi_\alpha)$ is almost independent of α but, as one can see in fig. (6.2), with dynamical fermion this is no longer the case: while $\rho_{\chi_1}(\tau)$ is compatible with zero already at short lag, $\rho_{\chi_5}(\tau)$ remains significantly different from zero up to $\tau \sim 50$. Differently from the topological charge, the auto-correlation functions of all other observables that we compared look very similar in the two cases.

6.1.2. Proposal for error estimates

The auto-correlation times that we have measured on the E5f-g and C1d runs are listed in table 6.2. The auto-correlation times of E5g are between 20% to 50% smaller than those of the E5f run, showing that also in simulations with dynamical fermions longer trajectories do help. For the $N_{\mathrm{f}} = 2$, O(a)-improved action we suggest the $a^{-5} \sim \exp(7\beta)$ scaling that we observed in the pure gauge theory. To calibrate the amplitude of the power law we use the upper bound of the largest value of τ_* that we have measured on E5g. This gives $\tau_*(\beta = 5.3) \simeq 50$ that translates in the law, for the action of ref. [33]

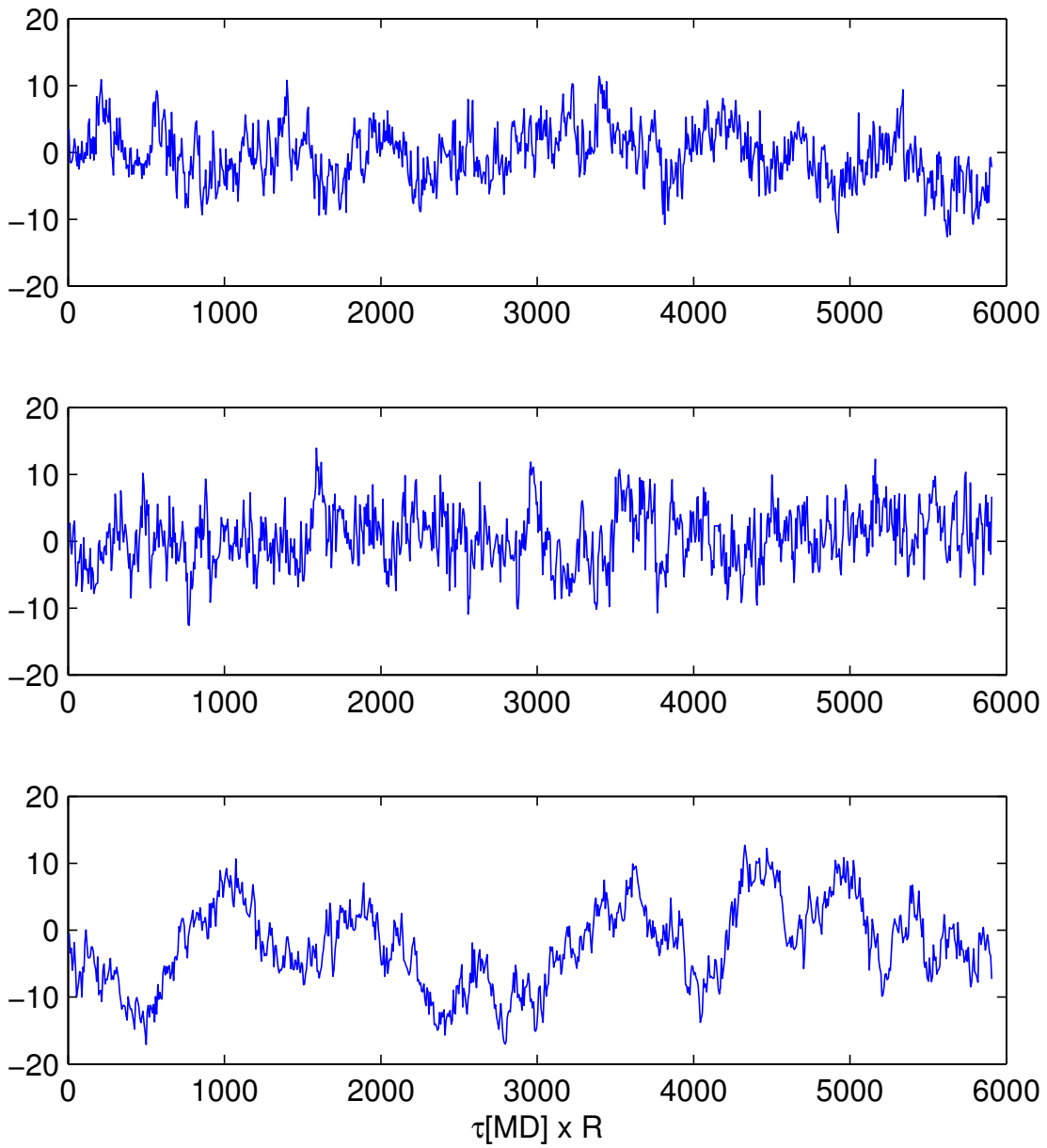$$\tau_{\exp}(\beta) \approx 200 \exp\left(7(\beta - 5.5)\right) \tag{6.1}$$

Figure 6.1.: Values of Q_5 measured on the E5f (**top**), E5g (**middle**) and C1d (**bottom**) chains: this last plot is cropped from the complete chain.
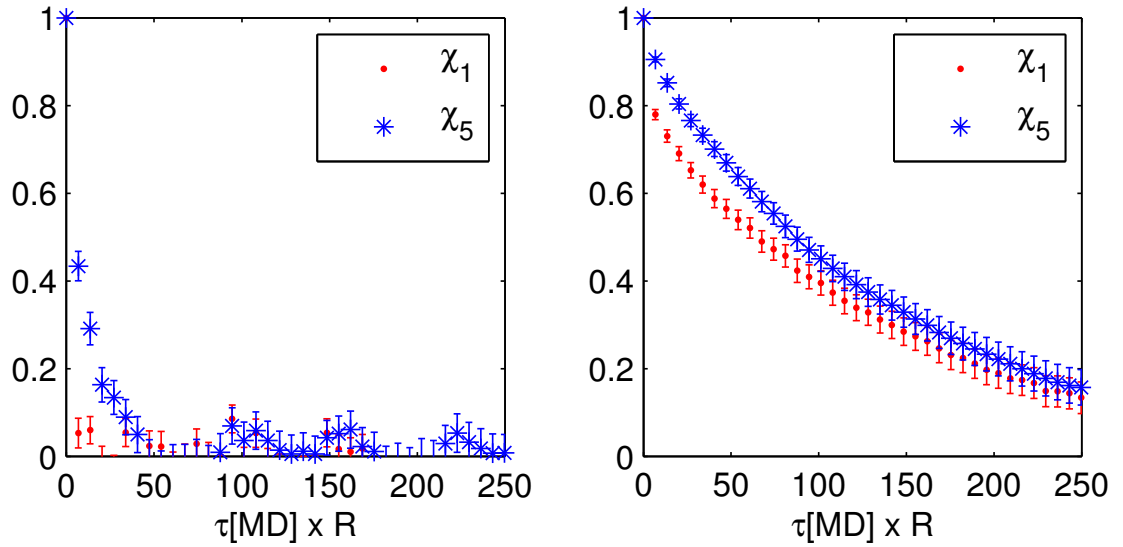
Figure 6.2.: Auto-correlation function of χ_{top} at different smearing levels. **Left:** E5g chain. **Right:** C1d chain.

where an error of a factor 2 seems reasonable for $5.2 \leq \beta \leq 5.7$. We remind here that in the case of DD-HMC the value of τ_{exp} is further increased by a $1/R$ factor, where R is the ratio of active links.

6.2. Error analysis of a full-QCD observable

As a practical application of the method that we have so far discussed we would now like to to show a determination of the lattice spacing with an error estimate that takes auto-correlations fully into account. This computation is done using the CLS ensembles of table 6.1. We will set the scale from the kaon decay constant f_K.

6.2.1. Strategy of the computation

Many simulations with dynamical fermions are performed at values of the pion mass different from its physical value $M_\pi \neq M_{\pi,\text{phys.}}$. This fact mostly reflects limitations of the algorithm used for generating the lattice configurations: smaller pion masses increase the cost of the computation and set a lower bound on the lattice volume through the stability requirement of $M_\pi L \geq 4$.

For this reason the value of computed observables has to be extrapolated to the physical point ($M_\pi = M_{\pi,\text{phys.}}$). The standard method adopted for performing this extrapolation is chiral perturbation theory (ChPT). The setup of our simulations consists of $N_f = 2$ degenerate quark flavours, this means that the contribution to the action coming from the strange and heavier quarks does not enter the path integral. Hadronic quantities

that have at least one valence quark that is not a sea quark (i.e. kaons) are said to be partially quenched (analogously to the hadronic observables in pure SU(3) simulations that are said to be quenched). In the case of partially quenched observables a theory that can be used for the extrapolations is partially quenched ChPT (PQChPT).

For the extrapolation we consider three quarks with hopping parameters $\kappa_1, \kappa_2, \kappa_3$. The first two correspond to the degenerate sea quarks $\kappa_1 = \kappa_2$. The pseudo-scalar meson whose valence quarks are the two sea quarks is the π, its mass is $M_\pi(\kappa_1)$ and at the physical point is given by $M_{\pi,\text{phys.}} = 134.8$ MeV. The kaons are composed by a sea quark and a quenched strange quark, their mass is $M_K(\kappa_1, \kappa_3)$ that at the physical point is given by $M_{K,\text{phys.}} = 494.2$ MeV.

A way to define kaons is through the dimensionless ratio

$$\frac{M_K^2(\kappa_1, \kappa_3)}{f_K^2(\kappa_1, \kappa_3)} = \frac{M_{K,\text{phys.}}^2}{f_{K,\text{phys.}}^2} \tag{6.2}$$

that can be imposed on the l.h.s. quantities at varying sea quark mass $M_1(\kappa_1)$ and gauge coupling β. The relation in eq. (6.2) fixes a value of $\kappa_3 = h(\kappa_1)$ as a function of the sea quark hopping parameter. At lowest order in ChPT we have that

$$[M_K^2(\kappa_1, \kappa_3)]_{\text{tree}} = \mu(M_1 + M_3) , \quad [f_K(\kappa_1, \kappa_3)]_{\text{tree}} = f \tag{6.3}$$

where f and μ are ChPT low energy constants. At this order eq. (6.2) fixes to a constant $M_3 + M_1 = \widehat{M} + M_s$ where $\widehat{M} = (M_u + M_d)/2$ and M_s is the mass of the strange quark. For this reason this procedure is should give a mild chiral extrapolation for $f_K(\kappa_1, \kappa_3)$ since this also is expected to be a function of the sum of the two quark masses.

After having determined the value of κ_3 (e.g. by interpolation) it remains to extrapolate the decay constant $af_K(\kappa_1, \kappa_3)$ to the physical point, defined by the dimensionless ratio

$$\frac{M_\pi^2(\kappa_1)}{f_K^2(\kappa_1, \kappa_3)} = \frac{M_{\pi,\text{phys.}}^2}{f_{K,\text{phys.}}^2} . \tag{6.4}$$

For this last step we use PQChPT of ref. [72], were the relevant one loop expression is found

$$\frac{[f_K(M_1, M_3)]}{f}_{\text{1-loop}} =$$
$$-\frac{1}{2}(y_{13} \log y_{13} + y_{11} \log y_{11}) - \frac{1}{8}\left(y_{11} \log \frac{y_{33}}{y_{11}} + y_{11} - y_{33}\right)$$
$$+ \frac{1}{2}\alpha_5 y_{13} + \alpha_4 y_{11} \tag{6.5}$$

with $y_{ij} = \mu(M_i + M_j)/(4\pi f)^2$ and with $\alpha_{4,5}$ low energy constants of the one loop

expansion. The functional form that we finally obtain is:

$$\frac{af_{\mathrm{K}}(M_1, M_3)}{af_{\mathrm{K}}(\widehat{M}, M_{\mathrm{s}})} = 1 + \overline{L}(\hat{y}_{11}, y_{\mathrm{K}}) + (\alpha_4 - \frac{1}{4})(\hat{y}_{11} - y_\pi) + \mathrm{O}(y^2) \tag{6.6}$$

$$\overline{L}(\hat{y}_{11}, y_{\mathrm{K}}) = L(\hat{y}_{11}, y_{\mathrm{K}}) - L(y_\pi, y_{\mathrm{K}}) \tag{6.7}$$

$$L(y, y_{\mathrm{K}}) = \frac{1}{2} y \log(y) + \frac{1}{8} y \log(2y_{\mathrm{K}}/y - 1) \, , \tag{6.8}$$

where the a is there as a reminder of the fact that the extrapolation is done at finite lattice spacing. The variables y are defined as

$$\hat{y}_{11} = \frac{M_\pi^2(\kappa_1)}{8\pi^2 f_{\mathrm{K}}^2(\kappa_1, \kappa_3)} \, , \quad y_{\mathrm{K}} = \frac{M_{\mathrm{K,phys.}}^2}{8\pi^2 f_{\mathrm{K,phys.}}^2} \, , \quad y_\pi = \frac{M_{\pi,\mathrm{phys.}}^2}{8\pi^2 f_{\mathrm{K,phys.}}^2} \, , \tag{6.9}$$

and w.r.t. eq. (6.5) we see that y_{13} cancels out since at leading order is constant, we substitute $y_{33} = 2y_{\mathrm{K}} - y + \mathrm{O}(y^2)$ and instead of the low energy constant f we use $f_{\mathrm{K}}(\kappa_1, \kappa_3)$. At one loop order of the chiral expansion this last change is consistent, and might even result in smaller corrections from the logarithmic terms. The lattice spacing can finally be computed with

$$a = \frac{af_{\mathrm{K}}(\widehat{M}, M_{\mathrm{s}})}{f_{\mathrm{K,phys.}}} \, . \tag{6.10}$$

6.2.2. Steps in the analysis

The primary quantities that enter the analysis are the C_{PP} and $C_{\mathrm{A_0P}}$ correlators of eq. (5.4) and eq. (5.5). From the correlators we estimate the lightest pseudo-scalar masses (the ones corresponding to the pions and the kaons), the matrix elements corresponding to these states and the PCAC bare quark masses.

Since lattices have finite time extent T with periodic boundary conditions, the computation of the properties of light mesons must address the fact that states with higher energy contribute to the correlation function in eq. (2.46) and that in general there are both forward and backward propagating contributions (e.g. mesons can travel both inside the lattice and through the boundaries). In general a correlator can then be expressed as

$$C(t) = \sum_{m,n} A_{nm} \exp(-tE_n - (T-t)E_m) \tag{6.11}$$

where in the case of C_{PP} the matrix A_{nm} is symmetric while for $C_{\mathrm{A_0P}}$ it is antisymmetric. In the specific case of these two correlators we write

$$C_{\mathrm{PP}} = \sum_{m=0, n=m}^{\infty} A_{nm} h_{\mathrm{s}}(t, E_n, E_m) \tag{6.12}$$

$$C_{\mathrm{A_0P}} = \sum_{m=0, n=m}^{\infty} B_{nm} h_{\mathrm{a}}(t, E_n, E_m) \tag{6.13}$$

where

$$h_{\mathrm{s}}(t, E, E') = \exp(-tE - (T-t)E') + \exp(-tE' - (T-t)E) \qquad (6.14)$$

$$h_{\mathrm{a}}(t, E, E') = \exp(-tE - (T-t)E') - \exp(-tE' - (T-t)E). \qquad (6.15)$$

As discussed in ref. [10], the leading contribution to zero momentum projected correlators (e.g. when the interpolators are the ones from eq. (2.48)) is given by $E_0 = 0$ and $E_1 = M_{\mathrm{PS}}$ where PS is a pseudo-scalar meson that can in our case either correspond to a pion or a to kaon, depending on the interpolating quark fields. For the computation of the lattice spacing we are interested in the mass and matrix element that corresponds to this leading contribution. In the case of the C_{PP} correlator these quantities can be extracted from a fit to $A\,h_{\mathrm{s}}(t, 0, M_{\mathrm{PS}})$, while for $C_{\mathrm{A_0P}}$ the fit is with the anti-symmetric formula. The choice of fit range has to be made such that systematic contributions coming from higher states are negligible compared with the size of the statistical errors. For this reason we have decided to fit both the ground state and the first excited state through the spectral representation, e.g. in the case of C_{PP} shown in fig. (6.3) we fit

$$C_{\mathrm{PP}}(t) \sim A_0 h_{\mathrm{s}}(t, 0, M_{\mathrm{PS}}) + A_1 h_{\mathrm{s}}(t, 0, M') \, . \qquad (6.16)$$

After having computed the effective mass as in eq. (5.6) and its statistical error $\delta M_{\mathrm{eff}}(t)$, we compare it to the size of the fitted contribution coming from the first excited state, as shown in fig. (6.4). We have finally used the criterion that systematic effects are negligible when the following condition is met

$$4\Delta_{\mathrm{sys.}}(t) < \delta M_{\mathrm{eff}}(t) \qquad (6.17)$$

where $\Delta_{\mathrm{sys.}}(t) = A_1 h_{\mathrm{s}}(t, 0, M')$. The first point t_1 that satisfies eq. (6.17) defines a range that is used in a single exponential fit for estimating the matrix element and M_{PS}. Our choice of fit range for the double exponential in eq. (6.16) has been always in the range $4 \le t_0/a \le 11$, and we have verified that t_1 does not vary much against a choice of $t_0 \pm a$.

The bare quark mass is determined from the PCAC relation of eq. (5.7), where the improvement coefficient c_{A} is the one of the two flavour theory determined in ref. [13]. In the case of the quark mass the initial time used for the plateau average has been chosen such that cutoff effects are negligible (inspecting the plots by eye) as shown for example in fig. (6.5).

From the single exponential fit of C_{PP} we obtain the square of the bare matrix element given by eq. (2.61). In turn this is used for extracting the bare decay constant f_{PS} that, together with M_{PS} and M_{PCAC} (computed at four different partially quenched hopping parameters), is the set of first-level derived observables that we have used for the second part of the analysis.

The next step in the analysis has been the determination of κ_3 from eq. (6.2). In all chains of table 6.1 we computed the correlators at the unitary point and four mixed
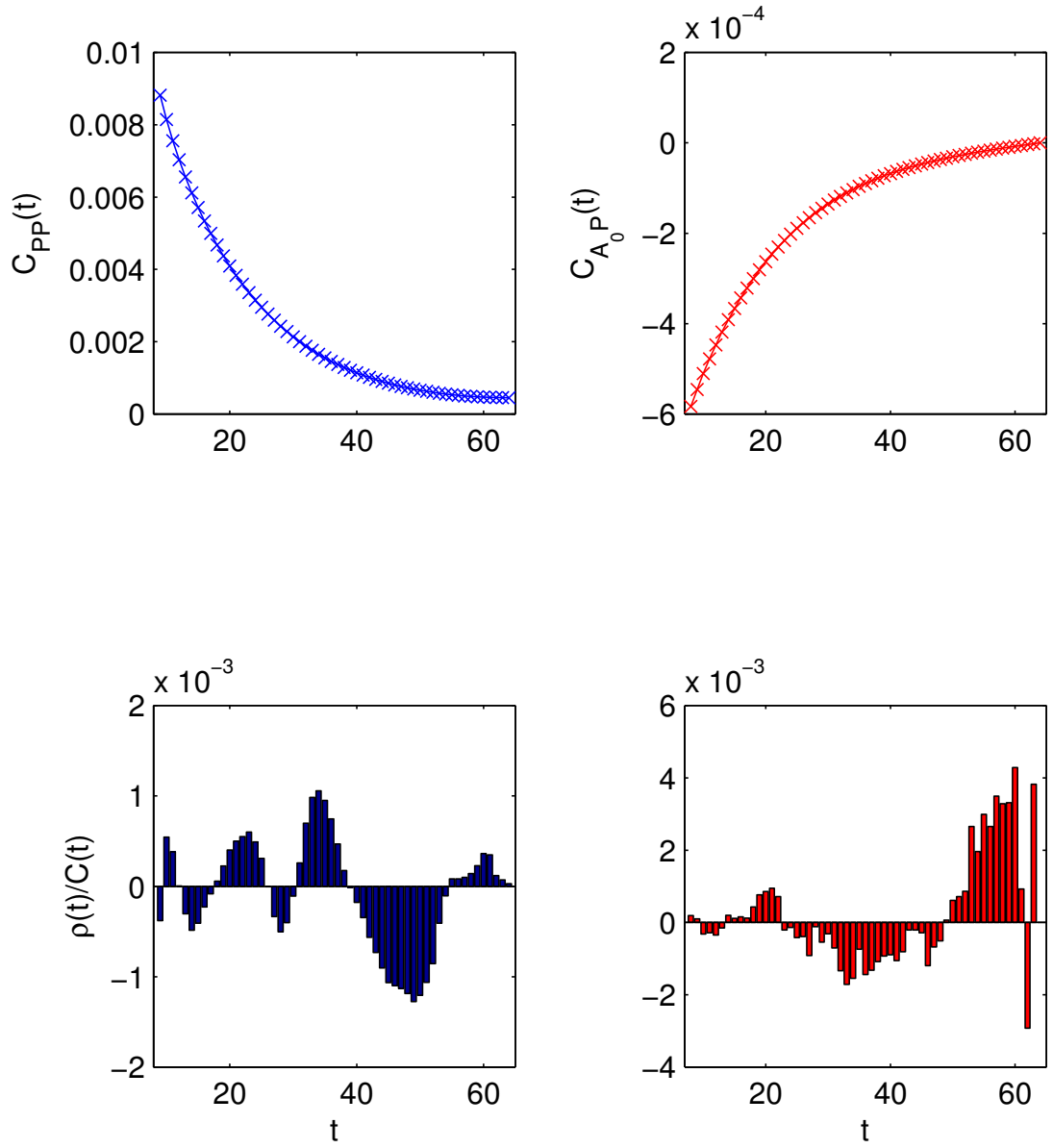
Figure 6.3.: Double exponential fit of the C_{PP} and C_{A_0P} correlators at the unitary point of the O7 chain. In the lower part we show the relative size of the residuals, where $\rho = C_{\text{fit}} - C$ and C stands for either C_{PP} or C_{A_0P}.
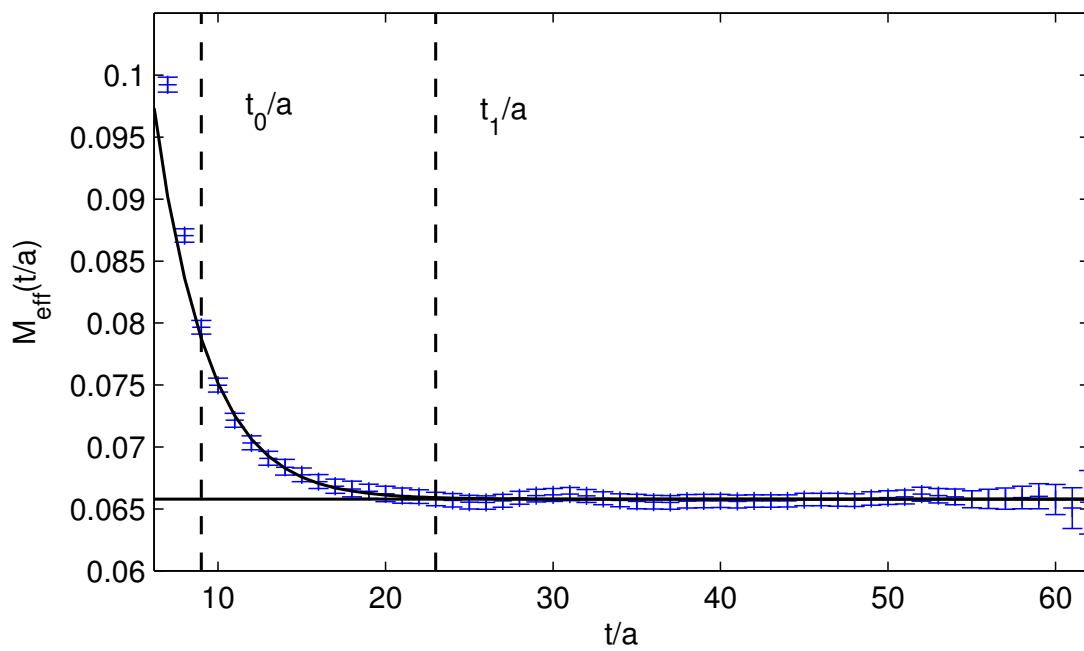
Figure 6.4.: Effective mass plot of the C_{PP} correlator at the unitary point. The vertical lines show t_0 and t_1, while the solid line is the result of the double exponential fit.
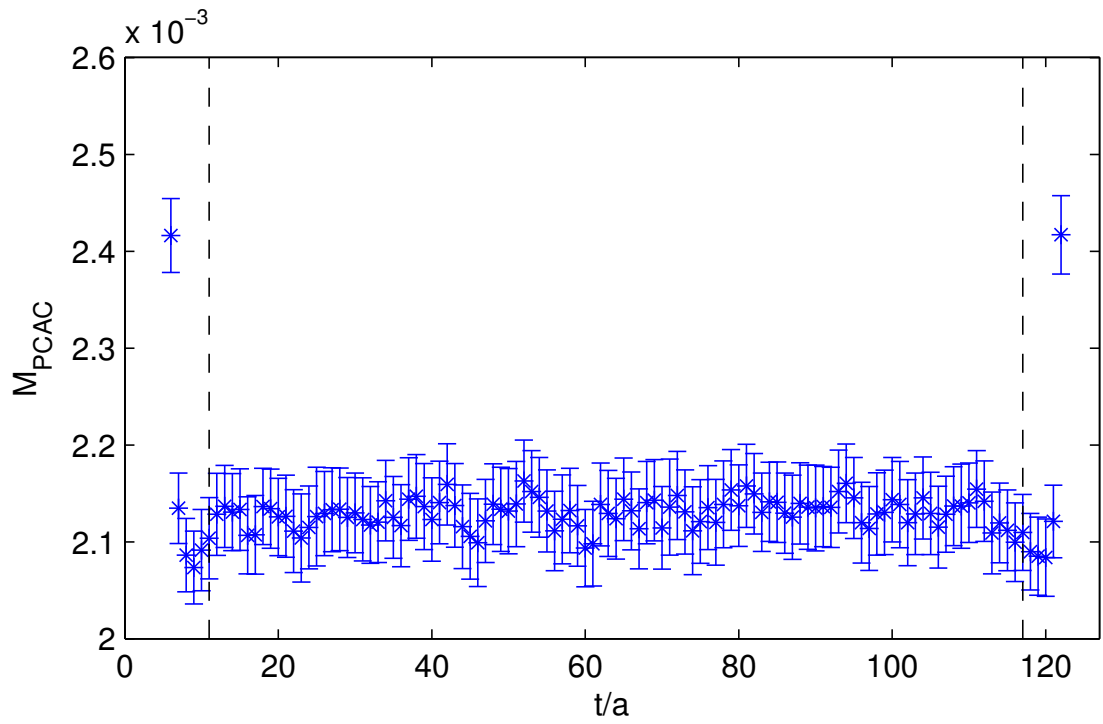
Figure 6.5.: M_{PCAC} of the O7 chain at the unitary point. The vertical lines show the range over which we average the expression in *eq.* (5.7).
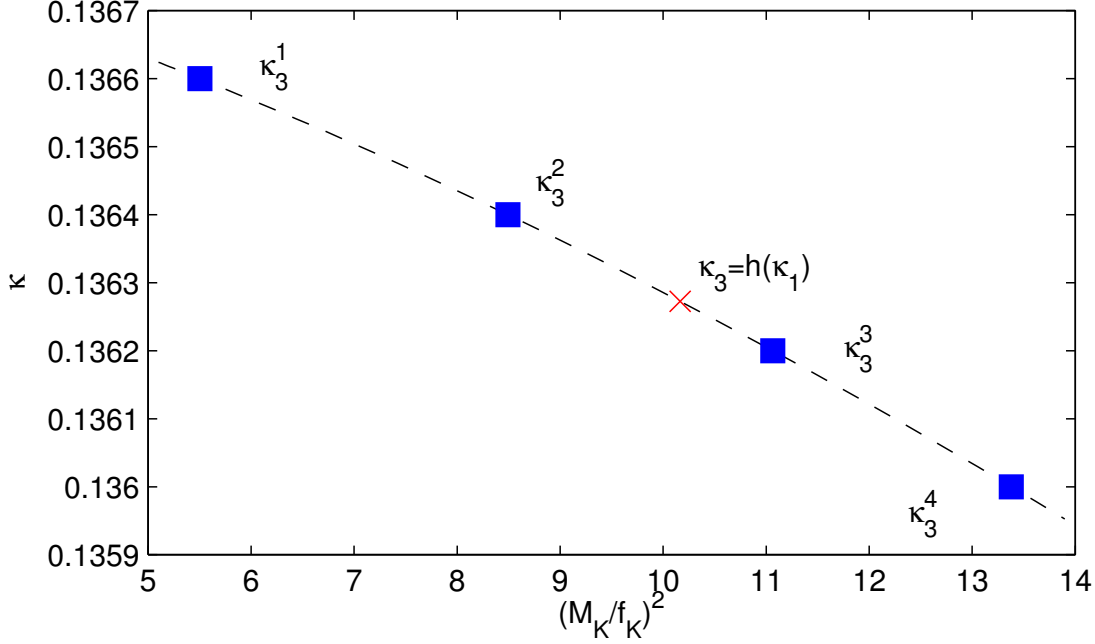
Figure 6.6.: Determination of κ_3 on the O7 chain, the ratio on the x-axis is between the pseudo-scalar mass and the renormalized decay constant.

correlators with the first hopping parameter fixed at its sea value $\hat{\kappa}$ and the second at $\kappa_3^i \sim \kappa_3$. These four values have been used for the interpolation of $h(\hat{\kappa})$, as shown in fig. (6.6), where the interpolation formula used is quadratic in $1/\kappa_3$.

The lattice spacing estimate is finally computed from the chiral fit defined in eq. (6.6) where the parameter α_4 (namely the slope of the linear part in the extrapolation) has been kept independent from the value of β. The resulting extrapolation is shown in fig. (6.7) where one can see that the three rightmost points even though they are excluded from the fit, they are still well described by the fitting function.

For the purpose of error analysis, the fit function is a derived quantity that depends on the value of derived quantities estimated on different ensembles, its general form is the one described by eq. (4.1). The error of the fit parameters (namely α_4 and $af_{\mathrm{K,lat.}}$) is computed with the method described in eq. (4.49), where the total error is split in the contributions coming from each ensemble. The error coming from each ensemble is estimated taking into account the slow modes of the algorithm by computing $\tau_{\mathrm{int}}^{\mathrm{u}}$. As a typical example in fig. (6.8) we show the auto-correlation function of the contribution that comes from the O7 ensemble to the bare decay constant $af_{\mathrm{K,lat.}}$ at $\beta = 5.5$ (in fig. (6.7) it correspond to the chiral extrapolation on the bottom). The contribution to the error that comes from the remaining ensembles is similarly calculated, and an
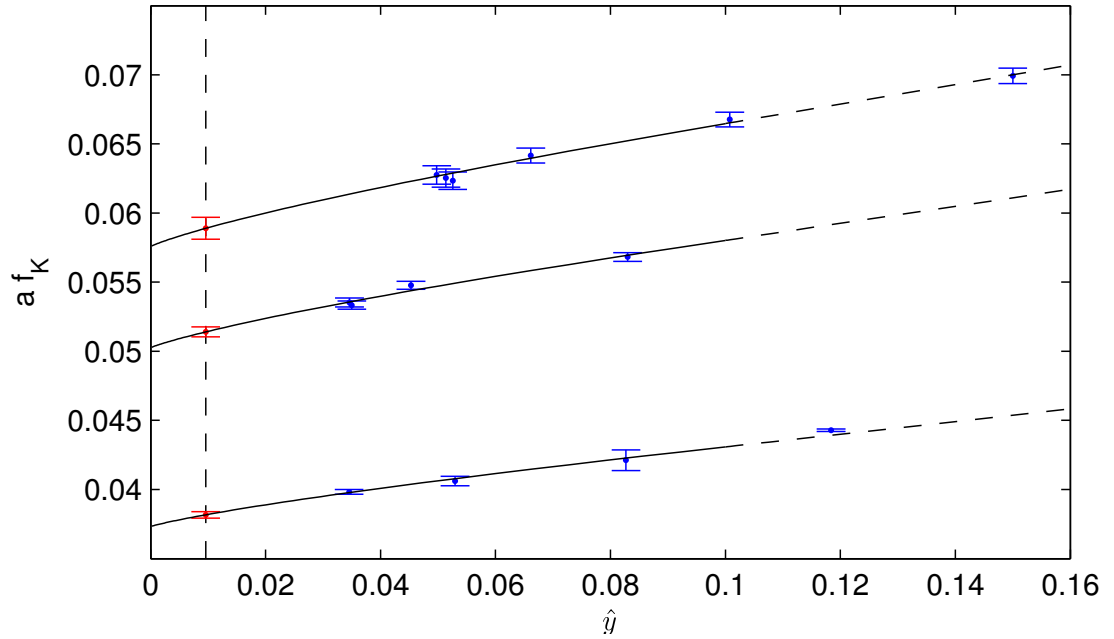
Figure 6.7.: Chiral extrapolation of the kaon decay constant in lattice units. The values of f_K have been multiplied by Z_A, but the error shown does not take the statistical error of the renormalization constant into account. The dashed line starts at $\hat{y}_{11} = 0.1$ where we perform a cut (only quantities below the cut participate to the fit). The vertical dashed line shows the physical point (the one at the physical value of the pion mass).
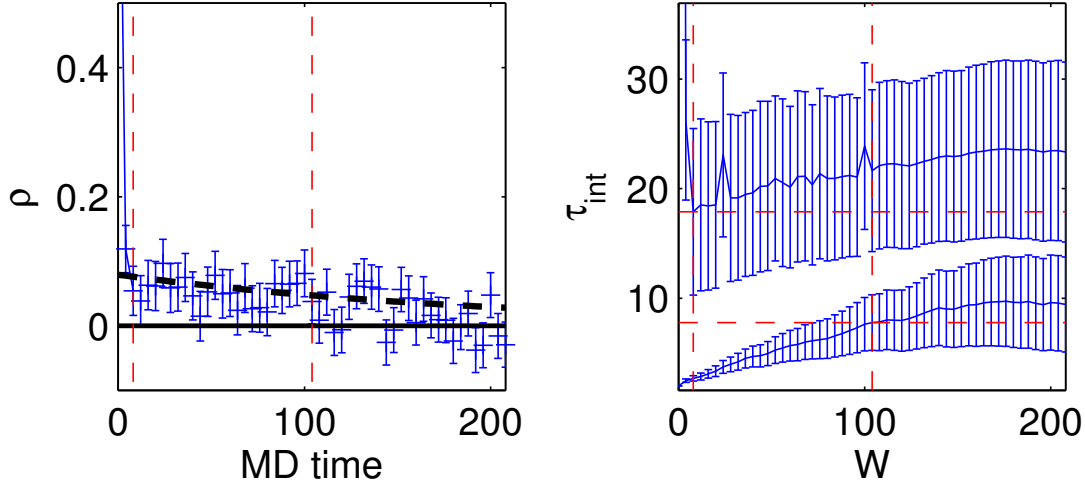
Figure 6.8.:   **Left:** normalized auto-correlation function of the contribution to the error to the determination of the lattice spacing at $\beta = 5.5$ coming from the O7 chain.   **Right:** integrated auto-correlation time and its upper bound, the vertical lines show W_{u} (the leftmost one) and W_{l} (this is computed setting the parameter in eq. (4.58) S=5.

interesting quantity to look at is the relative squared error budget defined as

$$\delta P|_{\eta,\mathrm{rel.}} = \frac{(\delta P|_\eta)^2}{\sum_{\eta=1}^{\mathrm{N\ error\ sources}}(\delta P|_\eta)^2} \tag{6.18}$$

where from eq. (4.3)

$$(\delta P|_\eta)^2 = \sum_{s,s'} \left. \frac{\partial p(\mathbf{X}^1,\dots)}{\partial X^{s,\eta}}\right|_{\mathbf{X}=\mathbf{H}} \Sigma^\eta(H^s,H^{s'}) \left. \frac{\partial p(\mathbf{X}^1,\dots)}{\partial X^{s',\eta}}\right|_{\mathbf{X}=\mathbf{H}}. \tag{6.19}$$

If the contributions come from an MCMC computation they are given by

$$(\delta P|_\eta)^2 = \frac{1}{N_\eta} \sum_{\tau=-\infty}^{\infty} \Gamma_{\mathrm{p}^\eta}(\tau) \tag{6.20}$$

while different kind of contributions must be accordingly propagated. In fig. (6.9) we show $\delta P|_{\eta,\mathrm{rel.}}$ coming from each ensemble, together with the error coming from the renormalization factor Z_{A} that has been computed in ref. [14]. Z_{A} enters as a multiplicative factor to the bare decay constant. We see that in both cases the largest contribution to the error comes from the error of Z_{A}.
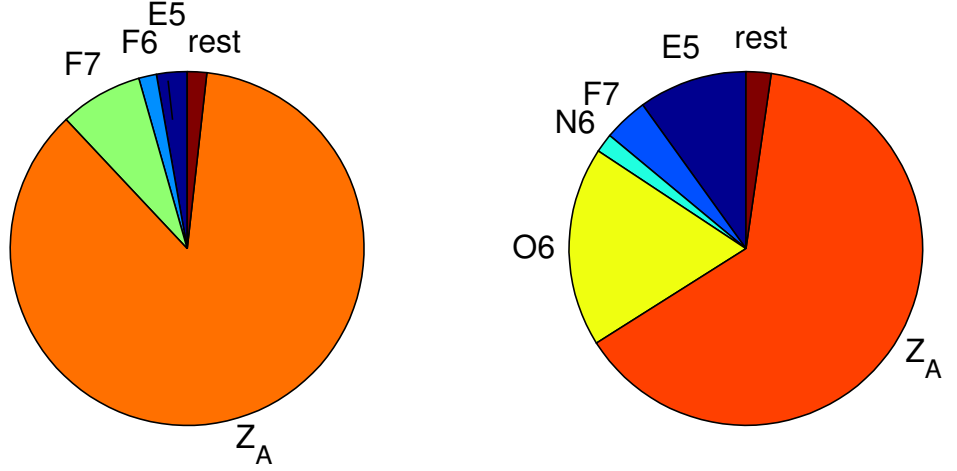
Figure 6.9.: Relative statistical error budget in the estimate of the lattice spacing, in both cases the largest contribution to the error comes from the error in the renormalization constant Z_A. **Left:** Estimate for $\beta = 5.3$. **Right:** Estimate for $\beta = 5.5$.

6.3. Wilson flow and slow observables

Quantities computed along the Wilson flow are less sensitive to the short range fluctuations of the gauge fields due to its smoothing properties. This makes them particularly suitable for monitoring the progress of lattice QCD computation, since slow modes tend to show up mostly in this class of observables.

The differential equation that describes the flow, eq. (2.67) must be discretized in order to solve it with numerical methods. We adopt here the Runge-Kutta scheme described in ref. [47]. The numerical integration requires a choice of step size that we set $\delta t_W = 0.02$. This value has been checked such that on the coarsest lattices it gives a relative error $< 10^{-5}$ on typical observables and it has been kept unchanged also at the larger values of β (even though on finer lattices the Wilson flow time scales with a^{-2} and the value of δt_W could have been increased accordingly).

The renormalized quantity E in eq. (2.68) can be used to define the scale t_0 introduced in ref. [47]

$$E(t_0)t_0^2 = 0.3 \tag{6.21}$$

where the arbitrary choice of 0.3 is justified by the observation that this typically corresponds to a smoothing radius of ~ 0.5 fm, this distance is neither too short (cutoff effects are expected to be small) nor too large, so that finite volume effects should also be well under control, in typical lattice volumes.

A possible use of slow observables is the determination of thermalization ranges. The
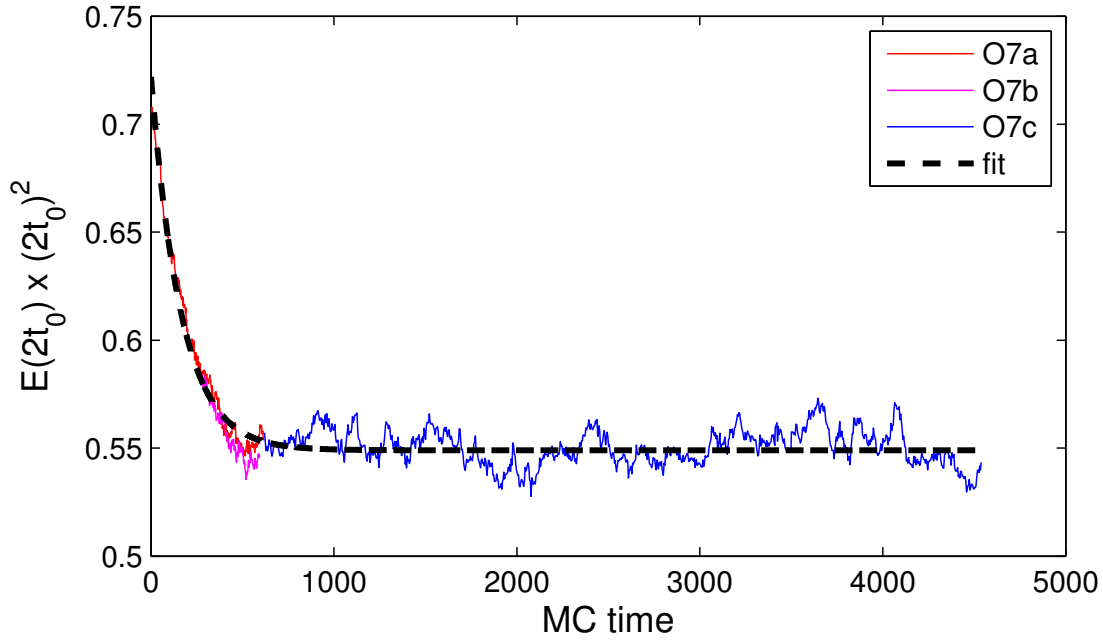
Figure 6.10.: Thermalization history of the O7 chain.

approach to equilibrium in a Markov chain is exponential and is dominated by τ_{exp} at large MC times. If the amplitude of the mode associated to τ_{exp} is large enough one can try to fit an exponential to the thermalization history, as we show in fig. (6.10). It is quite surprising that we see such behaviour from a single realization of the chain, since in general one would expect that a large number of independent realizations is needed. The value of the characteristic time that we read from the fit is ~ 170 that is very close to 200 that is the estimated value of τ_* at $\beta = 5.5$, from the interpolation formula.

7. Conclusions

The primary goal of this work was to develop understanding of the critical slowing down of algorithms used in current lattice QCD computations and to explore the implications for error analysis of observables computed in presence of long auto-correlations.

In a preliminary study within the quenched approximation we found that the topological susceptibility couples strongly to the slow modes of the HMC algorithm and suffers from critical slowing down with a critical exponent $z \simeq 5$. We have also studied other pure gauge and quenched observables that do not show the same critical behaviour. In particular for hadronic masses and matrix elements we have found a factor 50 suppression of the slow mode at intermediate lattice spacings. In QCD with two dynamical flavours we find that χ_{top} exhibits critical slowing down similar to the pure gauge case. The larger computational effort, due to the inclusion in the computation of a stochastic estimator of the fermionic determinant, prevents us from studying ensembles as large as the ones used for the pure SU(3) analysis. For the critical behaviour we have therefore assumed the power law behavior that we have found in the quenched approximation, calibrated with a calculation of $\tau_{\text{int}}(\chi_{\text{top}})$ done on a dynamical ensemble with high statistics at an intermediate lattice spacing of $a \sim 0.07$ fm. We have found that the value of τ_{exp} that we predict in this way at $a \sim 0.045$ fm is compatible with the exponential behaviour of the tail of the auto-correlation functions of some hadronic observables (namely matrix elements, pseudo-scalar masses and quark masses). We have also found empirical evidence of the goodness of our assumptions from an estimate of τ_{exp} that we obtain by fitting a single exponential to the approach to equilibrium of a slow observable.

In the course of the CSD analysis in many observables we have found evidence of long tails in the auto-correlation function. Even though we see that tails associated to τ_{exp} are suppressed at increasingly smaller lattice spacing, we analyzed the impact of underestimating their contribution in standard error analysis. In the case where statistics is too small to reliably estimate the auto-correlation function at large times (where the amplitude of the tail is much smaller than the typical size of the statistical errors) we proposed a method that includes the effect of a long tail in the error computation of LQCD observables. We have shown that the method works and in the case of an observable that couples to the slow mode it gives an upper bound to the statistical error that is not excessively conservative. The statistical error of the auto-correlation function and of τ_{int} has been computed with the well known approximate fromulas of ref. [74, 88, 43]. An investigation in the three dimensional ϕ^4 model shows deviations from the unbiased estimate of the error of the error (since in some cases the four point function is not completely dominated by disconnected pieces). In most cases the deviations are not too big, and even in presence of larger deviations the consequences for error analysis are minor.

7. Conclusions

The main conclusion that we draw is that simulations of lattice QCD become practically impossible to perform with current technology at $a \sim 0.04$ fm. Even though there have been some suggestions in the literature on how to push this limit to smaller lattice spacings [45, 50], none of the proposed methods has yet been succesfully applied to full QCD.

Acknowledgments

I would like to thank the colleagues at DESY for all the useful discussions and the nice evenings spent together. Hubert for all the counseling and for the great help he offered when I had to start my new life in Germany. My adviser Rainer for the uncountable hours of his time and for introducing us all to the magic of the Zeuthener See. The mythical SBP group for the great time we managed to squeeze out of Fridays Feierabends.

A particular thank goes to Stefan for helping me understand the insides of doing research and the many aspects of our numerical approach. To Ulli for the numerous teachings at the Monday seminars, and to all the other people at the Humboldt university for discussions and help.

I would finally like to thank all the people that were close to me and were patient enough to see the end of this work. My family for supporting me, in particular Julia for the moral help and the extra dose of patience needed.

Thank you all.

A. Error analysis software

The error analysis has been performed exclusively with MATLAB$^\text{®}$. The code is publicly available at `http://www-zeuthen.desy.de/alpha/public_software/index.html`.

A.1. MATLAB implementation of UWerrTexp

The program that implements the gamma method with the tail truncation bias correction is an extension of the code by U. Wolff publicly available[1] on the web. The function we implement is

```
function
  [value,dvalue,ddvalue,tauint,
   dtauint,qval,W, gammaout,drho]
  = UWerrTexp(Data,Parm,Nrep,Name,Quantity,varargin)
```

we have kept an interface that is fully compatible with the original code of U. Wolff. We describe here the meaning of the inputs and outputs, but practitioners with a working knowledge of `UWerr` will find all the extra information that is needed in the definition of the input argument `Parm`.

Input

Data it is an N x N_α matrix of measured (equilibrium!) data where N is the total number of measurements and N_α is the number of (primary) observables

Parm It is a vector of (up to 7) values:

1. Estimate of the ratio $S = \tau_*/\tau_{\text{int}}$. If $S = 0$, absence of auto-correlations is *assumed.*

2. Value of τ_* used to add a tail and give an upper bound to the error. If $\tau_* = 0$ the code performs a "standard" `UWerr` analysis.

3. It is the N_σ parameter that defines the point W_{u} that satisfies $\overline{\rho}(W_{\text{u}}) - N_\sigma \delta\overline{\rho}(W_{\text{u}}) \leq 0$. If $\tau_* \neq 0$ the exponential tail is attached at W_{u} (see also the discussion following eq. (4.73)).

4. A parameter W_{s} that defines a "small window". If $W_{\text{u}} < W_{\text{s}}$ a trial amplitude of the tail is taken to be either $\overline{\rho}(W_{\text{u}} + 1)$ or $2\delta\overline{\rho}(W_{\text{u}} + 1)$, whichever the largest. This

---

[1] original `UWerr`: `http://www.physik.hu-berlin.de/com/ALPHAsoft/`

new amplitude is accepted only if the resulting $\bar{\tau}_{\mathrm{int}}^{\mathrm{u}}$ is smaller than the previous one. This involved procedure prevents an excessive overestimate of $\tau_{\mathrm{int}}^{\mathrm{u}}$ in case when $\rho(\tau)$ decays very rapidly and the statistical errors are large. If $\bar{\rho}(W_{\mathrm{u}}) < 0$ this procedure is automatically applied.

5. This parameter is a Monte Carlo time conversion factor MCF. It is used in plots to rescale the time in user defined units.

6. This is a logical parameter, if set to 1 the output gives both the upper bound and the lower bound estimates for error, τ_{int} and W.

7. This is a logical parameter, if set to 1 it allows to propagate the error of quantities for which only the central value, the statistical and eventually also the systematic error is known. The way to pass the extra quantities and their error to the function is described below.

The default values for all these parameters are: $[1.5\ 0\ 3\ 5\ 1\ 0\ 0]$

Nrep It is a vector $[N_1\ N_2\ \ldots N_R]$ specifying a breakup of the N rows of `Data` into replicas of length N_1, N_2, … where $N = \sum N_r$. The replica distribution is plotted in a histogram and a Q-value (i.e. the probability to find this much or more scatter) is given when $R \geq 2$. Even though the code allows a splitting in realizations of different length, we recommend to use as often as possible replicas that have the exact same number of measurements. The default treats `Data` as a single chain of length N.

Name In case it is a string, it is the name of the observable in the titles of generated plots. Otherwise all plots are suppressed. The default is the string `"NoName"`.

Quantity It is a handle to a scalar function (@functionname) for the derived observable F. It has to operate on a row-vector of length N_α as first argument. Optional parameters P1, P2,…are passed on to this function as 2nd, 3rd, …If `Quantity` is an integer between 1 and N_α the analysis is performed on the α_{th} primary observable. The default value is 1.

If `Parm(7)` $\neq 0$ the function call changes to

```
function
  [value,dvalue,ddvalue,tauint,
   dtauint,qval,W, gammaout,drho]
  = UWerrTexp(Data,Parm,Nrep,Name,Quantity,UCData,varargin)
```

The extra parameter `UCData` is expected (i.e. if not set or set to `empty` it returns an error). All inputs are defined as before but the following

Quantity Scalar function handle (@functionname) for the derived observable F. It has to operate on a row-vector of length $N_\alpha +$ `NUCData` as first argument. Optional parameters P1, P2, . . . are passed on to this function as 2nd, 3rd, . . . argument.

UCData UnCorrelated Data. It is either an `NUCData x 2` or an `NUCData x 3` matrix. The first column contains the central value, the second contains the statistical error (that is summed in quadrature) and the third optional column is the systematic error (these contributions are summed linearly)

Output

value is the central estimate of `Quantity`.

dvalue is the statistical error (inclusive of auto-correlation effects). If `Parm(6) = 1` it is a vector of 2 values, namely `Stat = [lowerbound upperbound]`. If `Parm(7) = 1` returns one extra value, namely `[lowerbound upperbound systematic]`.

ddvalue statistical error of the error (only for the lowerbound)

tauint integrated auto-correlation time. If `Parm(6) = 1`, it returns a vector of 2 values namely $[\tau_{\text{int}}^{\text{l}} \ \tau_{\text{int}}^{\text{u}}]$.

dtauint statistical error of tauint. If `Parm(6) = 1`, returns a vector of 2 values: $[\delta\tau_{\text{int}}^{\text{l}} \ \delta\tau_{\text{int}}^{\text{u}}]$. $\delta\tau_{\text{int}}^{\text{u}}$ is computed assuming no error on τ_*.

qval Q-value of the replica distribution if $R \geq 2$ (it is the goodness of fit to a constant)

W it is the numerical value of the summation window. If `Parm(6) = 1`, it returns a vector of 2 values: $[W_{\text{l}} \ W_{\text{u}}]$.

gammaFbb Auto-correlation function (only up to 2W)

drho Error on the normalized auto-correlation function.

By default the routine generates plots of $\overline{\rho}(\tau)$ and $\tau_{\text{int}}^{\text{l}}$ with error bars in the relevant range to inspect the required plateau behaviour. In case τ_* is an input the plot shows also $\tau_{\text{int}}^{\text{u}}$ and the exponential tail together with the value of W_{u}. If there are two or more replicas their distribution is shown as a histogram with its Q-value in the title. In addition, in case that a primary observable is analyzed, a histogram of all estimates $a_\alpha^{i,r}$ is displayed.

A.2. Implementation of DerivedObservable

We have a separate implementation of a program that computes derived observables in the general case, namely when primary data comes either from one or from more than one different ensembles.

```
DerOBS = DerivedObservable(DATA,UCDATA,QTY,DQTY,varargin)
```

The function computes the derived observable from primary DATA. The derivative of the function specified by `QTY` can be explicitly given through the argument `DQTY`. Extra arguments of `QYT` are passed through `varargin`.

Input

Data is a cell array. Each cell contains data from a different ensemble. Data from each ensemble E_i can be either:

- An $N_i \times N_{\alpha_i}$ matrix of measured (equilibrium!) data where N_i is the total number of measurements on ensemble E_i and N_{α_i} is the number of (primary) observables on ensemble E_i.

- An $N_i \times N_{\alpha_i} \times R_i$ matrix of measured data. N_i is the total number of measurements on ensemble E_i, N_{α_i} is the number of (primary) observables on ensemble E_i and R_i is the number of replicas. If replicas consist of an uneven number of measurements, padding is required. Padding must be done after the last array element along the first dimention, with `NaN` elements.

UCData UnCorrelated Data. It is either an `NUCData x 2` or an `NUCData x 3` matrix. The first column contains the central value, the second contains the statistical error (that is summed in quadrature) and the third optional column is the systematic error (these contributions are summed linearly)
QTY scalar function handle (@functionname) for the derived observable F; it has to operate on a row-vector of length $\sum_n N_{\alpha_n} +$ `NUCData` as first argument; the first N_{α_1} arguments refer to the first ensemble, the following N_{α_2} to the second and so on... the last `NUCData` refers to the Uncorrelated Data set (`UCData`). Optional parameters P1, P2, ... are passed on to this function as 2nd, 3rd, ... argument
DQTY can be either

- scalar function handle (@functionname) for the gradient of the derived observable F; it has to operate on a row-vector of length $\sum N_{\alpha_n}$ as first argument; the first N_{α_n} arguments refer to the first ensemble, the following N_{α_n} to the second and so on... The function must also take a second argument specifying the variable w.r.t. which one is taking the derivative.

- Numeric value multiplying the increment used for calculating the numerical derivative.

- A vector of length $\sum_n N_{\alpha_n} + \mathtt{UCData}$ with logical entries (1 in case the approximated derivative of the observable in question has to be computed, 0 otherwise). $\mathtt{QTY}$ is assumed to get no contribution from observables whose derivatives are not computed (the implementer should check that this is actually the case!!)

Output

DerOBS cell array containing at each element the partial reduced observable for the quantity F, as in eq. (4.48). The error can then be constructed using eq. (4.49).

Bibliography

[1] B. Allés, G. Boyd, M. D'Elia, A. Di Giacomo, and E. Vicari. Hybrid monte carlo and topological modes of full QCD. *Phys. Lett.*, B389:107–111, 1996.

[2] Gunnar S. Bali et al. Quark mass effects on the topological susceptibility in QCD. *Phys.Rev.*, D64:054502, 2001. doi: 10.1103/PhysRevD.64.054502.

[3] Claude Bernard, Thomas A. DeGrand, Anna Hasenfratz, Carleton E. Detar, James Osborn, et al. Topological susceptibility with the improved Asqtad action. *Phys.Rev.*, D68:114501, 2003. doi: 10.1103/PhysRevD.68.114501.

[4] Ninoslav E. Bralić. Exact computation of loop averages in two-dimensional yang-mills theory. *Phys. Rev. D*, 22(12):3090–3103, Dec 1980. doi: 10.1103/PhysRevD. 22.3090.

[5] David J. E. Callaway and Aneesur Rahman. Lattice gauge theory in the microcanonical ensemble. *Phys. Rev. D*, 28(6):1506–1514, Sep 1983. doi: 10.1103/PhysRevD.28.1506.

[6] M.A. Clark and A.D. Kennedy. Accelerating dynamical fermion computations using the rational hybrid Monte Carlo (RHMC) algorithm with multiple pseudofermion fields. *Phys.Rev.Lett.*, 98:051601, 2007. doi: 10.1103/PhysRevLett.98.051601.

[7] Gilberto Colangelo, Stephan Durr, Andreas Juttner, Laurent Lellouch, Heinrich Leutwyler, et al. Review of lattice results concerning low energy particle physics. *Eur.Phys.J.*, C71:1695, 2011. doi: 10.1140/epjc/s10052-011-1695-1.

[8] M. Creutz. Global Monte Carlo algorithms for many-fermion systems. *Phys.Rev.*, D38:1228–1238, 1988. doi: 10.1103/PhysRevD.38.1228.

[9] Michael Creutz. Gauge Fixing, the Transfer Matrix, and Confinement on a Lattice. *Phys.Rev.*, D15:1128, 1977. doi: 10.1103/PhysRevD.15.1128.

[10] L. Del Debbio, Leonardo Giusti, M. Luscher, R. Petronzio, and N. Tantalo. QCD with light Wilson quarks on fine lattices. II. DD-HMC simulations and data analysis. *JHEP*, 0702:082, 2007. doi: 10.1088/1126-6708/2007/02/082.

[11] Luigi Del Debbio, Haralambos Panagopoulos, and Ettore Vicari. Theta dependence of SU(N) gauge theories. *JHEP*, 08:044, 2002.

[12] Luigi Del Debbio, Gian Mario Manca, and Ettore Vicari. Critical slowing down of topological modes. *Phys.Lett.*, B594:315–323, 2004. doi: 10.1016/j.physletb.2004.05. 038.

Bibliography

[13] Michele Della Morte, Roland Hoffmann, and Rainer Sommer. Non-perturbative improvement of the axial current for dynamical Wilson fermions. *JHEP*, 0503:029, 2005. doi: 10.1088/1126-6708/2005/03/029.

[14] Michele Della Morte, Rainer Sommer, and Shinji Takeda. On cutoff effects in lattice QCD from short to long distances. *Phys.Lett.*, B672:407–412, 2009. doi: 10.1016/j.physletb.2009.01.059.

[15] S. Duane and J.B. Kogut. The theory of Hybrid Stochastic Algorithms. *Nucl.Phys.*, B275:398, 1986. doi: 10.1016/0550-3213(86)90606-1.

[16] S. Duane, A.D. Kennedy, B.J. Pendleton, and D. Roweth. Hybrid Monte Carlo. *Phys.Lett.*, B195:216–222, 1987. doi: 10.1016/0370-2693(87)91197-X.

[17] Simon Duane and John B. Kogut. Hybrid Stochastic Differential Equations Applied to Quantum Chromodynamics. *Phys.Rev.Lett.*, 55:2774, 1985. doi: 10.1103/PhysRevLett.55.2774.

[18] Paul M. Fishbane, Stephen Gasiorowicz, and Peter Kaus. Stokes's theorems for non-abelian fields. *Phys. Rev. D*, 24(8):2324–2329, Oct 1981. doi: 10.1103/PhysRevD.24.2324.

[19] Roberto Frezzotti and Karl Jansen. A Polynomial hybrid Monte Carlo algorithm. *Phys.Lett.*, B402:328–334, 1997. doi: 10.1016/S0370-2693(97)00475-9.

[20] J. Gasser and H. Leutwyler. Chiral Perturbation Theory to One Loop. *Annals Phys.*, 158:142, 1984. doi: 10.1016/0003-4916(84)90242-2.

[21] Christof Gattringer and Christian B. Lang. Quantum chromodynamics on the lattice. *Lect.Notes Phys.*, 788:1–211, 2010. doi: 10.1007/978-3-642-01850-3.

[22] Leonardo Giusti and Martin Luscher. Chiral symmetry breaking and the Banks-Casher relation in lattice QCD with Wilson quarks. *JHEP*, 0903:013, 2009. doi: 10.1088/1126-6708/2009/03/013.

[23] Steven A. Gottlieb, W. Liu, D. Toussaint, R.L. Renken, and R.L. Sugar. Hybrid Molecular Dynamics Algorithms for the Numerical Simulation of Quantum Chromodynamics. *Phys.Rev.*, D35:2531–2542, 1987. doi: 10.1103/PhysRevD.35.2531.

[24] D.J. Gross and Frank Wilczek. Ultraviolet Behavior of Nonabelian Gauge Theories. *Phys.Rev.Lett.*, 30:1343–1346, 1973. doi: 10.1103/PhysRevLett.30.1343.

[25] Rajan Gupta, Gregory W. Kilcup, and Stephen R. Sharpe. Tuning the Hybrid Monte Carlo Algorithm. *Phys.Rev.*, D38:1278, 1988. doi: 10.1103/PhysRevD.38.1278.

[26] M. Hasenbusch. A Monte Carlo study of leading order scaling corrections of phi**4 theory on a three-dimensional lattice. *J.Phys.A*, A32:4851–4865, 1999. doi: 10.1088/0305-4470/32/26/304.

[27] M. Hasenbusch, K. Pinn, and S. Vinti. Critical exponents of the three-dimensional Ising universality class from finite-size scaling with standard and improved actions. *Phys.Rev.*, B59:11471–11483, 1999. doi: 10.1103/PhysRevB.59.11471.

[28] Martin Hasenbusch. Speeding up the hybrid Monte Carlo algorithm for dynamical fermions. *Phys.Lett.*, B519:177–182, 2001. doi: 10.1016/S0370-2693(01)01102-9.

[29] A. Hasenfratz, R. Hoffmann, and F. Knechtli. The static potential with hypercubic blocking. *Nucl. Phys. Proc. Suppl.*, 106:418–420, 2002.

[30] Anna Hasenfratz and Francesco Knechtli. Flavor symmetry and the static potential with hypercubic blocking. *Phys. Rev.*, D64:034504, 2001.

[31] Jochen Heitger and Andreas Jüttner. Lattice cutoff effects for F_{D_s} with improved Wilson fermions - a final lesson from the quenched case. *JHEP*, 05:101, 2009. doi: 10.1088/1126-6708/2009/05/101.

[32] Roland Hoffmann, Anna Hasenfratz, and Stefan Schaefer. Non-perturbative improvement of nHYP smeared Wilson fermions. *PoS*, LAT2007:104, 2007.

[33] Karl Jansen and Rainer Sommer. O(a) improvement of lattice QCD with two flavors of Wilson quarks. *Nucl. Phys.*, B530:185–203, 1998.

[34] Chulwoo Jung. Status of dynamical ensemble generation. *PoS*, LAT2009:002, 2009.

[35] A.D. Kennedy. Algorithms for dynamical fermions. 2006. 62 pages, 16 figures. Published by World Scientific in proceedings of the ILFTN workshop 'Perspectives in Lattice QCD'. Revised version corrects (or at least changes) some sign errors, and makes a few other improvements.

[36] A.D. Kennedy and Pietro Rossi. Classical mechanics on group manifolds and applications to Hybrid Monte Carlo. *Nucl.Phys.*, B327:782, 1989. doi: 10.1016/0550-3213(89)90315-5.

[37] Francesco Knechtli and Bjorn Leder. Scale r_0 and the static potential from the CLS lattices. *PoS*, LATTICE2010:233, 2010. * Temporary entry *.

[38] M. Lüscher. Selected topics in lattice field theory. . Lectures given at Summer School 'Fields, Strings and Critical Phenomena', Les Houches, France, Jun 28 - Aug 5, 1988.

[39] M. Lüscher. Construction of a selfadjoint, strictly positive transfer matrix for euclidean lattice gauge theories. *Commun. Math. Phys.*, 54:283, 1977.

[40] Martin Lüscher. DD-HMC algorithm for two-flavour lattice qcd. . URL `"http://luscher.web.cern.ch/luscher/DD-HMC/index.html"`.

[41] Martin Luscher. Advanced lattice QCD. pages 229–280, 1998.

[42] Martin Luscher. Solution of the Dirac equation in lattice QCD using a domain decomposition method. *Comput.Phys.Commun.*, 156:209–220, 2004. doi: 10.1016/S0010-4655(03)00486-7.

[43] Martin Luscher. Schwarz-preconditioned HMC algorithm for two-flavour lattice QCD. *Comput.Phys.Commun.*, 165:199–220, 2005. doi: 10.1016/j.cpc.2004.10.004.

[44] Martin Lüscher. Local coherence and deflation of the low quark modes in lattice qcd. *JHEP*, 07:081, 2007.

[45] Martin Luscher. Trivializing maps, the Wilson flow and the HMC algorithm. *Commun.Math.Phys.*, 293:899–919, 2010. doi: 10.1007/s00220-009-0953-7.

[46] Martin Luscher. Computational Strategies in Lattice QCD. 2010. * Temporary entry *.

[47] Martin Luscher. Properties and uses of the Wilson flow in lattice QCD. *JHEP*, 1008:071, 2010. doi: 10.1007/JHEP08(2010)071.

[48] Martin Luscher and Filippo Palombi. Fluctuations and reweighting of the quark determinant on large lattices. *PoS*, LATTICE2008:049, 2008.

[49] Martin Luscher and Filippo Palombi. Universality of the topological susceptibility in the SU(3) gauge theory. *JHEP*, 1009:110, 2010. doi: 10.1007/JHEP09(2010)110.

[50] Martin Luscher and Stefan Schaefer. Lattice QCD without topology barriers. *JHEP*, 1107:036, 2011. doi: 10.1007/JHEP07(2011)036.

[51] Martin Luscher and Peter Weisz. Perturbative analysis of the gradient flow in non-abelian gauge theories. *JHEP*, 1102:051, 2011. doi: 10.1007/JHEP02(2011)051.

[52] Martin Luscher, Stefan Sint, Rainer Sommer, Peter Weisz, and Ulli Wolff. Nonperturbative O(a) improvement of lattice QCD. *Nucl.Phys.*, B491:323–343, 1997. doi: 10.1016/S0550-3213(97)00080-1.

[53] N. Madras and A. D. Sokal. *J. Stat. Phys.*, 50:109, 1988.

[54] Marina Marinkovic and Stefan Schaefer. Comparison of the mass preconditioned HMC and the DD-HMC algorithm for two-flavour QCD. *PoS*, LATTICE2010:031, 2010.

[55] Marina Marinkovic, Stefan Schaefer, Rainer Sommer, and Francesco Virotta. Strange quark mass and lambda parameter by the alpha collaboration. *talk at Lattice 2011, USA*, 2011.

[56] N. Metropolis, A.W. Rosenbluth, M.N. Rosenbluth, A.H. Teller, and E. Teller. Equation of state calculations by fast computing machines. *J.Chem.Phys.*, 21: 1087–1092, 1953. doi: 10.1063/1.1699114.

[57] Christopher Michael and J. Peisa. Maximal variance reduction for stochastic propagators with applications to the static quark spectrum. *Phys.Rev.*, D58:034506, 1998. doi: 10.1103/PhysRevD.58.034506.

[58] Colin Morningstar. The Monte Carlo method in quantum field theory. 2007.

[59] Colin Morningstar and Mike J. Peardon. Analytic smearing of SU(3) link variables in lattice QCD. *Phys.Rev.*, D69:054501, 2004. doi: 10.1103/PhysRevD.69.054501.

[60] K.H. Mutter, K. Schilling, R. Sommer, and P. De Forcrand. Towards the limit of the quenched approximation in hadron mass calculations. 1986.

[61] Y. Namekawa et al. Light hadron spectroscopy in two-flavor QCD with small sea quark masses. *Phys.Rev.*, D70:074503, 2004. doi: 10.1103/PhysRevD.70.074503.

[62] Silvia Necco and Rainer Sommer. The N(f) = 0 heavy quark potential from short to intermediate distances. *Nucl. Phys.*, B622:328–346, 2002.

[63] Holger Bech Nielsen and M. Ninomiya. No go theorem for regularizing chiral fermions. *Phys. Lett.*, B105:219, 1981.

[64] K. Osterwalder and E. Seiler. Gauge field theories on a lattice. *Annals of Physics*, 110(2):440 – 471, 1978. ISSN 0003-4916. doi: DOI:10.1016/0003-4916(78)90039-8.

[65] Konrad Osterwalder and Robert Schrader. Axioms for Euclidean Green's Functions. 2. *Commun.Math.Phys.*, 42:281, 1975. doi: 10.1007/BF01608978.

[66] Politzer. Reliable Perturbative Results for Strong Interactions? *Phys.Rev.Lett.*, 30: 1346–1349, 1973. doi: 10.1103/PhysRevLett.30.1346.

[67] Politzer. Asymptotic Freedom: An Approach to Strong Interactions. *Phys.Rept.*, 14:129–180, 1974. doi: 10.1016/0370-1573(74)90014-3.

[68] M.B. Priestley. *Spectral analysis and time series.* Number v. 1-2 in Probability and mathematical statistics. Academic Press, 1982. ISBN 9780125649223.

[69] Y. Saad. *Iterative Methods for Sparse Linear Systems, 2nd edition.* SIAM, Philadelpha, PA, 2003.

[70] Stefan Schaefer. Simulations with the hybrid monte carlo algorithm: implementation and data analysis, 2010.

[71] Stefan Schaefer, Rainer Sommer, and Francesco Virotta. Critical slowing down and error analysis in lattice QCD simulations. *Nucl.Phys.*, B845:93–119, 2011. doi: 10.1016/j.nuclphysb.2010.11.020.

[72] Stephen R. Sharpe. Enhanced chiral logarithms in partially quenched QCD. *Phys.Rev.*, D56:7052–7058, 1997. doi: 10.1103/PhysRevD.56.7052,10.1103/ PhysRevD.62.099901.

[73] B. Sheikholeslami and R. Wohlert. Improved continuum limit lattice action for QCD with Wilson fermions. *Nucl. Phys.*, B259:572, 1985.

[74] A. D. Sokal. Monte Carlo Methods in Statistical Mechanics: Foundations and New Algorithms. *NATO Adv. Sci. Inst. Ser. B Phys.*, pages 131–192, 1997.

[75] Alan D. Sokal and Lawrence E. Thomas. Exponential convergence to equilibrium for a class of random-walk models. *Journal of Statistical Physics*, 54:797–828, 1989. ISSN 0022-4715. URL `http://dx.doi.org/10.1007/BF01019776`. 10.1007/BF01019776.

[76] R. Sommer. Leptonic decays of b and d mesons. *Nucl. Phys. Proc. Suppl.*, 42: 186–193, 1995.

[77] K. Symanzik. Continuum limit and improved action in lattice theories. 1. Principles and ϕ^4 theory. *Nucl. Phys.*, B226:187, 1983.

[78] K. Symanzik. Continuum limit and improved action in lattice theories. 2. O(N) nonlinear sigma model in perturbation theory. *Nucl. Phys.*, B226:205, 1983.

[79] (Ed.) 't Hooft, Gerard. 50 Years of Yang-Mills Theory. 2005. ISBN 981-238-934-2.

[80] G. 't Hooft. The making of the standard model. *Nature*, 448:271–273, 2007. doi: 10.1038/nature06074.

[81] Gerard 't Hooft. THE BIRTH OF ASYMPTOTIC FREEDOM. *Nucl.Phys.*, B254: 11–18, 1985. doi: 10.1016/0550-3213(85)90206-8.

[82] Gerard 't Hooft. When was asymptotic freedom discovered? or the rehabilitation of quantum field theory. *Nucl.Phys.Proc.Suppl.*, 74:413–425, 1999. doi: 10.1016/ S0920-5632(99)00207-8.

[83] Gerard 't Hooft. Nobel lecture: A confrontation with infinity. *Rev.Mod.Phys.*, 72: 333–339, 2000. doi: 10.1103/RevModPhys.72.333,10.1103/RevModPhys.74.1343. 1999 Nobel Lecture in Physics.

[84] Steven Weinberg. A Model of Leptons. *Phys.Rev.Lett.*, 19:1264–1266, 1967. doi: 10.1103/PhysRevLett.19.1264.

[85] Steven Weinberg. The Making of the standard model. *Eur.Phys.J.*, C34:5–13, 2004. doi: 10.1140/epjc/s2004-01761-1.

[86] Steven Weinberg. Effective Field Theory, Past and Future. *PoS*, CD09:001, 2009.

[87] Kenneth G. Wilson. Confinement of quarks. *Phys. Rev.*, D10:2445–2459, 1974.

[88] Ulli Wolff. Monte carlo errors with less errors. *Comput. Phys. Commun.*, 156: 143–153, 2004.

List of Figures

List of Figures

List of Tables

Eigenständigkeitserklärung

Ich erkläre, dass ich die vorliegende Arbeit selbständig und nur unter Verwendung der angegebenen Literatur und Hilfsmittel angefertigt habe.

Berlin, den 14.12.2011   Francesco Virotta